

Search for heavy neutrinos in the T2K experiment and upgrade of the near detector ND280

Suvorov Sergey

August 2019

CONTENTS

I Introduction

1 Neutrino physics	7
1 Historical overview	7
1.1 Discovery of the neutrino	7
1.2 Neutrino flavors	8
1.3 Neutrino in the Standard Model	8
1.4 Neutrino interactions	11
2 Neutrino oscillations	15
2.1 Theory	15
2.2 Experiment overview	21
2 Neutrino mass	27
1 Theory	27
1.1 Dirac mass term	27
1.2 Majorana mass term	28
1.3 Mixing Dirac and Majorana terms	29
1.4 Heavy Neutral Lepton	30
2 Experiments	31
2.1 Neutrino mass measurements	31
2.2 Search for Heavy Neutral Lepton	33
3 Prospects of the neutrino physics	37
1 Future neutrino experiments	37
4 The T2K experiment	39
1 Neutrino beam	41
1.1 Off-axis flux	42
1.2 Neutrino beamline	43
2 Near detector	46
2.1 INGRID	46
2.2 Near detector ND280	48
3 Super-Kamiokande	51
4 Analysis overview	53
4.1 Oscillation analysis	53
4.2 Neutrino cross-section measurements	57

II Heavy neutrino study

5 Prospects in T2K	61
6 HNL flux simulations	65
1 T2K flux simulation	65
2 HNL production	68
3 HNL decays	70
3.1 HNL daughter particles	73
7 HNL analysis	79
1 Time of flight correction	79
2 Event selection	80
2.1 Cuts description	81
2.2 Signal selection efficiency	86
2.3 Background suppression	87
3 Systematic uncertainties	90
3.1 Detector systematics	91
3.2 Flux systematics	94
3.3 Pile up	96
4 Statistical methods	96
8 Results	99
1 MC sensitivity estimations	99
2 Data unblinding	100
3 Prospects	103

III ND280 upgrade

9 Introduction	107
1 Beamline upgrade	108
2 Detector overview	109
2.1 Current detector limitations	109
2.2 New design proposal	111
10 Simulations	113
11 TPC	115
1 Concept	115
1.1 Resistive MicroMegas technology	115
2 Beamtest	115
2.1 Cosmic test	115
2.2 CERN beamtest	115
2.3 DESY beamtest	115
12 Super FGD	118
1 Concept	118
1.1 Assembly	118
2 Simulations	118
2.1 Expected light yield	118

2.2	Michell electron tagging	118
2.3	Pileups	118
3	Beamtest	118
3.1	First CERN beamtest	118
3.2	Second CERN beamtest	118
13	Neutron tagging in SuperFGD	119
1	Motivation	119
2	Geant4 simulation	119
3	Efficiency and energy resolution	119
4	Background estimations	119
5	Prospects for physics	119
IV Conclusion		
Bibliography		123

¹

Part I

²

Introduction

NEUTRINO PHYSICS

Exploration of the neutrinos is a relatively young but perspective direction of the research in particle physics. Over the last 60 years since its first experimental observation, lots of breakthroughs were made. Many of them have been awarded notable prizes. All this speaks of the great interest of the community on this topic. Many puzzles are still unsolved, plenty of challenging experiments are ongoing.

In this chapter, the brief history of the neutrino research and the current theory of the neutrino will be overviewed (section 1). The topic of the neutrino oscillations (section 2) will be described in more detail as the main subject of the current thesis. The experimental overview and the ongoing researches on this topic will be described in the subsection 2.2.

1 Historical overview

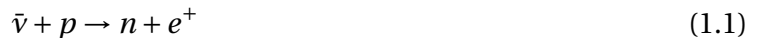
The prerequisites of the neutrino existence were found at the beginning of the XXth century. The spectrum of the electrons from the β -decay was measured as continuous but not discrete [1]. The β -decay was observed as a neutron transformation into electron and proton. Following the laws of both momentum and energy conservation, the electron produced in the 2-body decay should have fixed energy defined by the mass difference between the neutron and the proton. Non-discrete spectrum provoked plenty of theories such as energy non-conservation (by N. Bohr) or existence of the new hypothetical particle (by W. Pauli [2]). Later Enrico Fermi developed a complete theory of beta decay [3]. In the modern notation, the decay process was presented as $n \rightarrow p^+ + e^- + \bar{\nu}_e$, where neutrino is noted as ν .

1.1 Discovery of the neutrino

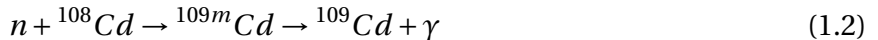
The experimental discovery of the neutrino was pretty challenging. Neutrinos are not taking part in the electromagnetic or strong interactions. The only way to detect them is through the weak interaction. Based on Fermi's theory the inverse beta decay $n + \nu \rightarrow p + e$ should exist that will allow the direct observation of the neutrino. But the expected cross-section for such a process was estimated at the level of $10^{-44} cm^2$. That was about a couple of dozen orders less than cross-

sections of the processes that were usually observed in the experiments at that time. That's why the neutrino discovery happened only 26 years after the idea of the neutrino existence had come.

After the proposal of the new particle few indirect measurements were performed, but the direct observation remained a challenge. The first successful neutrino detection was done by the group led by Frederick Reines and Clyde Cowan [4]. They performed a series of experiments trying to detect neutrino from the most powerful source at that time - nuclear power plant. Relatively brand new material a liquid scintillator was used as a target and detector. The inverse beta decay was used as a detection reaction:



The positron shortly annihilates with the emitting of the two photons that could be detected with PMTs. But not only neutrino interactions could cause such a signal. To suppress the background, the Cadmium isotope was added to the detector. Thus the neutrons would also be detected with reaction



As the ${}^{109m}Cd$ lifetime is few tens of microseconds the signal will have the unique signature: positron annihilation, and after a known time delay the gamma-ray emission. Both signals will come with well-defined energies. Thus rare signal events could be easily separated from the variety of the backgrounds.

Such a strategy lead to the successful discovery of the particle that was supposed to be "undetectable" before.

52

1.2 Neutrino flavors

The first neutrino detection was made using the nuclear reactor as a particle source. Such a source is extremely powerful but isotropic. For the precise measurements, it will be extremely useful to gain the statistics with the focused particle beam. For this, the accelerators could be used. The general idea is to use a proton beam hitting the target for the massive meson production. The charged meson could be focused with the magnetic field and further decay, producing the focused neutrino beam with high intensity. The description of such a scheme in the modern experiment could be found in section 1. First-time such an approach was used to determine if the neutrino has flavors [5]. At that time it was known that there are two generations of the charged leptons: electron and muon. The question was if the electron neutrino was different from the muon neutrino. The main idea of the experiment is to use the neutrino flux produced from the pion decay. Because of the mass difference between electron and muon charged pion decays mainly to the muon, e.g. $\pi^+ \rightarrow \mu^+ + \nu$. The experiment showed clearly that the reaction Equation 1.4 is severely suppressed comparing the reaction Equation 1.3.



That means that neutrino has flavors. It could be either produced or detected with the lepton of the same flavor. The existence of the different types of neutrino confirmed the doublet structure of the leptons. This fact will play an important role in the theory of neutrino oscillations.

71

1.3 Neutrino in the Standard Model

The first step towards the general model of particle physics was done by Yang and Mills by extending the concept of the gauge theory to the nonabelian groups. This made possible to describe

the phenomenon of strong interactions [6]. Later Glashow found a way to unify the electromagnetic and weak interactions [7]. Salam and Weinberg finished the theory with the implementation of the Higgs mechanism into the Glashow theory [8].

Plenty of experiments brilliantly confirmed the proposed model and demonstrated its incredible predictive power. For example, in the part of the electroweak interactions, the most breakthrough observations were: neutral current discovery [9], Z and W boson discovery [10], $\gamma - Z$ interference, neutrino generation number [10], Higgs boson discovery [11], and many others.

The schema describing the Standard Model is presented in [Figure 1.1](#).

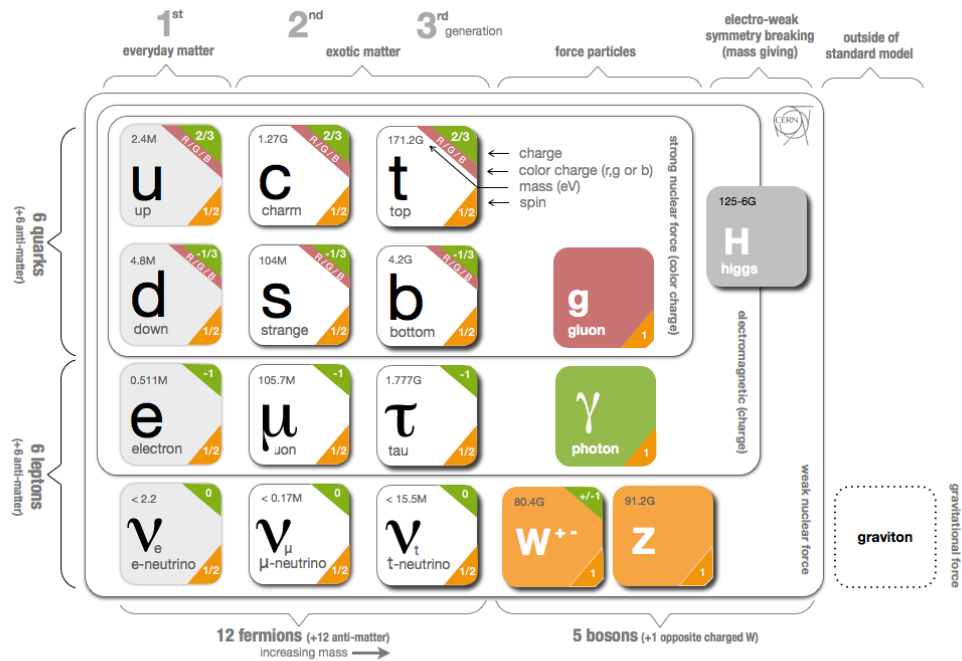


Figure 1.1: A schematic view of the Standard Model (SM) of particle physics.

In general, the SM is based on the YangMills theory with local $SU(3) \times SU(2) \times U(1)$ gauge symmetry. It could be divided into several parts:

- Quantum chromodynamics sector
- Electroweak sector
- Higgs sector
- Yukawa sector

In the context of the current thesis, we will discuss in detail the electroweak sector. It is based on the group $U(1) \times SU(2)_L$. It means that we will have two sets of generators: the weak hypercharge Y_W for $U(1)$ and Pauli matrices for $SU(2)_L$. Index L means that it affects only left-chiral fermions.

Helicity, polarity, chirality

Helicity is a projection of the spin onto the direction of the momentum.

$$h = \frac{\vec{s} \cdot \vec{p}}{|\vec{s}| |\vec{p}|} \quad (1.5)$$

The helicity could be “left” or “right” that corresponds to the spin direction opposite or co-directed with momentum. For the massless particles, helicity is Lorentz invariant. The polarization of the particle beam is a percentage of the particles with a given helicity. For example, 50% polarization means that half of the particles are “left” and half are “right”.

The chirality is a more fundamental characteristic comparing to helicity. It is determined by whether the particle wave function transforms with a right- or left-handed representation of the Poincare group.

Massless fermions keep chiral symmetry, i.e. independent rotation of the left- and right-handed components doesn't affect the theory. For them, the helicity is always the same as chirality.

The massive particles break the chiral symmetry explicitly. Also for the massive fermions, the helicity is not equivalent to the chirality as one could choose the reference frame moving faster than the particle and inverse the helicity.

In the SM fermions are described as doublets (subsection 1.2). For each charged lepton there is an appropriate neutrino. While charged lepton could be either right-handed or left-handed, the neutrino could be only left-handed. This part of the theory is based on the empirical observations [12] and this is strictly fixed in the model. Neutrino could interact with the charge current (CC) or neutral current (NC). The appropriate interaction terms are defined as:

$$\begin{aligned} -\mathcal{L}_{CC} &= \frac{g}{2} \sum_{\alpha} \bar{\nu}_{L\alpha} \gamma^{\mu} \ell_{L\alpha} W_{\mu}^{+} + h.c. \\ -\mathcal{L}_{NC} &= \frac{g}{\sqrt{2 \cos \theta_W}} \sum_{\alpha} \bar{\nu}_{L\alpha} \gamma^{\mu} \nu_{L\alpha} Z_{\mu}^0 \end{aligned} \quad (1.6)$$

Thus there is no chance for production or detection of the right-handed neutrino (left-handed anti-neutrino). The existence of such “exotic” particles is proposed in the various theories (subsection 1.4).



a Number of neutrino flavors

After the magnificent confirmation of the Standard Model with the discovery of the neutral current and W and Z bosons, it became possible to measure precisely the number of the neutrino generations. This analysis became possible with the massive production of the Z-bosons on the so-called Z-factory such as Large Electron-Positron Collider (LEP) at CERN.

The general idea of the study is to look at the different modes of the Z decays. All the decays could be classified into several groups:

$$\begin{aligned} Z &\rightarrow q\bar{q} \\ Z &\rightarrow \ell^{+}\ell^{-} \\ Z &\rightarrow \nu\bar{\nu} \end{aligned} \quad (1.7)$$

110 The total width of the boson decay sums up from these three parts. As for the width of $Z \rightarrow$
 111 $\ell^+ \ell^-$ is the same of all charged leptons and $Z \rightarrow \nu \bar{\nu}$ is the same for all neutrino types because of
 112 the lepton uniformity they could be multiplied by an appropriate number:

$$\Gamma_Z = \Gamma(Z \rightarrow \text{hadrons}) + N_\ell \times \Gamma(Z \rightarrow \ell^+ \ell^-) + N_\nu \times \Gamma(Z \rightarrow \nu \bar{\nu}) \quad (1.8)$$

113 During the experiment, the Γ_Z , $\Gamma(Z \rightarrow q\bar{q})$ and $\Gamma(Z \rightarrow \ell^+ \ell^-)$ were measured. The equality of
 114 the $\Gamma(Z \rightarrow e^+ e^-)$ and $\Gamma(Z \rightarrow \mu^+ \mu^-)$ was checked. The width of the decay into neutrinos came from
 115 the theory. The number of the neutrino generations remained the only unknown variable in the
 116 [Equation 1.8](#). The results of the precise measurements of the Z-boson resonance and predictions
 117 for 2, 3 and 4 neutrino generations are shown in [Figure 1.2](#). During the research at LEP, the number
 118 of neutrino generations was measured as $N_\nu = 2.9840 \pm 0.0082$. So we could conclude that in Stan-
 119 dard Model there are only three types of the left-handed neutrino with masses less than Z-boson
 120 mass.

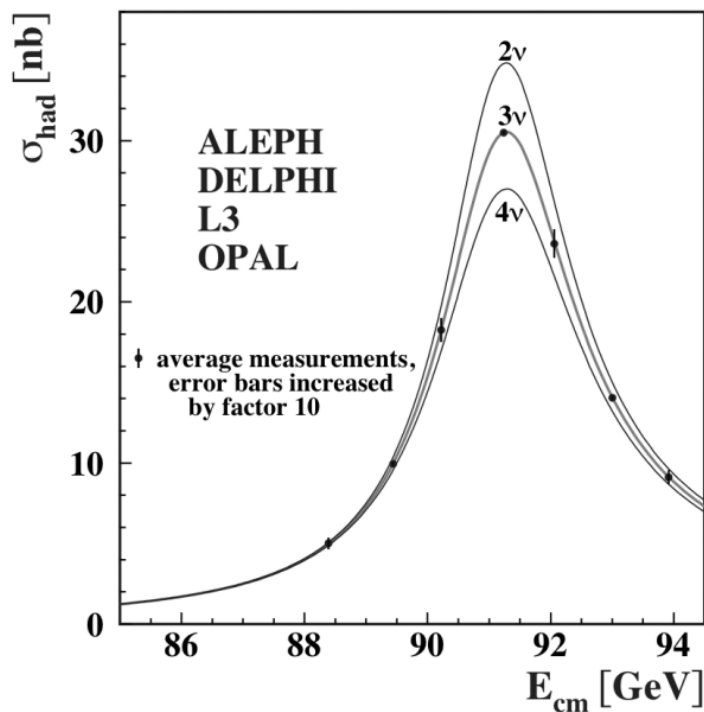


Figure 1.2: Measurement of the hadron production cross-section as a function of the LEP center-of-mass energy around the Z-boson resonance.

121

122

1.4 Neutrino interactions

123 The precise measurements in neutrino physics such as neutrino oscillation and search for CP-
 125 violation require accurate knowledge about the neutrino interactions' rates. This is still one of the
 126 dominating uncertainties in the neutrino oscillation experiments. Roughly we could divide the
 127 neutrino interactions with the matter on the interactions with electron and nucleus. The neutrino
 128 interactions with the single fermion are described very accurately with the Standard Model. So far
 129 no deviations are found in the experiment.

130

a Interactions with electron

131

133 Neutrino interactions with the single electron are the simplest ones. They could be described
 134 with the tree-level Feynman diagrams presented in [Figure 1.3](#). Electron neutrino could interact
 135 with the electron both through the scattering through the charged current ([Figure 1.3 \(a\)](#)) and
 136 neutral current ([Figure 1.3 \(c\)](#)), while muon and tau neutrino could scatter only via neutral cur-
 137 rent. These processes play an important role in the discovery of the neutrino oscillation as will be
 138 described in the [subsection 2.2](#).

139 The muon neutrino could also scatter over the electron through the charged current ([Figure 1.3](#)
 140 (b)), but this is a threshold process. The minimal neutron energy could be estimated by $E_\nu^{th} =$
 141 $(m_\mu^2 - m_e^2) / (2m_e) = 10.9\text{GeV}$ neglecting the neutrino mass. Thus the muon could not be produced
 142 by the neutrino from the Sun or other low-energy neutrinos.

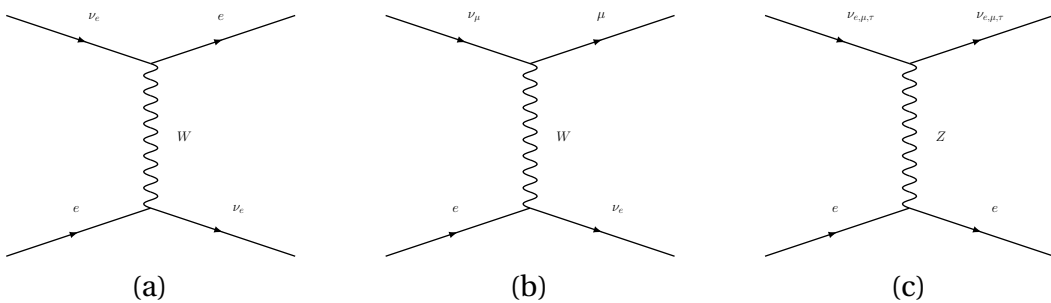


Figure 1.3: Tree-level Feynman diagrams of the neutrino interactions with electron: (a) and (b) electron and muon neutrino scattering through the charged current, (c) all-type neutrino scattering through the neutral current.

143 The anti-neutrino interaction with the electron could be described with the Feynman diagrams
 144 of the [Figure 1.4](#). Comparing with the neutrino, a muon anti-neutrino could not interact with the
 145 electron because of the charge conservation law.

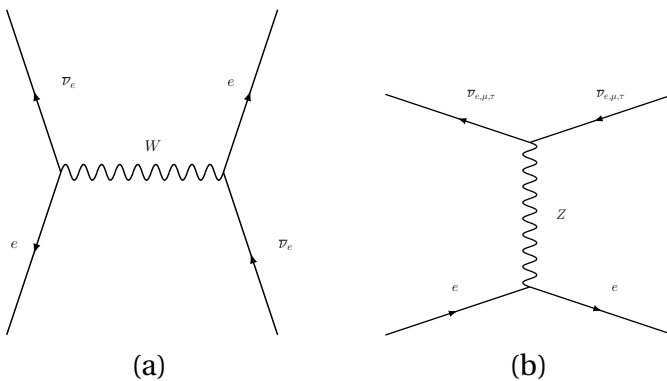


Figure 1.4: Tree-level Feynman diagrams of the anti-neutrino interactions with electron: (a) elec-
 tron anti-neutrino scattering through the charged current, (c) all-type anti-neutrino scattering
 through the neutral current.

146 The cross-sections for the processes mentioned above are presented on the [Figure 1.5](#).

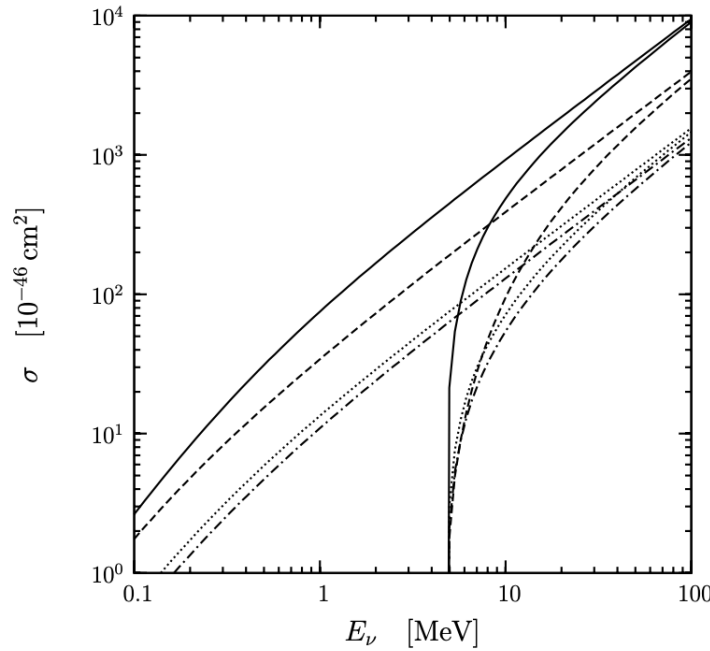


Figure 1.5: Neutrino-electron cross-sections as a functions of the neutrino energy E . Solid line: $\nu_e + e^- \rightarrow \nu_e + e^-$. Dashed line: $\bar{\nu}_e + e^- \rightarrow \bar{\nu}_e + e^-$. Dotted line: $\nu_{\mu,\tau} + e^- \rightarrow \nu_{\mu,\tau} + e^-$. Dash-dotted line: $\bar{\nu}_{\mu,\tau} + e^- \rightarrow \bar{\nu}_{\mu,\tau} + e^-$. For each scattering process the upper curve is the cross-section without a threshold for the kinetic energy of the recoil electron, whereas the lower curve is obtained with $T_e^{th} = 4.50 \text{ MeV}$, which corresponds to $E_\nu^{th} = 4.74 \text{ MeV}$. From [13]

147

b Interactions with nuclei

148

149

150 Neutrino interactions with a single fermion (e.g. quark) are very well described. But the atomic
 151 nuclei are complicated structures consists of plenty of particles that make the neutrino interaction
 152 description much more complicated. The reaction topology severely depends on the neutrino en-
 153 ergy. The following energy scales could be set:

- 154 ➤ $E_\nu < 0.1 \text{ GeV}$: neutrino interacts with the whole nucleus,
 155 ➤ $E_\nu \sim 0.1 - 20 \text{ GeV}$: neutrino interacts with one or few nucleons inside the nucleus,
 156 ➤ $E > \text{few GeV}$: neutrino interacts with the individual quarks

157 The energy scales above could be easily understood with De Broglie's wave approach. The in-
 158 coming neutrino wavelength should be compared with the target size.

159 From the experimental point of view, we could classify the neutrino interactions based on the
 160 outgoing particles. Thus we could divide all the reactions in the charged current and neutral cur-
 161 rent exchange. In the case of a charged current exchange, one will observe an outgoing charged
 162 lepton, while in case of neutral current exchange only hadrons and photons could be seen. Now
 163 we will define several topologies for the interactions via charged current. At the energies $\leq 1 \text{ GeV}$
 164 neutrino mostly interacts in the quasi-elastic way, transforming neutron into a proton. For the
 165 neutrinos with energies 1 GeV the most probable reaction is a Δ^{++} production with its further de-
 166 cay into proton and pion. Also at this energy region, we could see the coherent pion production,
 167 when a neutrino interacts with the whole nucleus or interactions with two nucleons simultane-

ously (2p2h interactions). With the energy growth, one will observe the dominance of the deep inelastic scattering with the various hadron production as a result of the broken nucleon. The Feynman diagrams for the processes mentioned above are shown in Figure 1.6.

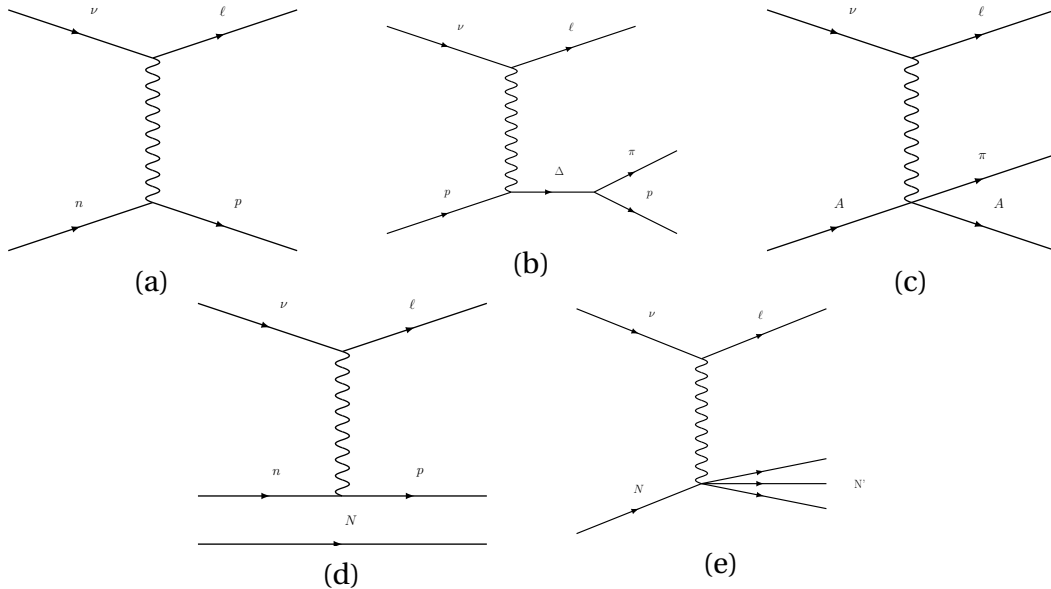


Figure 1.6: Feynman diagrams for the neutrino interactions with nucleus. The following reactions are shown: (a) quasi elastic scattering, (b) resonance pion production, (c) coherent pion production, (d) 2p2h, (e) deep inelastic scattering.

The evaluation of the neutrino and anti-neutrino cross sections with the energy is shown in Figure 1.7.

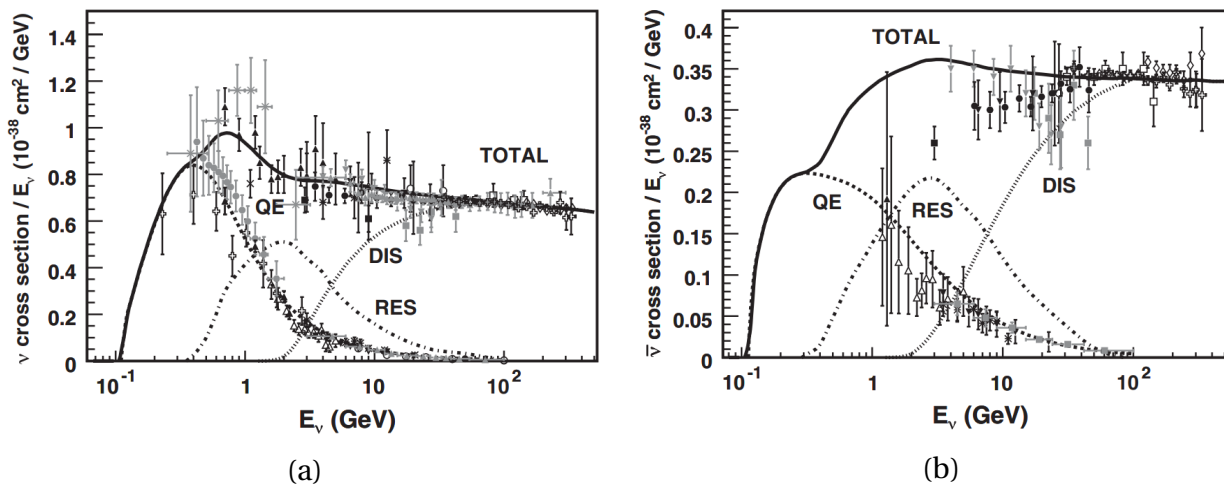


Figure 1.7: (a) neutrino and (b) anti-neutrino per nucleon CC cross sections from [14].

Discussing the neutrino interaction with nucleon it's worth mentioning the main problems of these reactions observation. Above we discussed mostly the interactions on the single nucleon. While in fact, it happens only for targets made from Hydrogen. In most of the experiments, the heavier targets are used to gain the number of neutrino interactions and detection accuracy. As a result, the neutrino interactions are affected by the following nuclear effects:

➤ Fermi motion. The nucleons are not at rest inside the nucleus. This effect is called Fermi motion. Several models could be used to parametrize this phenomenon, e.g. Relative Fermi

180 Gas (RFG) with the typical momentum depending on the nucleus. For example for Carbon
 181 $p_F \approx 220 \text{ MeV}/c^2$,

- 182 ➤ Final State Interactions (FSI). After the initial neutrino reaction, final state particles such
 183 as pions or nuclei could interact while propagating inside the nucleus. For example, pion
 184 could be absorbed, or additional hadrons could be produced. All these processes distort the
 185 neutrino reaction outcomes.
- 186 ➤ collective effects. The neutrino could interact with several nucleons at the same time. The
 187 most common case is the interaction with 2 particles – 2p2h. As the models of nucleons
 188 interactions are not precise enough this effect introduces relatively large uncertainty in the
 189 analysis.

190 The detailed description of the neutrino-nuclei interactions could be found in [14].

2 Neutrino oscillations

193 The neutrino oscillation phenomenon research is a very long story started from the phenomeno-
 194 logical prediction, followed by the puzzle of the small neutrino flux from the Sun, and reached a
 195 milestone recently with the robust confirmation of the effect. Many interesting discoveries were
 196 made in this way, e.g. non-zero neutrino mass, large mixing angles, hints for the CP-violation;
 197 many different ways to produce and study neutrinos were found. But many discoveries are still
 198 awaiting. In this section, the modern understanding of the phenomenon will be presented as well
 199 as the latest experimental results.

2.1 Theory

203 Soon after neutrino discovery, the experimental confirmation that neutrino and anti-neutrino
 204 interact differently came. Inspired by the observed oscillations of neutral kaons $K^0 \rightarrow \bar{K}^0$ Pon-
 205 tecorvo proposed the oscillations $\nu \rightarrow \bar{\nu}$ [15]. For such process neutrino should have small but
 206 non-zero mass. At that time the experimental confirmation of such a hypothesis was very chal-
 207 lenging as it could not be measured in the laboratory but with cosmological observations only.

208 The discovery of the muon neutrino provoked a different hypothesis of the neutrino flavor
 209 oscillations $\nu_e \rightarrow \nu_\mu$. Maki, Nagoya and Sakata proposed the theory of the 2-flavor neutrino oscil-
 210 lations [16].

a Phenomenology

214 The phenomenology of the neutrino oscillation will be described below with the quantum me-
 215 chanics approach. The state could be described either with a flavor basis $|\nu_\alpha\rangle$ or with a mass basis
 216 $|\nu_k\rangle$. The relation between them is defined with the mixing matrix $U_{\alpha k}$.

$$|\nu_\alpha\rangle = \sum_k U_{\alpha k}^* |\nu_k\rangle \quad (1.9)$$

218 where $\alpha = e, \mu, \tau$ and $k = 1, 2, 3$. Thus the mixing between the flavor and the mass states of the
 219 leptons is allowed. We measure the flavor of both produced and interacted neutrino with the flavor
 220 of the accompanying charged lepton. But the propagation of the particle is defined by its mass.

221 Within the quantum mechanics approach the Schroedinger equation will describe the changes of
 222 the system with time.

$$i \frac{d}{dt} |\nu_k(t)\rangle = \mathcal{H} |\nu_k\rangle \quad (1.10)$$

223 where the Hamiltonian of the system is defined as

$$\mathcal{H} |\nu_k\rangle = E_k |\nu_k\rangle \quad (1.11)$$

224 The changes with time will be described with the operator of the evolution

$$|\nu_k(t)\rangle = e^{-iE_k t} |\nu_k\rangle \quad (1.12)$$

225 As was mentioned above the production and detection of the neutrino should be described in
 226 the flavor states. Modifying [Equation 1.12](#) with [Equation 1.9](#) we will get

$$|\nu_\alpha(t)\rangle = \sum_{\beta=e,\mu,\tau} \left(\sum_k U_{\alpha k}^* e^{-iE_k t} U_{\beta k} \right) |\nu_\beta\rangle \quad (1.13)$$

227 The oscillation probability is a square of the matrix element

$$\begin{aligned} P_{\nu_\alpha \rightarrow \nu_\beta} &= \left| A_{\nu_\alpha \rightarrow \nu_\beta}(t) \right|^2 = \left| \langle \nu_\beta | \nu_\alpha(t) \rangle \right|^2 \\ &= \sum_{k,j} U_{\alpha k}^* U_{\beta k} U_{\alpha j} U_{\beta j}^* e^{-i(E_k - E_j)t} \end{aligned} \quad (1.14)$$

Neutrino masses are expected to be extremely small $\leq 1 \text{ eV}$ while we want to describe the energy scale above a few keV. In this case, an ultra-relativistic approximation is applicable.

$$\begin{aligned} E_k - E_j &\approx \frac{\Delta m_{kj}^2}{2E} \\ \Delta m_{kj}^2 &\equiv m_k^2 - m_j^2 \end{aligned} \quad (1.15)$$

228 Thus the oscillation probability versus the travel distance and neutrino energy will be defined as

$$P_{\nu_\alpha \rightarrow \nu_\beta}(L, E) = \sum_{k,j} U_{\alpha k}^* U_{\beta k} U_{\alpha j} U_{\beta j}^* \exp\left(-i \frac{\Delta m_{kj}^2 L}{2E}\right) \quad (1.16)$$

229 The neutrino oscillations could be classified into two major types:

- 230 ➤ “disappearance” — the phenomenon of observation less neutrino with the given flavor com-
 231 paring to the produced amount
- 232 ➤ “appearance” — the phenomenon of the observation of neutrino flavor which was not ini-
 233 tially produced, e.g. ν_e , while only ν_μ was produced

There is a common practice to split the real and imaginary part of the oscillation probability as they will demonstrate different behavior. For example, the real part is CP conservative, while the imaginary part violates CP symmetry. The “appearance” probability will be calculated with

$$\begin{aligned} P_{\nu_\alpha \rightarrow \nu_\beta}(L, E) &= \delta_{\alpha\beta} - 4 \sum_{k>j} \Re \left[U_{\alpha k}^* U_{\beta k} U_{\alpha j} U_{\beta j}^* \right] \sin^2 \left(\frac{\Delta m_{kj}^2 L}{4E} \right) \\ &\quad + 2 \sum_{k>j} \Im \left[U_{\alpha k}^* U_{\beta k} U_{\alpha j} U_{\beta j}^* \right] \sin \left(\frac{\Delta m_{kj}^2 L}{2E} \right) \end{aligned} \quad (1.17)$$

234 In its turn the “disappearance” phenomenon will be described by

$$P_{\nu_\alpha \rightarrow \nu_\alpha}(L, E) = 1 - 4 \sum_{k>j} |U_{\alpha k}|^2 |U_{\alpha j}|^2 \sin^2 \left(\frac{\Delta m_{kj}^2 L}{4E} \right) \quad (1.18)$$

Mixing matrix unitarity

In this section we assumed the unitarity of the mixing matrix

$$U^\dagger U = 1 \iff \sum_{\alpha} U_{\alpha k}^* U_{\alpha j} = \delta_{jk} \quad (1.19)$$

This assumption came from the fundamental laws of QFT. And it indeed should be true for mixing matrix of any dimension. As will be described in [chapter 2](#) the model with 3x3 mixing matrix is not essential for the explanation of the neutrino mass. Thus due to the existence of other neutrino states the mixing matrix of 3 left-handed neutrino is not unitary.

$$\sum_{\alpha=e,\mu,\tau} U_{\alpha k}^* U_{\alpha j} \neq \delta_{jk} \quad (1.20)$$

Though at the moment there is no experimental confirmation of such effect as it's expected to be much smaller than the sensitivity of the experiments.

235

b Mixing matrix parametrization

236

237

238 In this subsection, we will describe the most common parametrization of the 3-flavor neutrino
239 mixing matrix. This matrix was named Pontecorvo-Maki-Nagava-Sakata in order of the pioneers
240 of the oscillation theory. In the common representation, the matrix consists of 9 elements

$$\begin{pmatrix} \nu_e \\ \nu_\mu \\ \nu_\tau \end{pmatrix} = \begin{pmatrix} U_{e1} & U_{e2} & U_{e3} \\ U_{\mu 1} & U_{\mu 2} & U_{\mu 3} \\ U_{\tau 1} & U_{\tau 2} & U_{\tau 3} \end{pmatrix} \begin{pmatrix} \nu_1 \\ \nu_2 \\ \nu_3 \end{pmatrix} \quad (1.21)$$

241 for easier parametrization it's usually written as a multiplication of four matrices

$$U = \begin{pmatrix} 1 & 0 & 0 \\ 0 & \cos\theta_{23} & \sin\theta_{23} \\ 0 & -\sin\theta_{23} & \cos\theta_{23} \end{pmatrix} \times \begin{pmatrix} \cos\theta_{13} & 0 & \sin\theta_{13}e^{-i\delta} \\ 0 & 1 & 0 \\ -\sin\theta_{13}e^{+i\delta} & 0 & \cos\theta_{13} \end{pmatrix} \times \\ \times \begin{pmatrix} \cos\theta_{12} & \sin\theta_{12} & 0 \\ -\sin\theta_{12} & \cos\theta_{12} & 0 \\ 0 & 0 & 1 \end{pmatrix} \times \begin{pmatrix} \exp \frac{i\alpha_1}{2} & 0 & 0 \\ 0 & \exp \frac{i\alpha_2}{2} & 0 \\ 0 & 0 & 1 \end{pmatrix} \quad (1.22)$$

242 Such parametrization is done with three mixing angles: $\theta_{12}, \theta_{13}, \theta_{23}$ and three CP-violating
243 phases: δ and α_1, α_2 . Mixing angles define the transition from the mass state basis to the flavor
244 state basis. The clear schema of such rotation is shown in [Figure 1.8](#).

245 Rewriting equations [Equation 1.17](#) and [Equation 1.18](#) with the new parametrization for the ν_e
246 and ν_μ will result

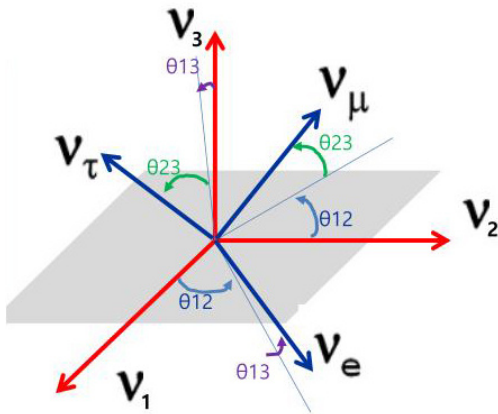


Figure 1.8: Reference rotation of the flavor basis versus the mass basis. The corresponding mixing angles are shown.

$$\begin{aligned}
 P_{\nu_\mu \rightarrow \nu_\mu} = & 1 - \sin^2 2\theta_{23} \sin^2 \frac{\Delta m_{13}^2 L}{4E_\nu} \\
 & + \left(\frac{1}{2} \cos^2 \theta_{12} \sin^2 2\theta_{23} - \sin \theta_{13} \sin^2 \theta_{23} \sin 2\theta_{23} \sin 2\theta_{12} \cos \delta \right) \times \\
 & \times \sin \frac{\Delta m_{12}^2 L}{4E_\nu} \sin \frac{\Delta m_{13}^2 L}{4E_\nu}
 \end{aligned} \quad (1.23)$$

247

$$\begin{aligned}
 P_{\nu_\mu \rightarrow \nu_e} = & \sin^2 \theta_{23} \sin^2 2\theta_{13} \sin^2 \frac{\Delta m_{13}^2 L}{4E_\nu} + \frac{1}{2} \sin 2\theta_{23} \sin 2\theta_{12} \cos^2 \theta_{13} \sin \frac{\Delta m_{12}^2 L}{2E_\nu} \times \\
 & \times \sin \frac{\Delta m_{13}^2 L}{2E_\nu} \cos \delta - \sin 2\theta_{23} \sin 2\theta_{13} \cos^2 \theta_{13} \sin \theta_{13} \times \frac{\Delta m_{12}^2 L}{2E_\nu} \sin^2 \frac{\Delta m_{13}^2 L}{4E_\nu} \sin \delta
 \end{aligned} \quad (1.24)$$

248 The visualization of the formulas above is provided in [Figure 1.9](#). The oscillation curves for
249 each initial state (e, μ, τ) and two L/E are shown. From such a plot, it's much easier to understand
250 the meaning of the oscillation parameters. The mixing angles define oscillation amplitude and the
251 mass difference defines frequency.

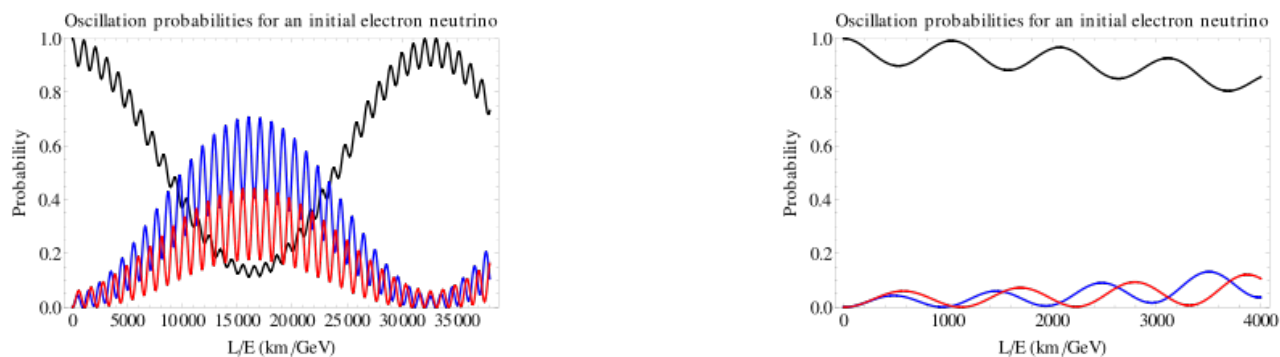


Figure 1.9: Oscillation probabilities for the initial electron neutrino state for two different L/E scales. The black line corresponds to the electron neutrino component, blue line for muon neutrino and red line for tau neutrino.

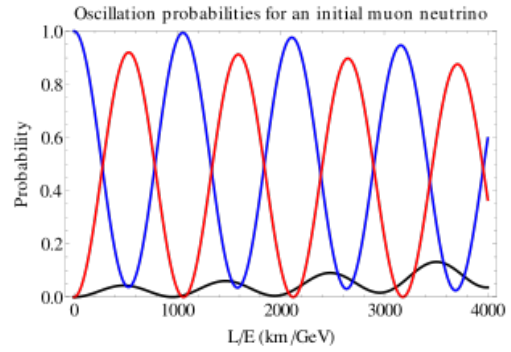
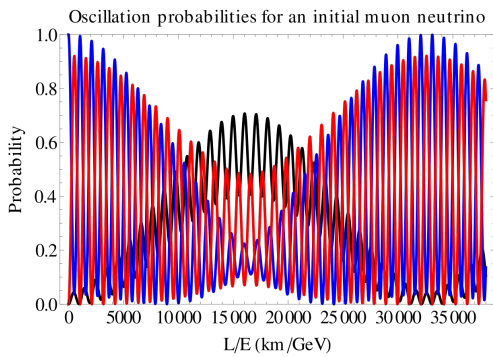


Figure 1.10: Oscillation probabilities for the initial muon neutrino state for two different L/E scales. The black line corresponds to the electron neutrino component, blue line for muon neutrino and red line for tau neutrino.

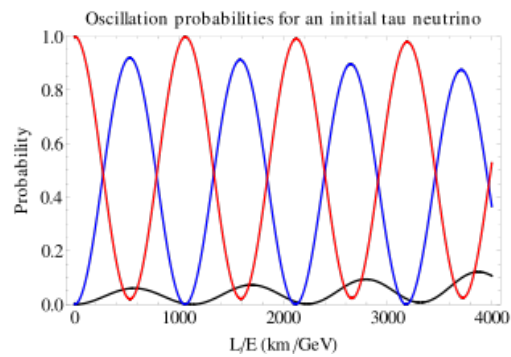
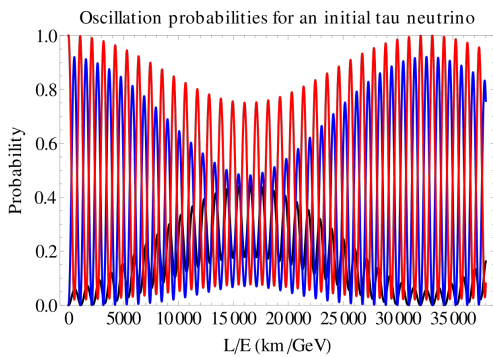


Figure 1.11: Oscillation probabilities for the initial tau neutrino state for two different L/E scales. The black line corresponds to the electron neutrino component, blue line for muon neutrino and red line for tau neutrino.

252

253

254

255 The phenomenon of the CP-violation in the neutrino oscillation is worth emphasizing. In the
 256 Universe the dominance of matter over the anti-matter was observed. The modern cosmology
 257 facing the problem of explanation of such a phenomenon. The fundamental conditions for the
 258 matter-dominance generation were developed by Sakharov [17]. One of the key conditions is the
 259 CP-violation. This phenomenon was observed in the quark sector [18]. But the precise measure-
 260 ments show that the amplitude of the CP-violation is not sufficient enough to generate the ob-
 261 served asymmetry in the Universe.

262 Plenty of hypotheses propose the generation of the matter dominance through the lepton sec-
 263 tor [19]. The non-zero CP-violation phase (Equation 1.22) is essential for such an effect. From the
 264 Equation 1.23 and Equation 1.24 we could clearly see that the CP-violating phase could be mea-
 265 sured only in the appearance channel and the total effect is scaled by the value of the mixing an-
 266 gle θ_{13} . According to the latest measurements, the value of the mixing angle is relatively large (in
 267 normal mass order assumption $\theta_{13} = 8.45^{+0.16}_{-0.14}$ [20]) that allows the direct search for the leptonic
 268 CP-violation in the experiment.

269 The latest results of the CP-violation in the neutrino oscillations will be presented in sub-
 270 section 2.2. It's important to note that the CP-violation is not essential to generate the matter-
 271 dominance in the early Universe. The existence of heavy neutrinos (subsection 1.4) is also neces-
 272 sary.

c CP violation in the neutrino oscillations

Symmetries: C, P, T

In particle physics there are three important symmetries: charge (C), parity (P) and time (T).

Parity inversion (P) flip the sign of the spatial coordinate $\mathcal{P}\vec{r} = -\vec{r}$. In the QFT it's described as $\mathcal{P}|\psi\rangle = c|\psi\rangle$. Where c is the eigenvalue of \mathcal{P} . The parity violation means a process that changes the eigenvalue of the parity transformation for some system. The theory of such a process was developed by Lee and Yang [21] and found in the Wu's experiment [22]. The asymmetry of the outgoing electrons from the Cobalt with respect to the nucleus polarization was the nice and clear proof for the effect.

Charge symmetry (C) transform particle to its anti-particle. $\mathcal{C}|\psi\rangle = \eta_C|\bar{\psi}\rangle$, where η_C is the eigenvalue of the transformation. The example of the eigenvalue non-conservation experimental observation could be found in [23].

Time transformation (T) inverse the time direction. After the discovery of the separate P and C violations, the combined symmetry breaking became the puzzle.

As it will be a hint towards T-symmetry breaking. The CP-violation was observed in the neutral kaons oscillations process [24]. Later such a process was confirmed with the direct measurements of kaon decays [25] and [26], B-meson decays [27] and [28], D-mesons [29].

Together they form a CPT symmetry. It's proved that any Lorentz invariant local quantum field theory with a hermitian Hamiltonian must be invariant under CPT.

273

d 2-flavor oscillations

274

275

276 In the previous section, the modern framework of the neutrino oscillations was described. His-
 277 torically the neutrino mixing theory was developed for 2 flavors. While 3-flavor oscillation proba-
 278 bility equations are quite complicated, a 2-flavor approximation often provides sufficient accuracy
 279 and suitable for the many experiments. In this approach, the mixing matrix transforms to a usual
 280 2×2 rotation matrix

$$U = \begin{pmatrix} \cos\theta & \sin\theta \\ -\sin\theta & \cos\theta \end{pmatrix} \quad (1.25)$$

281 and the oscillation probabilities will be written as

$$P_{\nu_\alpha \rightarrow \nu_\alpha} = 1 - \sin^2 2\theta \sin^2 \frac{1.27\Delta m^2 L}{E_\nu} \quad (1.26)$$

$$P_{\nu_\alpha \rightarrow \nu_\beta} = \sin^2 2\theta \sin^2 \frac{1.27\Delta m^2 L}{E_\nu} \quad (1.27)$$

282 in this notation the neutron energy unit is supposed to be GeV, the distance unit is km and the
 283 mass difference unit is eV^2/c^2 .

284

e Oscillation in matter

285

286

287 The framework presented above describes the oscillations in the vacuum. In the case of neu-
 288 trino propagation in matter, the effect will be different. Going through medium neutrino suffers
 289 from the forward elastic scattering with electrons and nucleons. This effect is similar to the phe-
 290 nomenon of light propagation in the matter. The new potential which is equivalent to the refrac-
 291 tion index needs to be taken into account. But the interaction types are slightly different for dif-
 292 ferent neutrinos. All neutrino types may scatter over electrons, protons and neutrons through the

neutral current exchange. In addition, electron neutrino scatters over the electrons with the charge current. The framework of the neutrino oscillations in matter was developed by Wolfenstein [30]. The mixing angle and the mass difference should be replaced by the effective ones, depending on the matter density.

The propagation of the neutrino in matter could be described with a Hamiltonian function that will be a sum of the neutrino energy and the potential of the neutrino interactions with electron.

$$H_{i,j} = \left(E_\nu + \frac{m_i^2}{2E_\nu} \right) \delta_{i,j} + U_{ei}^* U_{ej} \sqrt{2} G_F n_e \quad (1.28)$$

where U is a neutrino mixing matrix, G_F is a Fermi constant and n_e is electron density in matter. For the simplification I will estimate the changing of the oscillation parameters in the 2-flavor framework in the matter with a constant density. In vacuum the mixing angle and the mass difference are defined with θ and Δm . The new effective values in matter could be computed with:

$$\sin^2 2\theta_M = \frac{\sin^2 2\theta}{\cos^2 2\theta (1 - \lambda)^2 + \sin^2 2\theta} \quad (1.29)$$

$$\Delta m_M^2 = \Delta m^2 \frac{\sin 2\theta}{\sin 2\theta_M} \quad (1.30)$$

$$\lambda = \frac{2\sqrt{2}G_F E_\nu n_e}{\Delta m^2 \cos 2\theta} \quad (1.31)$$

In case of slightly changing density of the matter there is a region where the mixing angle reaches its maximum possible value $\pi/4$ [31]. This phenomenon is called MikheyevSmirnovWolfenstein (MSW) effect.

It's interesting to notice that non-zero mass difference is not necessary for the neutrino oscillations in matter. The flavor change is observable even in the case of $\Delta m = 0$ only because of the non-zero mixing angles [32].

f Modern neutrino oscillation understanding

In spite of the clear explanation of the neutrino oscillation phenomenon within the quantum mechanics framework (section 2), this method suffers from incompleteness. For instance, the assumption of the same momentum (or the same energy) of the different eigenstates is quite strong but fully empirical. Also, the normalization of the transition amplitude is not properly justified.

Another approach could solve some of the problems above. In the case of the neutrino description only as a propagator between production and detection point (QFT framework) the normalization and all the conservation laws will come out of the box without manual tuning [33].

Another interesting notice refers to the charged lepton oscillation problem. For instance, mixing in the quark sector involves all the 9 quarks, while the oscillations in the lepton sector are usually notated as "neutrino oscillations" affecting only 3 uncharged leptons. In fact Pontecorvo-Maki-Nagoya-Sakata matrix affects also charged leptons. But the coherence will be imminently ruined when the macroscopic sizes of source and detector are taken into account [34].

2.2 Experiment overview

The neutrino oscillation story starts from the Raymond Davis experiment in the Homestake mine (USA) [35]. The idea of the experiment was to measure the neutrino flux from the Sun core using the 400 m^3 barrel with C_2Cl_4 . The inverse beta-decay was used to detect the neutrinos $\nu_e +$

326 $^{37}\text{Cl} \rightarrow ^{37}\text{Ar} + e^+$. After every 70 days of the exposition the radioactive ^{37}Ar isotopes were blown
 327 up from the reservoir, and their decays were counted. The total neutrino flux was estimated as one
 328 third of the expectations. The observation was confirmed later with the following experiments:
 329 GALLEX [36], SAGE [37], Kamiokande [38]. Thus it was two possible results interpretation:

- 330 ➤ The Standard Solar Model (SSM) is incorrect and the number of the produced neutrino is
 331 different from expectations
- 332 ➤ Neutrinos are oscillating (changing flavor) on the way from the production to detection.
 333 Since only electron neutrino was used for the observations the possible transformation of
 334 the electron neutrino to muon and tau neutrino could explain the anomaly
- 335 ➤ All the experiments had the same uncounted systematic error

336 The third option is very disfavorable as the different targets ad different analysis methods were
 337 used. The decision between the first and second options could be done with the detection of all
 338 kinds of neutrinos from the Sun. Such an experiment, called SNO, was performed in the Sudbury
 339 mine. The heavy water D_2O was used as a neutrino target. The benefits of usage of the deuterium
 340 are the possibility to measure both the electron neutrino flux through the charge current (CC)
 341 interactions and the total neutrino flux through the neutral current (NC) interactions. Also, the
 342 electron neutrino flux estimations could be cross-checked with the measurements of the electron
 343 neutrino elastic scattering over electrons through both CC and NC.

$$\nu_e + d \rightarrow p + p + e^+ \quad (1.32)$$

$$\nu_\alpha + d \rightarrow p + n + \nu_\alpha \quad \alpha = e, \mu, \tau \quad (1.33)$$

$$\nu_e + e^- \rightarrow \nu_e + e^+ \quad (1.34)$$

344 Thus it could be found out is it a deficit of all kinds of neutrinos or only electron ones. It was
 345 proved that the total neutrino flux is in a perfect agreement with SSM, but the electron neutrino
 346 flux is lower than expected [39]. The Super-Kamiokande confirmed the SNO result with measure-
 347 ments of both solar and atmospheric neutrinos [40]. The discovery of the atmospheric neutrino
 348 oscillations was a breakthrough since the solar neutrino oscillation points only to the non-zero
 349 mixing angles, while the atmospheric ones point to the non-zero mass-difference between neu-
 350 trino eigenstates (subsubsection 2.1.e). Thus the neutrino mass was discovered.

351 But even after such brilliant confirmations of the phenomena the prove of the effect with the
 352 well-known source was essential. Such confirmation came with the measurements of the reactor
 353 antineutrinos with the KamLAND experiment [41]. It was the final confirmation of the neutrino
 354 oscillation phenomena.

a Modern experimental results

357 After the discovery of the neutrino oscillations, many experiments study the phenomenon with
 358 different techniques.

- 360 ➤ Solar neutrinos: experiments Borexino, Super-Kamiokande. These experiments are powerful
 361 in θ_{12} could also measure Δm_{21}^2 and θ_{13}
- 362 ➤ Reactor experiments: KamLand [41], RENO [42], Double Chooz [43], Daya Bay [44]. These
 363 experiments study the electron anti-neutrino disappearance and are very sensitive to the
 364 θ_{13} and could measure θ_{12} , Δm_{21}^2 , Δm_{32}^2

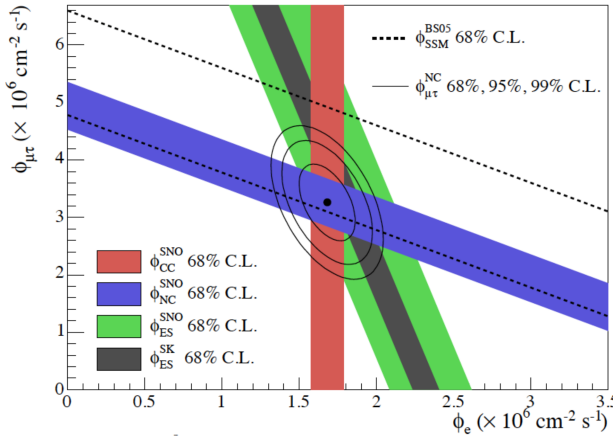


Figure 1.12: The comparison of the fluxes ν_e and $\nu_{\mu,\tau}$ based on the measurements by SNO and Super-Kamiokande.

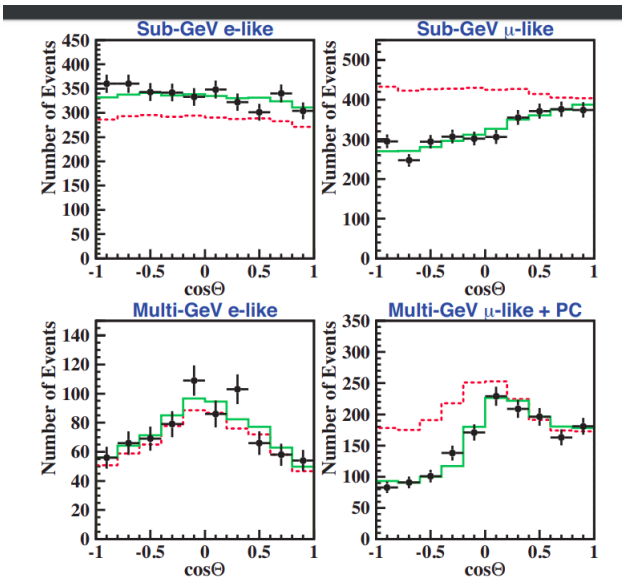


Figure 1.13: The angular distribution of the muon and electron events in the Super-Kamiokande. The dotted histograms represented the simulation results w/o the neutrino oscillations and solid histograms corresponds to the best fit with oscillation hypothesis.

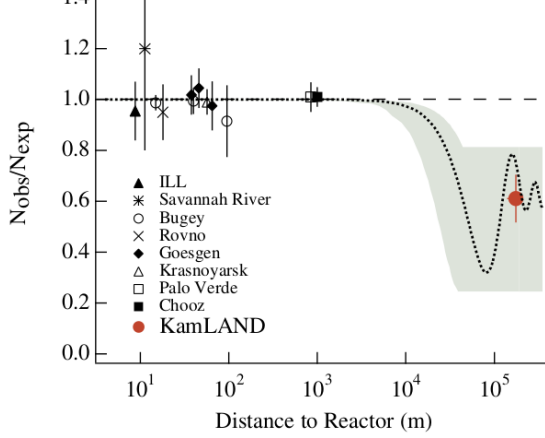


Figure 1.14: The ratio of the observed and expected neutrino flux from reactors. Figure from [41].

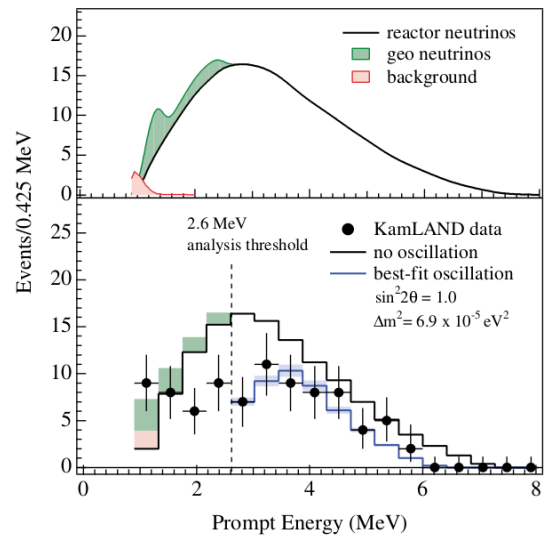


Figure 1.15: The energy spectrum of the neutrinos observed in the KamLAND experiment comparing to the expectations w/o neutrino oscillations. Figure from [41].

365 ➤ Accelerator experiments: K2K [45], MINOS [46], T2K [47], NOvA [48]. These experiments
 366 started with studying muon (anti-)neutrino disappearance and MINOS, T2K and NOvA man-
 367 aged to observe the electron neutrino appearance, OPERA observed the tau neutrino ap-
 368 pearance. Thus these experiments are very precise in measurements of the θ_{23} and sensitive
 369 to the CP-violation. They could also measure θ_{13} and δm_{32}

370 ➤ Atmospheric and cosmology neutrinos: Super-Kamiokande [49], IceCube. They could probe
 371 the interesting processes in cosmology and also measure θ_{23} , θ_{13} , Δm_{32} and δ_{CP}

372 So far the neutrino oscillation parameters are measured very precisely ([Table 1.1](#)), but there is
 373 still room for the improvements.

param	Normal Order		Inverse Order	
	best fit value	3σ range	best fit value	3σ range
$\frac{\sin^2 \theta_{12}}{10^{-1}}$	3.20	2.73→3.79	3.20	2.73→3.79
$\theta_{12}/^\circ$	34.5	31.5→38.0	34.5	31.5→38.0
$\frac{\sin^2 \theta_{23}}{10^{-1}}$	5.47	4.45→5.99	5.51	4.53→5.98
$\theta_{23}/^\circ$	47.7	41.8→50.7	47.9	42.3→50.7
$\frac{\sin^2 \theta_{13}}{10^{-2}}$	2.160	1.96→2.41	2.220	1.99→2.44
$\theta_{13}/^\circ$	8.45	8.0→8.9	8.53	8.1→9.0
$\delta_{CP}/^\circ$	218	157→349	281	202→349
$\frac{\delta m_{21}^2}{10^{-5} eV^2}$	7.55	7.05→8.24	7.55	7.05→8.24
$\frac{\delta m_{32}^2}{10^{-3} eV^2}$	2.42	2.334→8.24	-2.50	-2.59→-2.39

Table 1.1: Summary of the neutrino oscillation parameters measurements from [18] for both normal and inverse neutrino mass order.

374 The visual representation of the neutrino oscillation parameters constraints is presented in [Fig-](#)
 375 [ure 1.16](#).

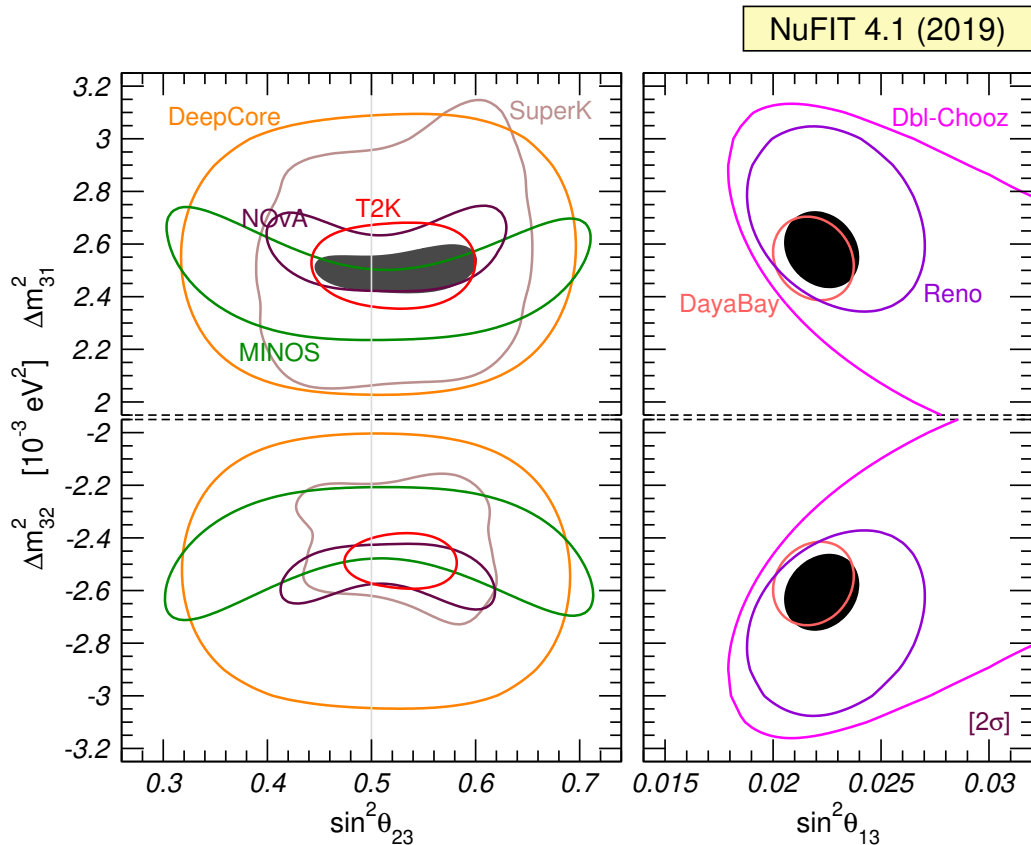


Figure 1.16: The global fit of the neutrino oscillation parameters and results from the particular experiments used in the fit. The upper figures corresponds to the normal mass order and lower figures for inverted mass order. The figure from [50].

376

377

NEUTRINO MASS

378 As presented in the [section 2 of chapter 1](#) during the exploration of the neutrino oscillation phe-
379 nomenon, the non-zero difference between neutrino eigenstates was observed. That leads to the
380 conclusion that at least two of the three eigenstates should be massive. While in the SM the neu-
381 trinos are massless ([subsection 1.3 of chapter 1](#)). The theory explaining the mass origin of the
382 neutrino is required.

383 The easiest solution is to try to implement the same process which gives mass to all other
384 particles in the SM — Higgs mechanism [51] (also called EnglertBroutHiggsGuralnikHagenKibble
385 mechanism for all contributed scientists). There are several problems in this way:

- 386 ➤ the scale of the neutrino mass is very different from the other particles in the SM. The neu-
387 trino masses are less than 1 eV [52], while the other particles masses are $\gtrsim 1$ MeV, which gives
388 us a difference of at least 6 orders. It could be even larger up to 8 orders in the case of min-
389 imum possible neutrino mass. It's hard to believe that the same mechanism is responsible
390 for the generation of mass at so different scales.
- 391 ➤ as described in the [subsection 1.3](#) only left-handed neutrinos and right-handed anti-neutrinos
392 were observed. While for the Higgs mechanism both left and right-handed particles are re-
393 quired.

394 That leads to the fact that we need to implement some new mechanisms or/and new funda-
395 mental particles to explain the origin of the neutrino masses.

396

1 Theory

397

398 In this section, the main models of neutrino mass generation will be overviewed. Dirac and Ma-
399 jorana mass terms will be presented as well as a “mixed” model of merging these two approaches
400 (a seesaw mechanism).

402

1.1 Dirac mass term

403

404 In the Standard Model of particle physics, the masses of all the particles are generated with the
406 Higgs mechanism. For example, the Higgs-lepton Yukawa Lagrangian provides a natural explana-

407 tion for the masses for the charged leptons

$$\mathcal{L}_{H,L} = - \sum_{\alpha,\beta=e,\mu,\tau} Y'_{\alpha\beta} \overline{L'_{\alpha L}} \Phi \ell'_{\beta R} + h.c. \quad (2.1)$$

Applying the same approach for the neutrino mass generation we will get the Lagrangian

$$\begin{aligned} \mathcal{L} &= - \sum_{\alpha\beta=e,\mu,\tau} \bar{\nu}_{L,\alpha} (m_D)_{\alpha\beta} \nu_{R,\beta} + h.c. = \\ &= - \overline{\nu_L} m_D \nu_R + h.c. \end{aligned} \quad (2.2)$$

408 where m_D is a 3x3 complex matrix. It could be diagonalized $m_D = U^\dagger m V$, where U and V are
409 unitary and $m_i \delta_{ik}$, $m_i > 0$. After diagonalization, we could separate

$$\begin{aligned} \nu_{\alpha L} &= \sum_i U_{\alpha i} \nu_{i L} \\ \nu_{\alpha R} &= \sum_i V_{\alpha i} \nu_{i R} \end{aligned} \quad (2.3)$$

410 and define $\nu \equiv \nu_L + \nu_R$. Thus the Dirac mass term will be expressed as

$$\mathcal{L}_{mass}^D = - \sum_i m_i \overline{\nu_i} \nu_i \quad (2.4)$$

411 where ν_i , $i = 1, 2, 3$ are neutrino mass eigenstates and $\nu_{\alpha L}$ are left-handed neutrino flavor eigen-
412 state. The transition between them is defined with PMNS matrix (Equation 1.9).

413

1.2 Majorana mass term

414

415 Neutrino could be described with the Majorana equation in the case $\psi = \psi^C$. This equation
416 gives a definition to the Majorana fermion - this is a particle invariant under C symmetry or the
417 particle that is equal to its anti-particle. Is it true in the case of the neutrino is still an open question.
418 To generate the mass for such a particle we need only one chiral fermion field. As neutrino is left-
419 handed let us notate it as ν_L . To write the mass term for this specific case we need to use ν_L alone.
420 Modifying Equation 2.4

$$\mathcal{L}_{mass}^D = -m \bar{\nu} \nu = -m (\overline{\nu_R} \nu_L + \overline{\nu_L} \nu_R) = -m \overline{\nu_R} \nu_L + h.c. \quad (2.5)$$

422 Here ν_R should be replaced with the right-handed function of the ν_L . in fact it's a charge con-
423 jugated field

$$\nu_L^C = \mathcal{C} \overline{\nu_L}^T \quad (2.6)$$

424 Thus the Majorana mass term could be expressed as

$$\mathcal{L}_{mass}^M = -\frac{1}{2} m \overline{\nu_L^C} \nu_L + h.c. \quad (2.7)$$

425 The Majorana mass term provides an interesting mechanism of the generation of the neutrino
426 mass. But it implements also physics beyond the SM. The lepton number is invariant in the SM
427 because of the U(1) symmetry. With the Majorana model it there is no such symmetry anymore.
428 This leads to the processes when the lepton number is violated, e.g. neutrino-less double beta
429 decay. Also, such theory contains a product of fields with energy dimensions five.

430

1.3 Mixing Dirac and Majorana terms

433 The most perspective approach is a combination the both Dirac and Majorana terms. In this
 434 case, the model is very flexible and could provide the natural explanation of the neutrino masses
 435 with minimum extensions over the Standard Model. The mass term will be written with

$$\mathcal{L}_{mass}^{D+M} = \mathcal{L}_{mass}^D + \mathcal{L}_{mass}^R + \mathcal{L}_{mass}^L \quad (2.8)$$

where

$$\mathcal{L}_{mass}^L = \frac{1}{2} \sum_{\alpha, \beta} \nu'_{\alpha L} C^\dagger M_{\alpha \beta}^L \nu'_{\beta L} + h.c. \quad (2.9)$$

$$\mathcal{L}_{mass}^R = \frac{1}{2} \sum_{s, s'} \nu_{s R}^T C^\dagger M_{s s'}^R \nu'_{s' R} + h.c. \quad (2.10)$$

$$\mathcal{L}_{mass}^D = - \sum_{s=s_1, \dots, s_{N_s}} \sum_{\alpha} \bar{\alpha} \nu_{s R} M_{s s'}^D \nu'_{\alpha L} + h.c. \quad (2.11)$$

436 In the equations above the Greek indexes, as usual, corresponds to the flavor states, L and R
 437 illustrate the chirality and s_i describes the sterile neutrino types. Thus matrix M^L will be symmetric
 438 3×3 , M^R — symmetric $N_s \times N_x$ and M^D — $N_s \times 3$. The mass matrix for some of these three
 439 components will be written with

$$M^{D+M} \equiv \begin{pmatrix} M^L & M^{D T} \\ M^D & M^R \end{pmatrix} \quad (2.12)$$

440 and the mass states will be presented with

$$\nu_R^C \equiv \begin{pmatrix} \nu_{s_1 R}^C \\ \vdots \\ \nu_{s_{N_s} R}^C \end{pmatrix} \quad N'_L \equiv \begin{pmatrix} \nu_L' \\ \nu_R' \end{pmatrix} \quad (2.13)$$

441 And the mass term [Equation 2.8](#) with new notations will be rewritten as

$$\mathcal{L}_{mass}^{D+M} = \frac{1}{2} N'^T C^\dagger M^{D+M} N'_L + h.c. \quad (2.14)$$

442 There are plenty of ways to combine Dirac and Majorana terms. With different initial assumptions,
 443 the theory result could be quite different. Here there are the main hypotheses. The notation
 444 below m_D describes the Dirac mass, m_L , m_R describe Majorana mass and the $m_{1,2}$ describes the
 445 mass eigenstates observable in the experiment.

- 446 ➤ Maximal mixing. $m_L = m_R$, $m_{2,1} = m_L \pm m_D$, $\Delta m^2 = m_2^2 - m_1^2 = 4m_L m_D$
- 447 ➤ Dirac limit. $m_L = m_R = 0$, $m_{2,1} = \pm m_D$
- 448 ➤ Pseudo-Dirac neutrinos. $|m_L|, m_R \ll m_D$, $m_{2,1} \approx \frac{m_L + m_R}{2} \pm m_D$
- 449 ➤ Seesaw mechanism. $m_D \ll m_R$, $m_L = 0$

450

a Seesaw mechanism

451

452

453 Among all of the theories with Dirac and Majorana mixing the seesaw mechanism seems to be
454 the most perspective. Here are the main advantages of this hypothesis:

- 455 ➤ The gauge symmetry is not broken as $m_L = 0$
- 456 ➤ The only “exotic” part (SM extension) is the implementation of m_R
- 457 ➤ The Dirac mass could be easily explained with the Higgs method as m_D is close to the mass
458 of the SM particles
- 459 ➤ Tiny mass of the observed neutrino eigenstates could be described with mixing

So, how could we explain the fact that observed neutrino mass is so small? m_D is generated with a Higgs mechanism and could be GeV scale. m_R is an exotic part of the theory. As it is a Majorana term it will violate the lepton number. But it will take place only at extremely high energies, much more than the electroweak scale. The observed neutrino mass will be given by the mixing:

$$m_1 \approx \frac{m_D^2}{m_R} \ll m_D \quad m_2 \approx m_R \gg m_D \quad (2.15)$$

460 and the mixing angle will be set as

$$\theta \approx \frac{m_D}{m_R} \ll 1 \quad (2.16)$$

461 For example, imagine the Dirac mass is fixed with $m_D = 170\text{GeV}$ and observed neutrino mass
462 $m_1 = 5 \times 10^{-2}\text{eV}$, then the Majorana mass will be at an extremely high energy scale $M_R \approx 10^{15}\text{GeV}$.
463

1.4 Heavy Neutral Lepton

464 In the previous section, it was proved that the extension of the SM is necessary to explain the
465 neutrino mass. The seesaw mechanism is a minimal extension that could provide such an expla-
466 nation. But there is no hint for the mass scale of the proposed new particles.

467 For example, the implementation of the 1 eV neutrino will mostly affect the neutrino oscilla-
468 tion probabilities. To meet the agreement with the LEP results of the Z boson decay measurements
469 ([subsubsection 1.3.a](#)) the 4th neutrino should not couple with the Z boson. That's why such a parti-
470 cle is notated as a “sterile” neutrino. Also, their mixing with the other three active neutrinos should
471 be quite small $|U_{e4}|, |U_{\mu 4}|, |U_{\tau 4}| \ll |U_{s4}|$ as in most of the neutrino oscillation experiments 3-
472 flavor neutrino model describes the observation pretty well. However, in some experiments, the
473 anomaly that could be explained with the 4th neutrino with $\Delta m_{41}^2 \approx 1\text{eV}$ was found. The first such an
474 experiment was LSND [53], that inspired the short-baseline neutrino oscillation research program.
475 Some anomalies have also been found in the experiments with neutrinos from reactors and with
476 solar neutrinos in the gallium experiments. Though there is no final statement is it a significant
477 observation or the result of the unaccounted systematic error. Plenty of experiments are running
478 now in order to figure out the nature of the phenomenon. We could generally divide them in the
479 short-baseline accelerator experiments: MicroBooNE, ARAPUCA, ICARUS and others and reactor
480 experiments: NEOS [54], DANSS [55], STEREO [56], PROSPECT [57], NEUTRINO-4 [58], SoLid, and
481 others.

482 More information about the light sterile neutrino could be found in [59]. The implementation
483 of the heavier neutrinos will be overviewed in the next section.

486

a Neutrino Minimal Standard Model (ν MSM)

487

The minimal extension of the SM introducing the neutrino mass explanation was developed by the Asaka and Shaposhnikov [60]. The existence of three heavy neutrinos N_1, N_2, N_3 was proposed. It's worth mentioning that there are plenty of extensions of the SM with different numbers of additional particles. ν MSM is highlighted because of this minimalism, which has always been an advantage of the physics theory.

Long living (comparing to the Universe's age) N_1 with a mass around keV could be responsible for the phenomenon of the Dark Matter. It could be produced in the early Universe and still exists. N_1 could explain the known middle-distance gravitational anomalies such as galaxies mass and galaxy rotation speed.

N_2 and N_3 are two nearly degenerated fermions with mass $140\text{MeV} < M < 80\text{GeV}$. The model contains 6 CP-violating phases that allow the violating of the lepton number L . Through the mixing with the active neutrino, such an asymmetry could be transferred to the active leptons. With the help of the sphaleron mechanism, the violation of the lepton number could cause the violation of the baryon number B , but conserving the $B - L$. Such a model could explain the observed baryon asymmetry of the Universe [61].

504

2 Experiments

505

Despite the Standard Model assumption about the neutrino massless nature, there were plenty of attempts to measure its mass. After the confirmation of the fact that neutrino has mass from the neutrino oscillation phenomenon (section 2), these measurements became essential.

510

2.1 Neutrino mass measurements

In this section, both direct and non-direct methods of the neutrino mass measurements will be overviewed. The latest experimental results will be presented.

515

a Beta decay

516

The straightforward way for the neutrino mass measurements is a search for the effect of the nonzero neutrino mass in the beta decay spectrum. One needs to measure the energy of outgoing electrons and look at the far end of the distribution. The variation of the neutrino mass changes dramatically the energy spectrum in this particular region. For the electron source, the deuterium or a tritium isotope is usually chosen. The main technological issues are to perform extremely precise measurements of the electron energy. The most accurate limits obtained with this method for a long time belonged to Mainz [62] and Troitsk [63] experiments. Recently KATRIN experiment announced more precise neutrino mass limits $m_\nu < 1.1\text{eV}$ with 90% C.L. [52].

It's important to notice what is a "neutrino mass" m_ν that is measured in the beta decay.

$$m_\nu \equiv m_\beta \equiv \sqrt{\sum_i |U_{ei}|^2 m_i^2} \quad (2.17)$$

527

More details about the neutrino mixing will be presented in section 2.

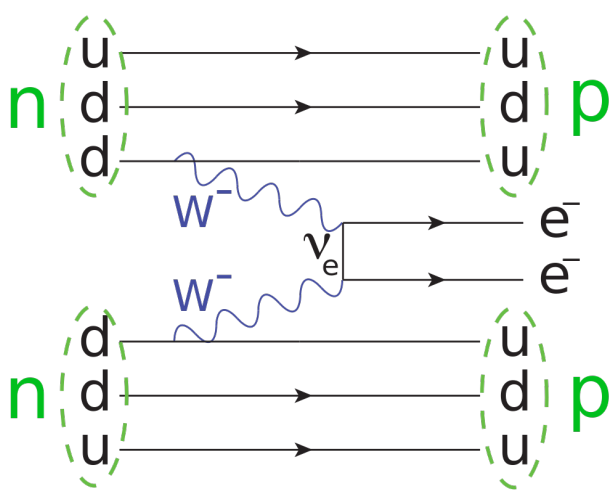


Figure 2.1: Feynman diagram for the neutrinoless double beta decay

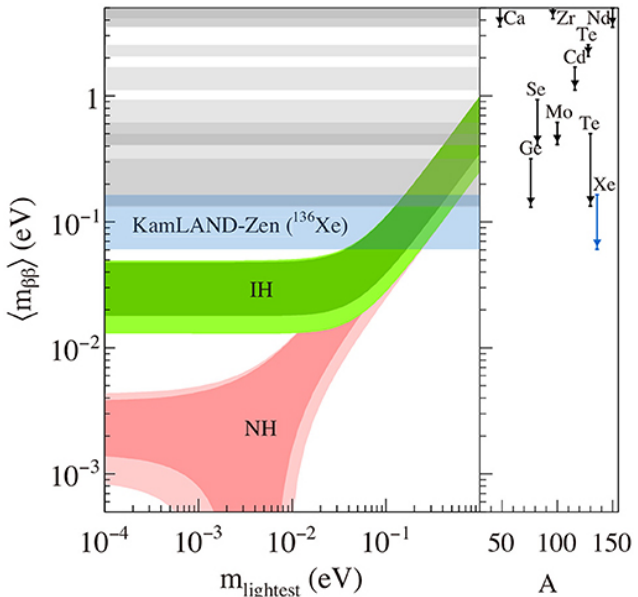


Figure 2.2: The current limits on the $m_{\beta\beta}$ and the allowed regions for both normal and inverse mass order.

528

b Neutrinoless double beta decay

529

530

531 In case neutrino has a Majorana nature, it's possible to measure the $m_{\beta\beta}$ in the process of the
532 neutrinoless double beta decay. The Feynman diagram of the process is shown in Figure 2.1.

$$m_{\beta\beta} = \sum_i U_{ei}^2 m_i \quad (2.18)$$

533 All the $0\nu\beta\beta$ experiments are putting the limits of the $m_{\beta\beta}$ value. The most precise result was
534 obtained by KamLAND-Zen experiment $m_{\beta\beta} < (61 - 165)\text{meV}$ 90% C.L. [64]. The summary of all
535 the constraints from different experiments is shown in Figure 2.2. One should keep in mind that
536 successful measurement possible only in the case of Majorana neutrino nature.

537

c Cosmology

538

540 Cosmology provides different possibilities for neutrino mass measurements. One of the earliest
541 attempts was done based on the timing measurements of the neutrinos from SN1987 — the
542 earliest and so far the only observation of the neutrino from the supernova collapse.

543 The other method is a precise observation of the evolution of the early Universe. The combination
544 of the cosmic microwave background (CMB) and baryon oscillation provides the limit on
545 the neutrino mass $m_\nu = \sum_i m_{\nu_i} < 0.12\text{eV}$ 90% C.L. [65].

546 The main problem of such analysis is a dependence on the theoretical models such as supernova
547 collapse or early Universe evolution.

548

2.2 Search for Heavy Neutral Lepton

550 As mentioned in the subsection 1.4, there is plenty of hypotheses proposing the existence of the
 552 Heavy neutral Lepton (HNL). Various analyses in different experiments were performed in order
 553 to find the HNL. In this section we will describe the search for the HNL in the context of the ν MSM
 554 framework, but the results could be applied for any other models introducing the heavy neutrino
 555 via mixing with the active one.

556

a HNL at keV scale

558

559 The lightest HNL at the keV scale could be detected through its decays $N_1 \rightarrow \nu v \bar{\nu}$ and $N_1 \rightarrow \gamma v$.
 560 While the first reaction is undetectable from the practical point of view, the latter will produce the
 561 observable X-rays. There is plenty of analyses searching for the X-ray signal from the cosmological
 562 object (e.g. Galaxy core, other galaxies, etc.) [66, 67]. The latest results are presented in Figure 2.3.

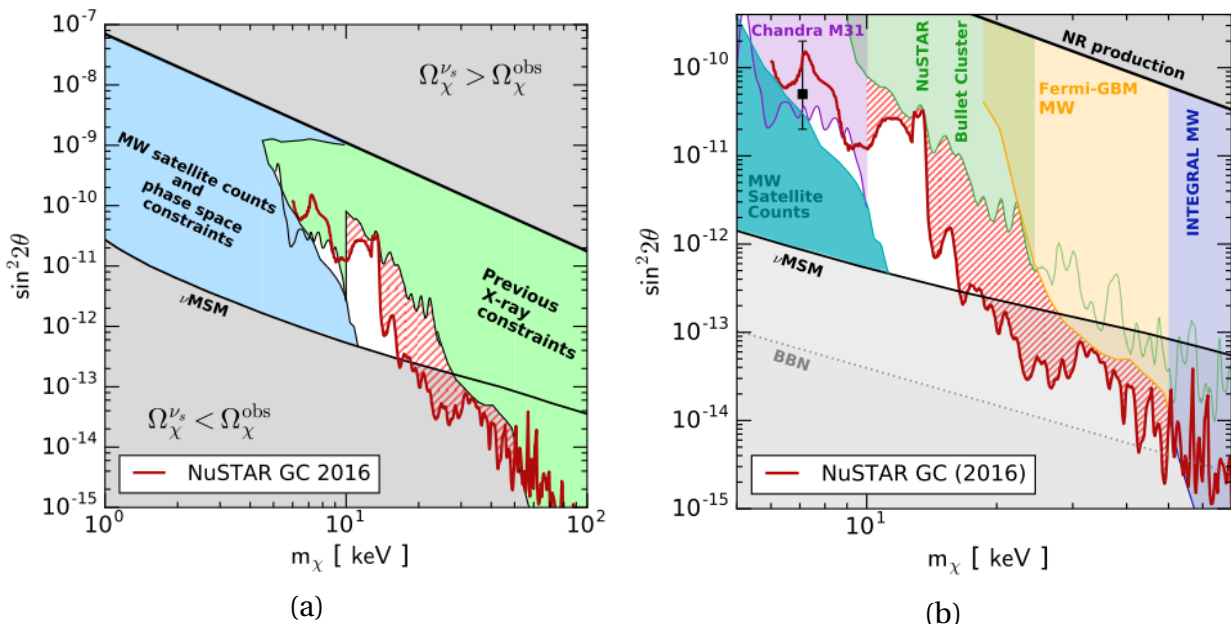


Figure 2.3: The constraints on the mixing angle of N_1 with respect to its mass: (a) the general figure and (b) the detailed view at the region of interest. Figure provided by [67].

563 So far the region is almost excluded but there is still a possibility to find N_1 from ν MSM [68].

564

b HNL at GeV scale

565

566

567 This is a scale where we expect to find the heavy neutrinos N_1 and N_2 from the ν MSM. Its mass
 568 allowed the direct search through the decay into SM particles. The work [69] provides a detailed
 569 overview of the HNL production and the decay modes. The main production mode it a meson
 570 two-body decay.

$$H \rightarrow \ell + N \quad (2.19)$$

571 Thus we could expect the HNL production in the decays of π , K , D , B and heavier mesons. The
 572 HNL is unstable hence the decay channel into the active lepton is open. While the decay modes to

573 the lighter HNL $N_{1,2} \rightarrow N_1 + \dots$ is strongly suppressed. The most probable modes are

$$N \rightarrow \bar{\nu}\nu\nu, \mu e\nu, \pi^0\nu, \pi e, \mu\mu\nu, \pi\mu, K\mu, \eta\nu, \rho\nu, \dots \quad (2.20)$$

574 Two-body decay mode is more probable over the three-body decay modes, hence there are
 575 more preferable for the direct search in the experiment. Also, the channels with at least two charged
 576 particles in the final state are much easier for the observation. Thus 3ν and $\pi^0\nu$ modes are often
 577 not considered in the analysis due to extremely hard detection.

578 In general, the HNL search could be separated into several categories:

- 579 ➤ analysis of the meson decay. The effect is proportional to $|U|^2$. For example, E949 and NA62
 580 explored the decay $K^+ \rightarrow \mu^+ N$. Thus the region of the HNL mass $M_{HNL} < m_K - m_\mu = 388 \text{ MeV}/c^2$
 581 could be explored.
- 582 ➤ direct search for the HNL decay. For example, PS191 experiment searched for the HNL pro-
 583 duced with $\pi/K \rightarrow eN$ and $\pi/K \rightarrow \mu N$ and further decayed into $e\pi, \mu\pi, \mu e\nu$. Slightly different
 584 analyzes were done by DELPHI and LHCb. They still look for the HNL decays, but produced
 585 in the Z boson decay.
- 586 ➤ joint search for HNL production and decay. For example, ATLAS and CMS performed the
 587 search for the two leptons with the same charge: one lepton along with HNL production the
 588 other comes from its decay. Such a process is possible only in the Majorana nature of the
 589 HNL.

590 So far, no evidence of the HNL existence was found and the upper limits on the mixing ele-
 591 ments were set. The latest results from all the experiments could be found in [Figure 2.4](#), [Figure 2.5](#)
 592 and [Figure 2.6](#).

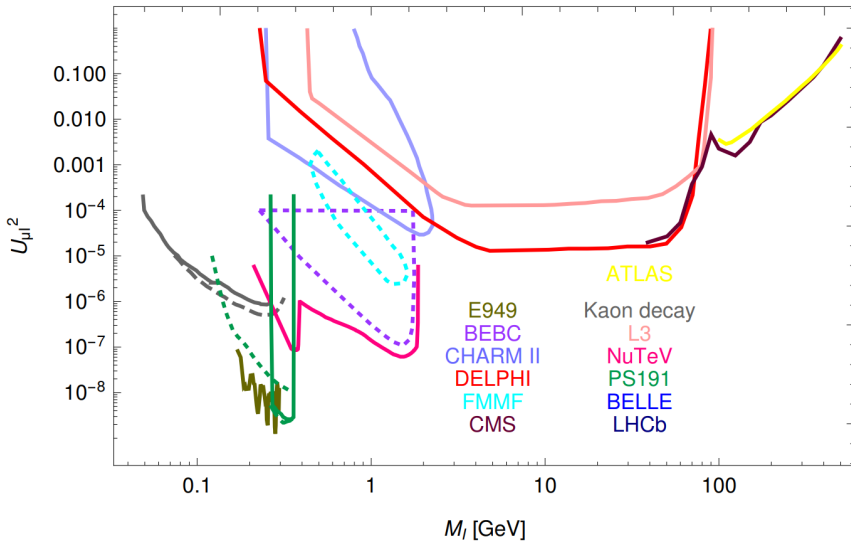


Figure 2.4: Constraints on the mixing matrix element $|U_\mu|^2$ from the experiments CMS [70], DEL-
 PHI [71], L3 [72], LHCb [73], BELLE [74], BEBC [75], FMMF [76], E949 [77], PIENU [78], TRI-
 UMF/TINA [79], PS191 [80], CHARMII [81], NuTeV [82], NA3 [83] and kaon decays in [84, 85]. The
 plot is similar to Ref. [86], some comments on the interpretation can be found in that article and
 references therein.

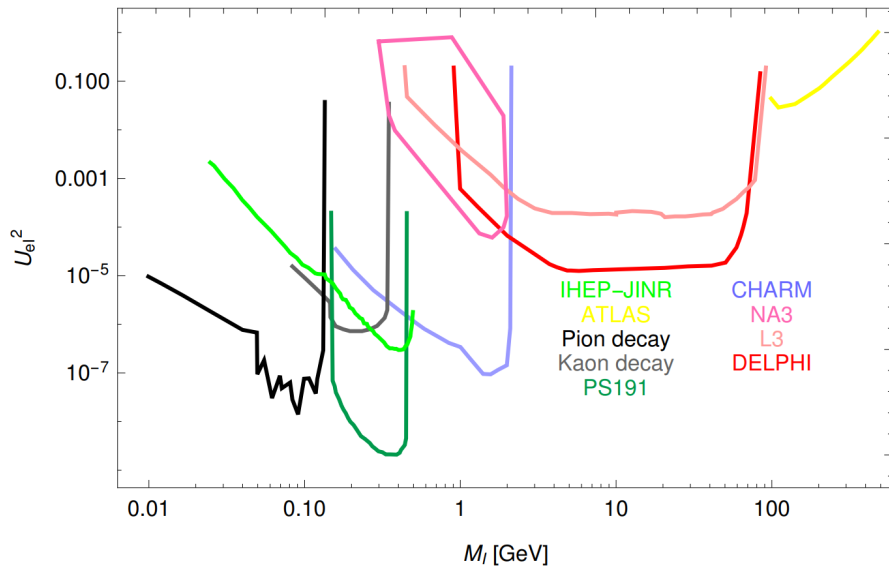


Figure 2.5: Constraints on the mixing matrix element $|U_e|^2$ from the experiments DELPHI [71], L3 [72], PIENU [78], TRIUMF/TINA [79], PS191 [80], CHARM [87], NA3 [83], IHEP-JINR [88] and kaon decays [84]. The plot is similar to Ref. [86], some comments on the interpretation can be found in that article and references therein.

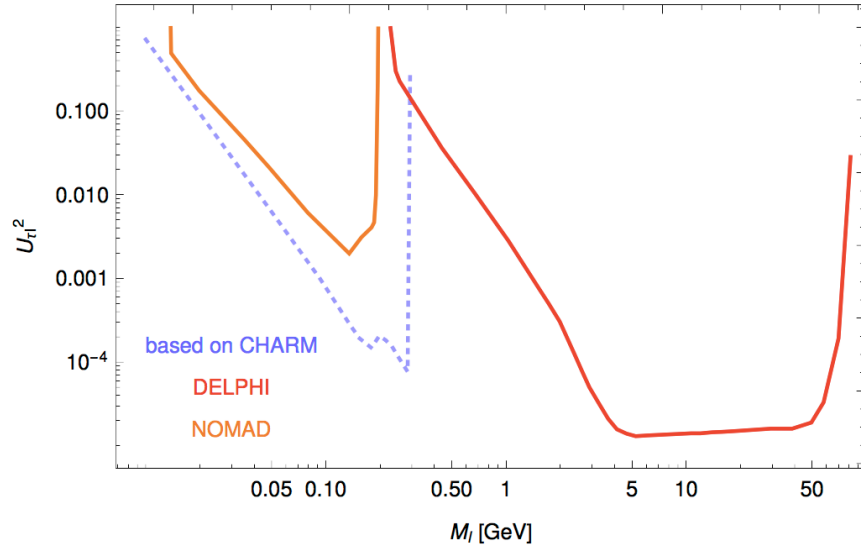


Figure 2.6: Constraints on the mixing matrix element $|U_t|^2$ from the experiments CHARM [89], NOMAD [90], DELPHI [71] and L3 [72], some comments on the interpretation can be found in that article and references therein.

593

594

PROSPECTS OF THE NEUTRINO PHYSICS

595 The the introduction part there was highlighted several times that we still have plenty of open
596 questions in the neutrino physics. The most important among them are:

- 597 ➤ CP-violation in the lepton sector. Does it exist?
- 598 ➤ Is neutrino a Dirac or a Majorana fermion?
- 599 ➤ What is the neutrino mass order? $m_1 < m_2 < m_3$ or $m_3 < m_1 < m_2$?
- 600 ➤ What are the absolute values of the neutrino mass?
- 601 ➤ What is the nature of the neutrino mass?
- 602 ➤ What are the other neutrinos except known 3 generations?
- 603 ➤ Could neutrino (or heavy neutrino) solve the problems of modern cosmology: Dark Matter
604 existence and the matter-dominance in the Universe?

605 Answer for any of them will be a remarkable step forward in our understanding of fundamental
606 physics.

1

Future neutrino experiments

608 609 Plenty of experiments are working on solving the problems above. Many proposals were made
610 about future experiments.

612 The ongoing long-baseline accelerator experiments T2K and NOvA already observed a hint for
613 the maximal CP-violation in the neutrino oscillations. The T2K experiment will be able to reach
614 3σ sensitivity for some values of the δ_{CP} [91]. The future experiments Hyper-Kamiokande [92] and
615 DUNE [93] are proposed to reach 5σ sensitivity for almost all the values of the δ_{CP} .

616 The JUNO experiment [94] is going to perform the extremely precise measurements of the re-
617 actor neutrino oscillations. With the help of these observations the neutrino mass order could be
618 determined.

619 Plenty of experiments are looking for the neutrino-less double-beta decay. They are looking
620 for the small signal in the low background environment. Different isotopes are used as a sup-
621 posed source of the $0\nu\beta\beta$ decay. KamLAND-ZEN uses the ^{136}Xe isotope, GERDA [95] uses ^{76}Ge ,

622 CUORE [96] ^{82}Se and SNO+ ^{130}Te . Any of the positive results will indicate the Majorana nature of
623 the neutrino.

624 Astrophysics experiments are studying neutrino from the sources outside the Solar System.
625 Usually, they are using Cerenkov light from the lepton or other particles produced in the neutrino
626 interactions. The probability of such events is relatively low, so the fiducial volume is extended as
627 much as possible. But the energy of such events is quite high. The examples of such experiments
628 are IceCube [97] using 1 km^3 of ice at the South Pole; Antares — the first sea neutrino telescope;
629 proposed experiment KM3NeT [98] is a one cubic kilometer neutrino telescope in the Meridian
630 sea. These experiments could detect the neutrinos from the supernova core or active galaxy core
631 that makes them very powerful for testing the cosmological models.

632 The very important class of the experiments are searching for sterile neutrino in the reactor
633 experiment. Some anomalies, e.g. lack of the neutrino events in the short-baseline reactor exper-
634 iments or Gallium experiments could be explained with the implementation of the 4th neutrino
635 flavor. The extremely short-baseline reactor experiments are very sensitive to its existence. Some
636 of them are able to change the baseline with the detector moving. The oscillations are modulated
637 by the ration of the energy to distance E/L . With the unmovable detector, the effect is measured
638 only varying the energy, hence the very precise knowledge of the reactor energy spectrum is essen-
639 tial. With the movable detector, this source of uncertainty is severely suppressed. The experiment
640 examples are: NEOS [54], DANSS [55], STEREO [56], PROSPECT [57], NEUTRINO-4 [58], SoLid.
641 These experiments will give a clear answer about the existence of the sterile neutrino in the near
642 future.

643 In the context of current tithes the future experiments dedicated to the search of the heavy
644 neutrino worth mentioning. Actually, any experiment with the intensive meson production could
645 be used for this propose. Thus DUNE [93], Hyper-Kamiokande [92], FCC [99] experiments will be
646 able to perform HNL search. But there is a proposal of the standalone experiment aimed only for
647 the heavy neutrino search. SHiP (Search for Hidden Particles) will study exclusively decays of the
648 HNL in the vacuum vessel. SHiP (Search for Hidden Particles) experiment [100] will use 400 GeV/c
649 proton beam for the production of the D and B mesons. The wide range of the heavy neutrino
650 mass will be explored with this setup.

651

652

THE T2K EXPERIMENT

653 The T2K (Tokai to Kamioka) is a long-baseline accelerator neutrino experiment. Its main propose
654 is precise measurements of the neutrino oscillation parameters. T2K is a continuation of the suc-
655 cessful history of the previous accelerator experiments: KEK, MINOS, etc. At the beginning of the
656 T2K era, the main challenge was the measurements of the θ_{13} mixing angle. Its value was not mea-
657 sured at all at that moment and $\theta_{13} = 0$ was possible. The value of this angle is important as the
658 amplitude of the CP-violation (subsubsection 2.1.c of chapter 1) is scaled with θ_{13} . Even with the
659 maximum value of the δ_{CP} , the effect could vanish with zero mixing angle. Thus θ_{13} measurements
660 became the main goal at the beginning of the T2K era.

661 The θ_{13} could be measured in both appearance ($\nu_\alpha \rightarrow \nu_\beta$) and disappearance ($\nu_\alpha \rightarrow \nu_\alpha$) chan-
662 nels. The reactor experiments are very powerful in the analysis of the $\bar{\nu}_e \rightarrow \bar{\nu}_e$ disappearance
663 process and thus could measure θ_{13} precisely. But the CP-violation effect could take place only
664 in the appearance channel (subsubsection 2.1.c of chapter 1). The $\nu_e \rightarrow \nu_\mu$ channel is extremely
665 challenging from the experimental point of view. To reconstruct the flavor of the ν_μ the charged
666 muon need to be produced. Thus the neutrino energy should be greater than the muon mass
667 $m_\mu = 105 \text{ MeV}/c^2$. There is no easy way to create an intensive pure beam of high energetic electron
668 neutrinos. On the contrary, the $\nu_\mu \rightarrow \nu_e$ channel is very promising. The charged mesons (e.g. pi-
669 ons, kaons) decay mainly into the muon neutrino. And the intensive and focused beam of charged
670 mesons could be easily created with the particle accelerator. Thus the accelerator experiments are
671 the only way to probe the CP-violation. Also, they are very powerful in the measurements of the
672 θ_{13} , θ_{23} and Δm_{32}^2 .

673 The approach of the accelerator oscillation experiment is to measure the energy spectrum of
674 the neutrino beam at the far detector and compare it to the expectations without the oscillations.
675 The reconstruction of the energy is critical as neutrino oscillates along L/E_ν . While the baseline L
676 is fixed neutrino with different energies will arrive at the far detector in the different phase of the
677 oscillation. The expected neutrino flux could be constrained with the measurements of the un-
678 oscillated neutrinos with the near detector. In the T2K the neutrino energy is reconstructed with
679 the water Cherenkov detector Super-Kamiokande (section 3) and the magnetized near detector
680 ND280 (subsection 2.2). The water detector measures the energy of the particle with the opening
681 angle of Cherenkov radiation and the ND280 measures the momentum with the track curvature
682 in the magnetic field. The energy of all the products of the neutrino interaction should be recon-
683 structed for the precise neutrino energy estimation. The easiest way to do it is to work in the energy
684 region where the most probable neutrino interaction is quasi-elastic $\nu_\ell + n \rightarrow \ell^- + p$ ($\bar{\nu}_\ell + p \rightarrow \ell^+ + n$)

685). As this is a two-body process and the incoming neutrino direction is known the neutrino energy
 686 could be calculated with the outgoing lepton kinematics only. This reaction dominates at energies
 687 below 1 GeV. But if the neutrino has higher energy then plenty of particles could be produced.
 688 Some of them could be low energetic or neutral. That makes the neutrino energy reconstruction
 689 extremely tricky. The problem is that the mesons with the wide energy range are produced in the
 690 proton beam interactions in the target. That results in a very wide neutrino spectrum. To deal with
 691 this T2K uses the “off-axis” beam to produce quasi-monoenergetic neutrino flux ([subsection 1.1](#)).

692 T2K was designed to measure the appearance process $\overset{(-)}{\nu}_\mu \rightarrow \overset{(-)}{\nu}_e$ which was expected to be ex-
 693 tremely rare. First of all the signal rate should be enlarged as much as possible. The J-PARC acceler-
 694 ator provides a very intensive muon neutrino beam. Further improvement is considered ([section 1](#)
 695 of [chapter 9](#)). Secondly, all the processes that could mimic the $\nu_\mu \rightarrow \nu_e$ signal should be suppressed
 696 or precisely controlled. One of the main concerns is the electron neutrinos initially produced in the
 697 beamline. The meson’s decay mostly leads to the muon and muon neutrino production. But the
 698 muon decay will result in the electron anti-neutrino $\mu \rightarrow e\bar{\nu}_e\nu_\mu$. To suppress such a process, the
 699 length of the meson decay volume is limited. Produced muons are stopped in the dump just after
 700 the decay pipe and emit the electron neutrinos isotropically, not pointed towards the far detector.
 701 The second process of concern is the neutral pion production in the neutrino interactions through
 702 the neutral current. The π^0 will further decay into two photons. At our energies, photons will con-
 703 vert into the electron-positron pair. One of the components of the pair could be lost resulting in
 704 the detection of the electron-like event. To estimate the rate of the neutral pion production the
 705 special π^0 subdetector was built in the near detector complex ([subsubsection 2.2.a](#)).

706 When studying the CP-violation it’s critical to distinguish neutrino and anti-neutrino oscilla-
 707 tions since the effect is the opposite for them. The Super—Kamiokande could not separate elec-
 708 trons from positrons and μ^- from μ^+ as Cherenkov rings will be similar for them. Thus the neutrino
 709 could not be distinguished from the anti-neutrino. The near detector ND280 is magnetized. Neu-
 710 trino and anti-neutrino will produce leptons of the opposite charge. Their tracks will curve in the
 711 contrary directions and could be easily separated.

712 The sketch of the T2K setup is shown in [Figure 4.1](#). In brief, the working process of the T2K
 713 experiment is the following:

- 714 1. Proton beam hits the carbon target producing mesons.
- 715 2. The mesons are focused with horns into the decay volume. The horn polarity defines whether
 716 positive or negative mesons will be focused.
- 717 3. In the decay volume, the mesons decay mostly into the muon neutrino or anti-neutrino.
 718 Thus the horn polarity defines the neutrino mode: ($H \rightarrow \mu^+ \nu_\mu$ or $\overline{H} \rightarrow \mu^- \bar{\nu}_\mu$). The energy
 719 spectrum of the off-axis neutrino beam is quasi-monoenergetic peaking around 0.6 GeV.
- 720 4. The muons from the meson decays are mostly stopped in the beam dump, preventing the
 721 large electron neutrino contribution in the flux.
- 722 5. The neutrino beam intensity and direction are constantly monitored by the muon monitor
 723 and the on-axis detector INGRID.
- 724 6. The energy spectrum of the non-oscillated neutrino beam is measured with the off-axis
 725 ND280 detector([section 2](#))
- 726 7. After traveling 295 km neutrino beam reach the far detector complex Super-Kamiokande
 727 ([section 3](#)). The baseline and neutrino energy are tuned to the first oscillation maximum
 728 ($\Delta m_{32}^2 L/E \approx 1$).

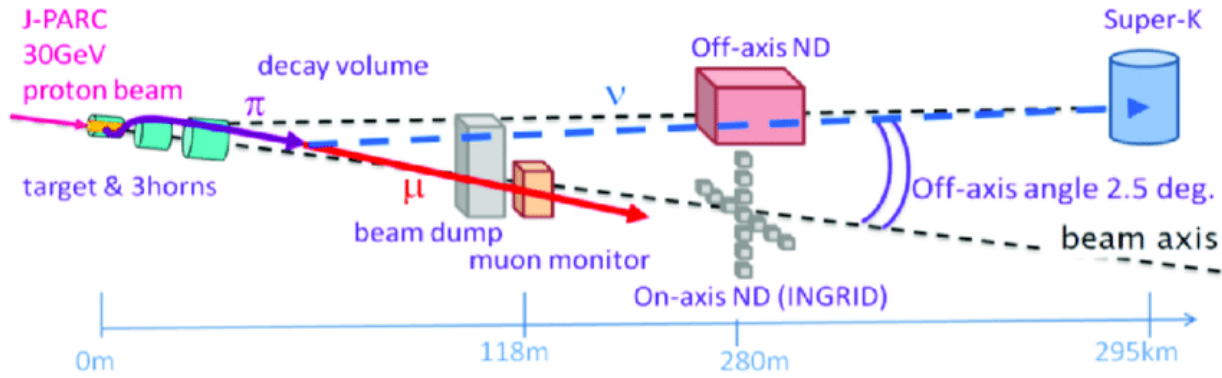


Figure 4.1: The sketch of the T2K setup shows all the key elements of the experiment.

The main goals of the T2K experiment are:

- precise measurements of the oscillation parameters Δm_{23}^2 and θ_{23} with the muon neutrino disappearance $\nu_\mu \rightarrow \nu_\mu$ and $\bar{\nu}_\mu \rightarrow \bar{\nu}_\mu$
- measurements of the θ_{13} with the electron appearance $\nu_\mu \rightarrow \nu_e$ and $\bar{\nu}_\mu \rightarrow \bar{\nu}_e$
- search for the CP violation $\sin \delta_{CP} \neq 0$ with studying the difference between $\nu_\mu \rightarrow \nu_e$ and $\bar{\nu}_\mu \rightarrow \bar{\nu}_e$
- along with the oscillation measurements, the neutrino interactions are studied carefully to reduce the systematic uncertainty. Thus the neutrino cross-sections on carbon, water and iron are measured.

Alongside reactor experiments, T2K successfully measured the non-zero value of the θ_{13} [43] thus opening the way for the CP-violation search. At the moment it's a major goal of the experiment together with more precise measurements of other oscillation parameters. In this chapter, the details about the T2K setup as well as an analysis technique will be overviewed.

1 Neutrino beam

For the production of the T2K neutrino beam the proton accelerator is used. The 30 GeV/c protons from the J-PARC accelerator hit the target producing mesons. At these energies mainly pions are produced. There is still some minor contribution of kaons in the meson flux. Mesons with the proper charge are focused in the decay volume. At the same moment, wrong-charged mesons are dis-focused and neutral particles remain unfocused. In the decay volume, the mesons decay mainly into the muon and muon neutrino. The decay to the electron and electron neutrino is suppressed by 4 orders by the kinematics of the decay. The mesons of the same charge always produce neutrino or anti-neutrino. Thus the wrong-sign component of the neutrino beam is severely suppressed with the meson focusing system. The polarity of the focusing system may be changed resulting in the pure neutrino or anti-neutrino beam.

The accelerator neutrino experiment has lots of benefits from the man-made neutrino beam. It is focused, thus extremely intensive, high energetic and precisely controlled. It mostly consists of the neutrino of the same flavor. The possibility to switch between the neutrinos or anti-neutrinos beam is very helpful for the CP-violation search. To constrain the δ_{CP} the difference between neutrino and anti-neutrino oscillations should be studied. The beam monitoring reduces a lot the systematic uncertainties related to the flux. The intensive pure beam of the muon neutrino is es-

761 sential for the precise studies of the $\nu_\mu \rightarrow \nu_e$ oscillations. The purity of the beam will minimize the
 762 electron neutrino events in the far detector that are the background for the ν_e appearance process.
 763 The lower background will make easier the signal observation. In this section, the details about the
 764 beam production and monitoring within the T2K experiment will be presented.

765

1.1 Off-axis flux

766 Mesons produced in the proton collisions have a wide energy spectrum. That leads to a wide
 767 range of neutrino energies. It makes the oscillation analysis pretty tricky. Neutrino oscillates along
 768 L/E_ν . Thus only neutrinos with the given energy will demonstrate the maximum appearance or
 769 disappearance. All the neutrinos with other energies will be less affected by the oscillations and
 770 could mask the process of interest. As mentioned in the introduction, to gain energy reconstruc-
 771 tion precision only quasi-elastic interactions are used. It means that we are looking for events with
 772 one lepton and nothing more. The energy is estimated assuming the quasi-elastic interaction as
 773 well. This is a dominant topology of the neutrino interactions at the energies below 1 GeV. With
 774 energy growth, the cross-section of the neutrino interactions dramatically increases. The main re-
 775 action becomes the inelastic processes with a production of plenty of different particles. If the
 776 particle energy is lower than the threshold of Cherenkov radiation emission it is completely invis-
 777 ible in the Super-Kamiokande. Thus high energy neutrinos are very dangerous for the T2K. They
 778 interact more often and produce many particles that could be low energetic. Hence we could rec-
 779 ognize such an event as quasi-elastic and reconstruct the neutrino energy with the completely
 780 wrong assumption. It will lead to the wrong oscillation measurement.

781 To handle this T2K experiment uses a so-called “off-axis” concept to obtain a quasi-monoenergetic
 782 neutrino beam. The key idea is to use not the neutrinos pointed along the beam axis, but directed
 783 at a slight angle. Such neutrinos will have a relatively narrow energy spectrum. The dominating
 784 neutrino production mode in the T2K is a pion decay $\pi \rightarrow \mu\nu$. The neutrino energy in the two-
 785 body decay will be given by

$$E_\nu \approx \left(1 - \frac{m_\mu^2}{m_\pi^2}\right) \frac{E_\pi}{1 + \gamma^2 \theta^2} \quad (4.1)$$

786 where γ is the pion kinematic parameter and θ is a neutrino direction angle w.r.t. pion momen-
 787 tum. The equality of the derivative of the neutrino energy over the pion energy to zero means full
 788 independence of the first from the latter. In case $\theta = \gamma^{-1}$ $dE_\nu/dE_\pi = 0$ that means that neutrino
 789 energy depends weakly on the parent pion energy. Finally, we will get

$$E_\nu \approx \left(1 - \frac{m_\mu^2}{m_\pi^2}\right) \frac{m_\pi}{2\theta} \approx \frac{29.8 \text{ MeV}}{\theta} \quad (4.2)$$

790 The T2K beamline allows varying of the peak neutrino energy by tuning the off-axis angle. The
 791 energy spectra for different angles are provided in [Figure 4.2](#). The figure provides also the oscil-
 792 lation probability of the muon neutrino at a distance of 295 km versus the energy. Thus with the
 793 off-axis angle tuning the maximum oscillation effect could be measured. Though the high energy
 794 neutrinos are harmful to the oscillation analysis nevertheless high energy mesons could be useful
 795 for other studies. For example, they could be helpful for the Heavy Neutral Lepton (HNL [subsec-
 796 tion 1.4](#)) search. High energy mesons decay will result in the focused HNL beam while low energy
 797 mesons will produce HNL in a very wide angle. The heavy neutrino study is one of the main topics
 798 of the current thesis ([chapter 5](#)).

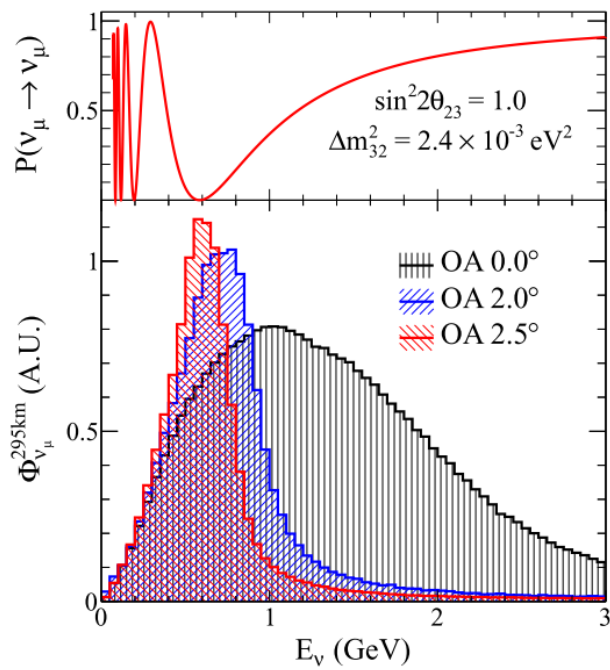


Figure 4.2: Muon neutrino survival probability at 295 km and neutrino fluxes for different off-axis angles. Figure from [101].

801

1.2 Neutrino beamline

804 The T2K neutrino beamline could be generally divided into two stages: primary beamline and
 805 secondary beamline. The first takes the protons from the J-PARC accelerator main ring, performs
 806 measurements of the beam parameters and focuses it on a carbon target. The secondary beamline
 807 focuses the produced mesons with the horns into the decay volume and monitors its decay. The
 808 general scheme of the beamline is shown in Figure 4.3. The detailed description could be found
 809 in [101].
 810

a Primary beamline

811 The primary beamline takes the proton from the J-PARC main ring. The beam is structured
 812 into the spills coming with 0.5 Hz rate. Each spill is $5 \mu\text{s}$ wide and consists of 8 bunches with
 813 $\sigma \approx 18 \text{ ns}$ and 58 ns separation. Per each spill, 3×10^{14} protons could be delivered. Thus the total
 814 maximum power of the beamline could be estimated as 750 kW. The total number of protons hit
 815 into the target is used as the main characteristic of the statistics collected in the T2K experiment
 816 (POT - Protons On Target). The evolution of the accumulated statistics, as well as the beam power,
 817 is shown in Figure 4.4.

818 The initial beam is bounded with the arc section made with superconducting magnets and
 819 horizontally aligned with the direction to the detectors. At this stage, the measurements of the
 820 beam parameters are performed. The beam intensity is measured with current transformers that
 821 use toroidal coils around a cylindrical ferromagnetic core. The uncertainties of the measurements
 822 are estimated at the level of 2%. The beam position is measured with electrostatic monitors and
 823 secondary emission monitors. First measures the beam position with the accuracy of $450 \mu\text{m}$ the

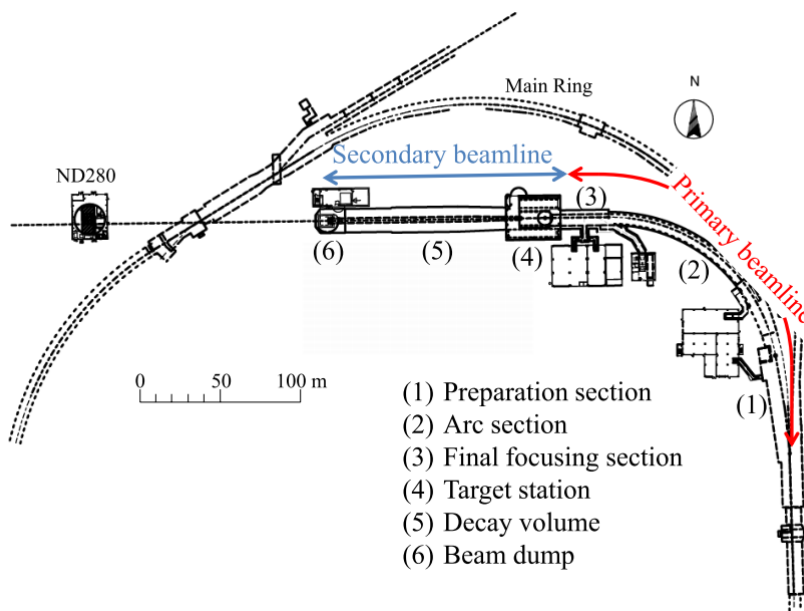


Figure 4.3: The scheme of the T2K neutrino beam line. Primary beamline (proton line) is shown in red and secondary beamline is shown in blue.

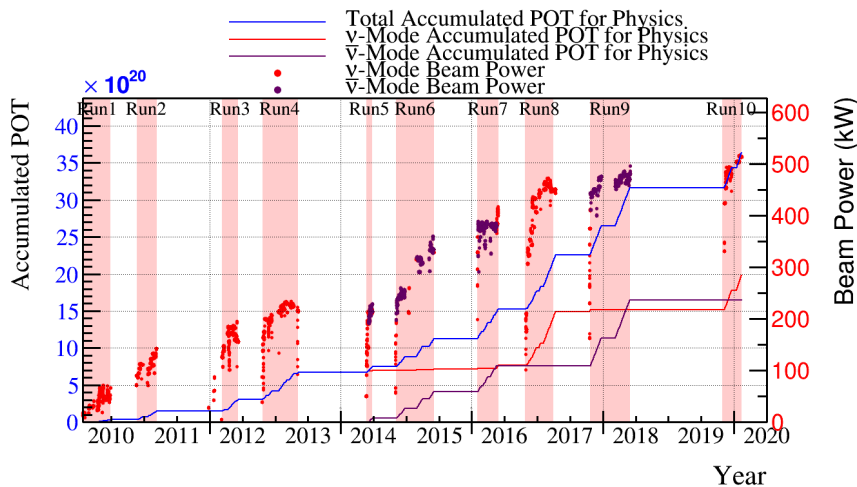


Figure 4.4: The collected statistics in the T2K experiment in POT (Proton On Target) together with the beam intensity along the data accumulation.

826 latter measures the beam width with the precision $200 \mu\text{m}$. After the measurements, the beam is
827 directed downward and focused on the carbon target.
828

b Secondary beamline

831 The secondary beamline is responsible for neutrino production. The target for protons is made
832 of Carbon cylinder 2.6 cm width and 91.4 cm length (1.9 interaction length). Target heats up to
833 800°C during the irradiation. The core is put with the titanium case for fast heat transfer to the
834 water cooling system. The target is inserted into the first magnetic horn, so the mesons are affected
835 by the focusing magnetic field from the moment of production.

836 The meson focusing system consists of three magnetic horns. The first one contains the target
 837 where the mesons are produced. The horns are operated with the pulsed current at the level of 250-
 838 320 kA. The polarity could be changed to focus negative or positive mesons resulting in neutrino
 839 or anti-neutrino production. The dramatic gain of the horn usage for the neutrino beam intensity
 840 is shown in [Figure 4.5](#).

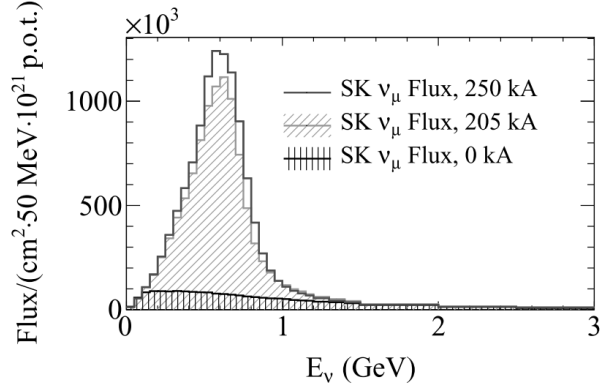


Figure 4.5: The effect of horn usage on the beam intensity at the far detector

The hadrons are focused into the decay volume. It's a 96 m tunnel widening from $1.4 \times 1.7 \text{ m}^2$ at the beginning up to the $3.0 \times 5.0 \text{ m}^2$ at the end. The volume is filled with argon gas and is cooled with water. The parent particles are considered as possible neutron sources are π^\pm, K^\pm, K_L^0 and μ^\pm . The most probable neutrino production reactions are:



841 The energy spectra divided into neutrino flavor and parent particle are provided in [Figure 4.6](#).

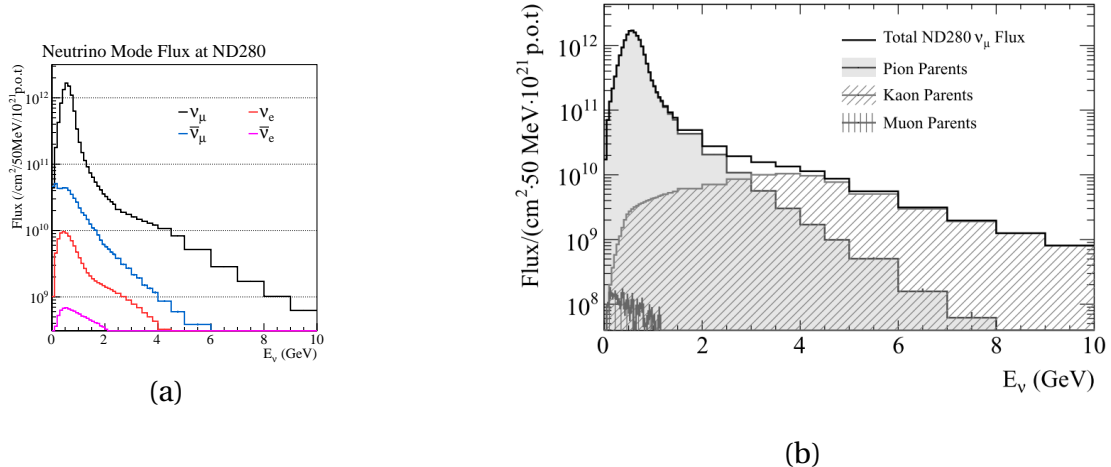


Figure 4.6: The neutrino beam at the near detector side divided into (a) neutrino flavor and (b) parent particle.

842 The beam dump is placed just after the decay pipe. It's made of 75 tons of graphite and sup-
 843 press all the charged particles except the high energy muons ($E > 5 \text{ GeV}$). Thus low energy muons
 844 will not decay in flight, producing electron neutrinos pointed to the far detector. It's critical for the

845 successful oscillation analysis. High energy muons could be used for the neutrino beam stability
 846 monitoring. They are mostly produced along with neutrino in the 2-body meson decays. Thus the
 847 muon direction fluctuation will explicitly indicate the fluctuation of the neutrino beam. The de-
 848 tector is made with an array of ionization chambers and another array of silicon PIN photodiodes.
 849 The center of the muon profile is reconstructed with 3 cm precision resulting in 0.25 mrad angular
 850 accuracy.

851 The overview of the T2K secondary beamline together with the near detector complex is pre-
 852 sented in [Figure 4.7](#).

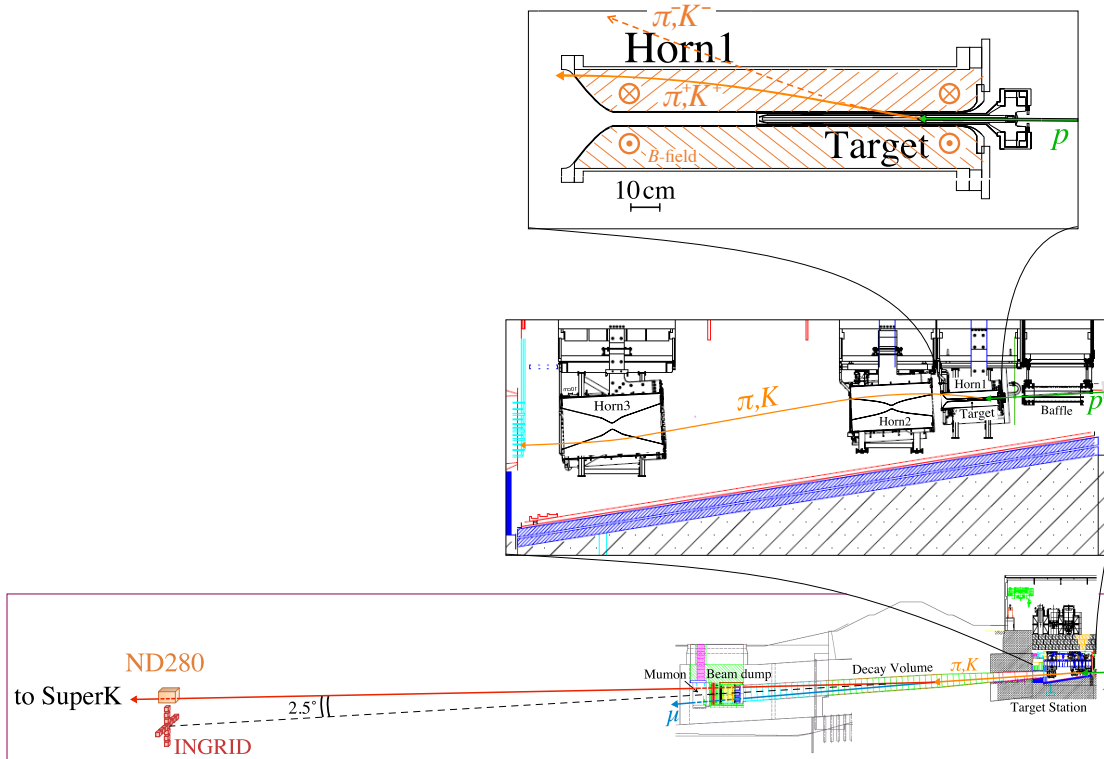


Figure 4.7: The overview of the T2K secondary beamline and the near detectors.

853

2 Near detector

854

855 Precise knowledge about the initial neutrino beam is essential for the accurate oscillation mea-
 856 surements. The T2K near detector complex is placed in 280 meters from the proton target and its
 857 main goal is the monitoring of the unoscillated beam. Two detectors are used for this propose:
 858 on-axis INGRID and off-axis ND280. The schematic views of both detectors are presented in [Fig-](#)
 859 [ure 4.8](#).
 860

861

2.1 INGRID

862

863 The main goal of the INGRID detector is controlling the position and intensity of the neutrino
 864 beam. It consists of 14 modules arranged in a cross with two additional modules placed outside

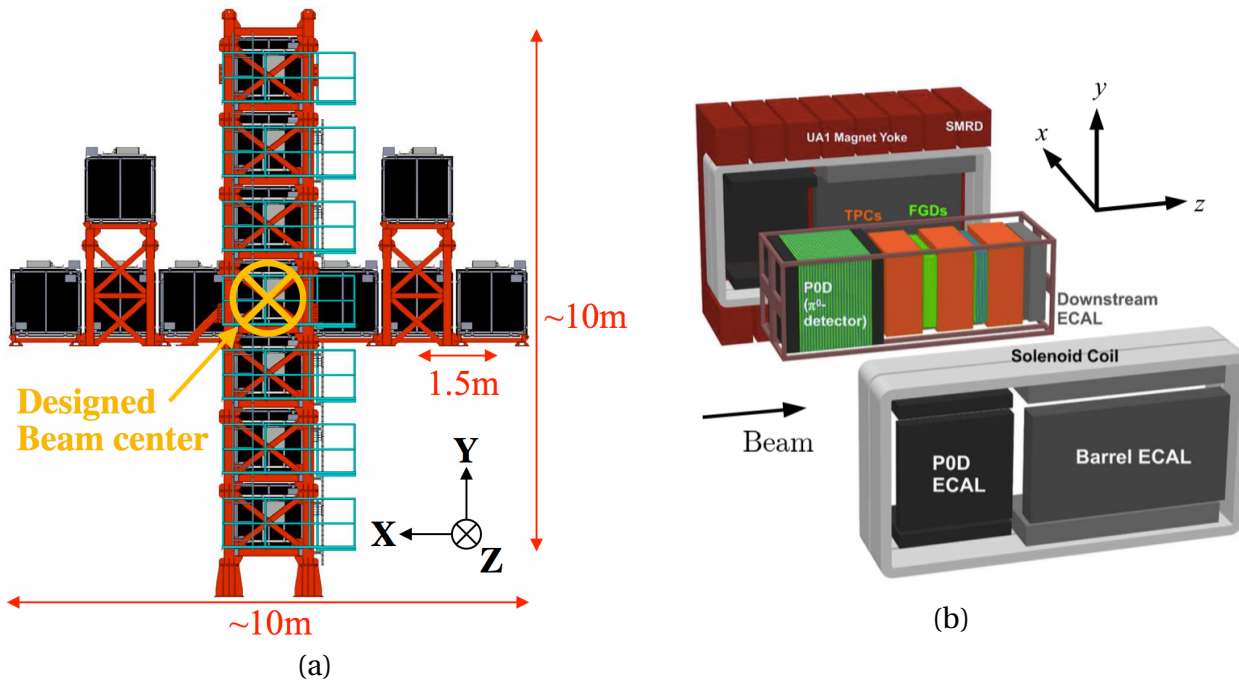


Figure 4.8: An exploded view of the near detector complex: (a) on-axis INGRID detector, (b) off-axis ND280 detector.

866 the main cross (Figure 4.8 (a)). The center of the cross is placed at 0° angle w.r.t. proton beam
 867 direction. Each detector module consists of a sandwich of iron and tracking planes. We expect
 868 enough neutrino interactions in the iron targets every day for the day-to-day monitoring of the
 869 neutrino beam parameters. Figure 4.9 represents the results of such measurements. Both intensity
 870 and direction variations are small and the related uncertainties in the oscillation analysis are far
 871 from dominating.

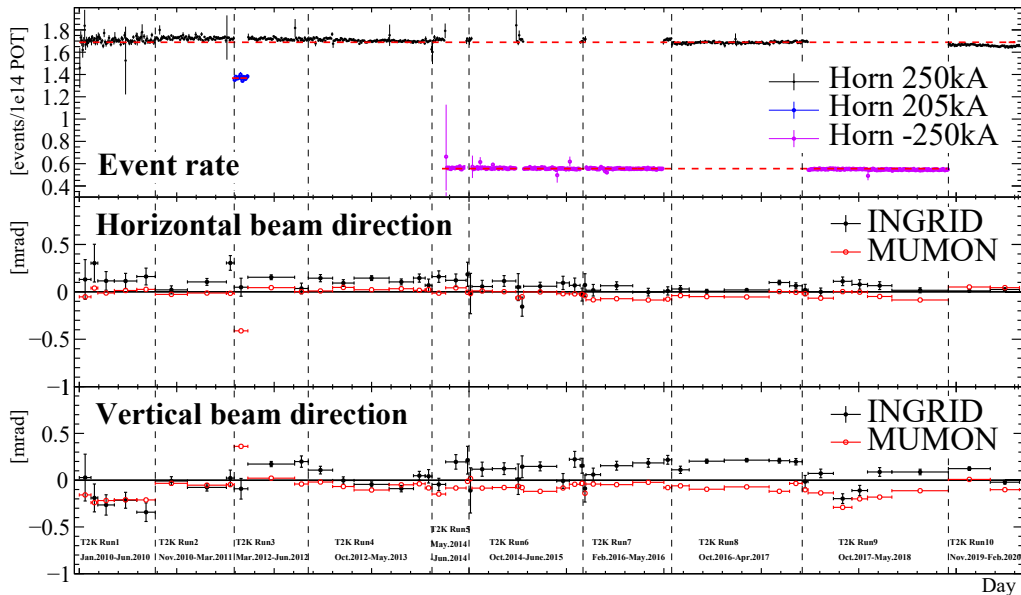


Figure 4.9: The INGRID measurements of the neutrino beam intensity and position.

872

873

2.2 Near detector ND280

874

875

876

877

878

879

880

881

882

883

884

885

886

887

888

889

890

891

892

893

894

895

896

897

898

899

900

901

902

903

904

905

906

907

908

909

910

911

912

913

914

915

916

917

918

The ND280 is an off-axis detector placed at the direction from the target towards the far detector Super-Kamiokande. Its goal is neutrino interaction measurements dividing them into neutrino sign, flavor and the reaction topology. The neutrino energy is measured as well. For this propose the detector is composed of plenty of different sub-detectors. The Fine Grained Detectors (FGD) are used as a target for neutrino interaction and the tracking of the outgoing particles. The gaseous Time Projection Chambers (TPC) are used for the charged particle tracking. The particle sign and momentum are measured with the track curvature in gas. The type of the particle is also reconstructed with the ionization energy losses. Thus the incoming neutrino type (neutrino/anti-neutrino), flavor and energy could be determined. Electromagnetic calorimeter (ECAL) detect the gamma conversion and improve electron and muon separation. The SMRD detector works as a trigger for the cosmic rays and may help with the muon identification. The P0D detector is used for the measurements of the π^0 production in the neutrino interactions. At the beginning of the T2K, it was a big concern about the neutral pion production as the main background for the far detector.

The ND280 measurements are used to constrain the parameters of the flux and the theoretical models of the neutrino interactions. The fact that we know the neutrino sign, flavor, energy and the reaction type allows us to probe plenty of the models' parameters independently. This will result in the smaller uncertainty of the global oscillation analysis. The subdetectors structure and features will be overviewed in the following subsections.

a π^0 detector (P0D)

The primary goal of the P0D detector is to measure the cross-section of the π^0 production in the neutrino interactions through the neutral current (NC). As was mentioned in the introduction it was supposed to be the main background in the far detector. The photons from the π^0 decay could be misreconstructed as $\nu_\mu \rightarrow \nu_e$ signal and bias the oscillation analysis a lot. The same flux and the same target material should be used for the accurate background treatment. As the detector is aimed to detect the NC π^0 production it should be good in the charged particle tracking to distinguish CC and NC interactions. Also, it should be effective for photon detection. The sensitive volume of the P0D is made from the scintillator bars aligned along X and Y axis (perpendicular to the beam axis). The readout is done with the wavelength shifting fibers (WLS). The XY scintillator layers are alternated with brass sheets and water bags. Such a structure allows efficient reconstruction of the charged particle tracks as well as electromagnetic showers. The latter are used for photon detection. The scintillator layers are alternated with the lead sheets instead of water bags in the upstream and downstream parts of the detector. This improves the containment of the EM showers. The measurements of the NC π^0 production could be done with and without water target, thus the cross-section on water could be extracted.

b Fine grained detectors (FGD)

Two FGD modules [102] are used as a target for the neutrino interactions. The size of the module is $2 \times 2 \times 0.3$ m³. They consist of a sandwich structure of bars made with plastic scintillators and oriented along X and Y axis, while the beam is coming along Z axis. The bars are pierced with WLS for the light collection and transportation to the photosensors. The light readout is done with

919 multi-pixel photo counters (MPPC) that provide high detection efficiency and sufficient dynamic
 920 range.

921 In the second FGD the plastic layers are alternated with the water modules. Thus the measure-
 922 ments of the neutrino interaction with the water could be done. Such a measurement is important
 923 in the context of T2K as far detector uses water target only. The difference between neutrino inter-
 924 action cross-section with Carbon and Oxygen could be a source of systematic uncertainty.
 925

c Time projection chambers (TPC)

926
 927
 928 The TPCs [103] are gaseous detectors that perform the 3D reconstruction of the charged parti-
 929 cle's track. The scheme of the detector is presented in Figure 4.10.

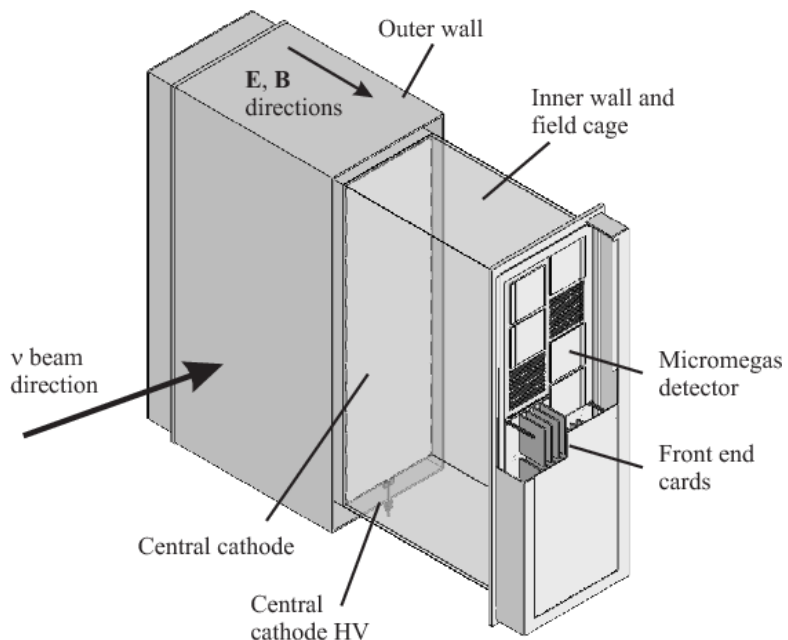


Figure 4.10: The scheme of the TPC module

930 The general principle of the TPC operation and the key characteristics of the T2K TPCs are pre-
 931 sented in Figure 4.11. The active volume of the detector is filled with the gas mixture of Argon, CF₄
 932 (tetrafluoromethane) and iC₄H₁₀ (isobutane) in the volume proportions 95:3:2. A charged particle
 933 going through the gas volume loses the energy through the ionization. The electrons from the ion-
 934 ization drift against the direction of the electric field — from the cathode towards the micromegas.
 935 The positive ions are drifting towards the cathode. The Argon was chosen as a main component
 936 of the gas mixture because it's a noble gas. It's very easy to ionize thus we will have a lot of initial
 937 electrons. Also, it will not subject to a chemical reaction. It is especially important in the ampli-
 938 fication region, where chemical reactions are most probable. Isobutane also serves for the higher
 939 precision of the measurements absorbing photons emitted in the electron avalanches and prevent
 940 quenching. CF₄ is responsible for the speed up of the electron drift. Such a mixture is very powerful
 941 resulting in high speed, low diffusion, and good performance with micromegas chambers.

942 The electric field strength is constant in the drift region, ideally, there should be no amplifi-
 943 cation there. The voltage between the cathode and micro mesh is 25 kV at a distance of 1 meter.
 944 The signal is dramatically amplified between the micro mesh and micromegas as the voltage 350

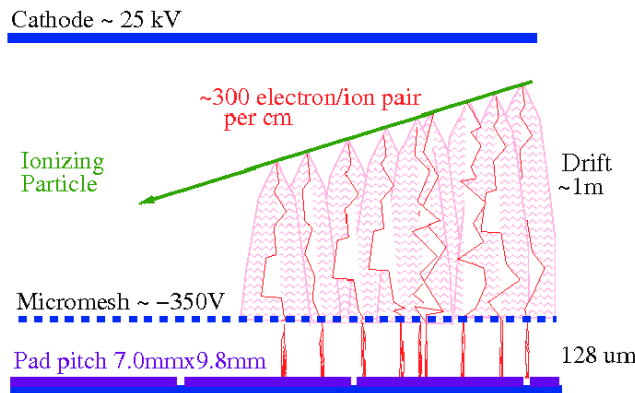


Figure 4.11: The general concept of the TPC operation.

945 V is applied for the $128 \mu\text{m}$ gap. The produced avalanches are detected with the $6.9 \times 9.7 \text{ mm}^2$
 946 pads. Here the electrons are transformed into the analog signal that will be later digitized with the
 947 electronics.

948 In total, the readout surface of one TPC module consists of 12 micromegas 48×36 pads each.
 949 The 2D projection (YZ) of the track could be easily reconstructed with the hit pads. The X coor-
 950 dinate depends on the electron drift time. Though the time delay from different parts of the track
 951 is measured precisely this is an arbitrary measurement. The track curvature in XY plane is known
 952 but the external detector (FGD) is essential for the absolute position.

953 The core of the ND280 — the tracker, consists of 3 TPCs alternated with 2 FGDs. Such a struc-
 954 ture is aimed at the effective detection of the lepton produced in the neutrino interactions inside
 955 FGDs. The particle type, sign and momentum could be precisely measured with such a setup.
 956

d Electromagnetic calorimeter (ECaL)

957
 958
 959 The calorimeters are used for the detection of the gammas from the π^0 , produced in the neu-
 960 trino interactions. They also could help with the particle identification. Electrons and hadrons will
 961 produce showers while muons will have a clear clean track. The calorimeters are surrounding the
 962 inner detectors of the ND280. They consist of the sandwich structure of plastic bars $4 \times 1 \text{ cm}^2$ in
 963 cross-section, alternating with 1.75 mm thick absorber layers made with lead. The downstream
 964 ECAL consists of 34 layers and provides the most precise results, while P0D and barrel ECAL con-
 965 sists of 31 layers.
 966

e Side muon range detector (SMRD)

967
 968
 969 The SMRD is surrounding the whole ND280 and is a multifunction detector. It could eject the
 970 events triggered by the cosmic rays or the neutrino interactions in the outer detectors or concrete
 971 of the pit. SMRD is useful for the detection of the muons that exit the detector with high angles.
 972 Since there is no TPC in this direction the momentum measurement could be done only with
 973 SMRD. The detector itself consists of 440 1.7 cm thick plastic scintillator modules that are inserted
 974 in the gaps between 4.8 thick steel plates of the magnet yoke.

975

3 Super-Kamiokande

877 The far detector of the T2K experiment is Super-Kamiokande (SK) [104] located 295 km away
 979 from the proton target in the Kamioka mine. 50 tons of water is used as a target for the neutrino.
 980 The water tank is viewed by 13 thousand of the photomultipliers (PMT) aimed at the detection
 981 of Cherenkov light from the charged lepton produced in the neutrino interactions. The schematic
 982 view of the detector is presented in Figure 4.12.

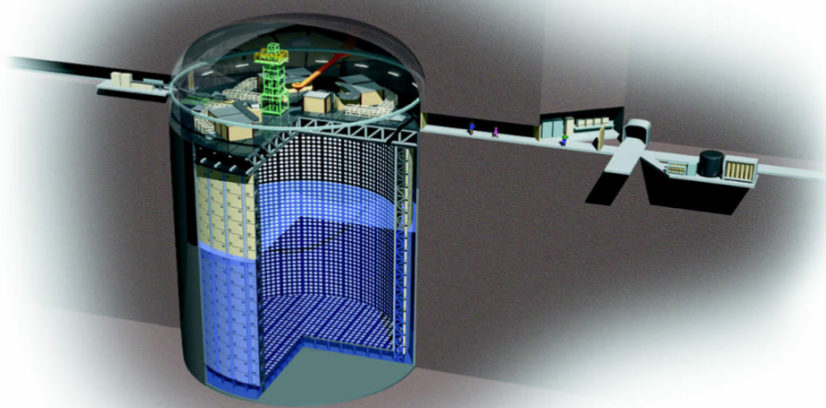


Figure 4.12: The scheme of the Super-Kamiokande detector.

983 The working principle of the detector is based on the effect of Cherenkov radiation. When a
 984 charged particle passes through a dielectric medium at a speed greater than the phase velocity
 985 of light in that medium the conic wavefront is formed. The opening angle of the cone is defined
 986 by the particle speed and the refraction coefficient of the medium $\cos\theta = 1/n\beta$, where $\beta = v/c$.
 987 The emission of the radiation is a threshold effect. As could be seen from the equation above, the
 988 wavefront could be formed only if the particle is fast enough $\beta > 1/n$. For the water detector, the
 989 thresholds are 1.4 GeV for protons, 160 MeV for muons and 775 keV for electrons. The maximum
 990 angle is also limited by $\theta_{max} = \arccos(1/n) \approx 42^\circ$.

991 Super-Kamiokande continues the successful history of the neutrino detectors in the Kamioka
 992 mine. The first experiment KamiokaNDE (Kamioka Nucleon Decay experiment) started looking
 993 for the nucleon decays in 1983. The neutrino interactions were supposed to be the main back-
 994 ground. During the detector operation, nice performance of the neutrino detection was observed
 995 and the experiment was refocused on the neutrino analysis. Since then the detector was massively
 996 improved, new setups were built: Kamiokande II, Super-Kamiokande. The latter is operating now
 997 as a far detector of the T2K experiment. The ultimate experience collected during the studies in
 998 Kamioka allows excellent physics performance.

999 There are many challenges in neutrino studies with water Cherenkov detectors. First of all, the
 1000 statistics is limited due to the small cross-section. To increase the number of events the detector
 1001 was enlarged several times from 3 kt (KamiokaNDE) to 50 kt (Super-Kamiokande). But the detec-
 1002 tion of Cherenkov light becomes an issue with larger tank. The intensity of such a light is quite low.

1003 Thanks to the hard work of the SK collaboration the water purity is remaining extremely high. The
 1004 transparency is very stable at the level of 100 meters. The other issue is photon detection itself.
 1005 The photo coverage of the active area surface is 40% aiming at the collection as many photons
 1006 as possible. Large 20-inch PMTs with high detection efficiency are used for it. The wavelength of
 1007 Cherenkov light is tending to the ultraviolet region, while the efficiency of the photocathodes is
 1008 quite low there. The light intensity decreases as λ^3 with the increasing of the wavelength, that's
 1009 why the excellent performance of the PMT is essential for the successful detector operation.

1010 The other challenge is a background suppression. The detector is placed in the mine in order
 1011 to reduce the flux of the cosmic rays. Though extremely high muons could reach the water tank.
 1012 Also, muons could be produced by the neutrino interactions in the rock close to the detector. The
 1013 Super-Kamiokande is divided into two volumes: inner and outer detectors. They are isolated for
 1014 the light, so the signal detection in the outer volume will explicitly indicate the out-of-tank particle
 1015 production. Only leptons produced in the inner detector are considered for the neutrino analysis.
 1016 The active volume is reduced with 2 m tolerance from each wall reducing the fiducial volume to
 1017 22.5 tons. It was done because the outer detector could fail to detect the external particle and the
 1018 part of the inner detector works as an additional veto. The vertex position reconstruction accuracy
 1019 is close to 2 meters, so if the particle is detected 2 m away from the wall we are quite sure that it
 1020 originates from the inner volume.

1021 The detector allows separating Cherenkov ring produced by muon and electron. Due to lighter
 1022 mass electrons are more subject to breaking radiation. Since the critical energy for the electrons in
 1023 water is tens MeV and the typical energy of the electrons produced by the T2K neutrinos is hun-
 1024 dreds MeV, we expect to see electromagnetic showers that will distort Cherenkov ring. The exam-
 1025 ples of the events are presented in Figure 4.13. The left image demonstrated a much less distorted
 1026 ring from the muon while the right image demonstrates the result of the electron showering. Up to
 1027 now the Super-Kamiokande separates these two topologies with the excellent purity of 99%. That's
 1028 extremely important for the oscillation experiment. The neutrino will produce the charged lepton
 1029 of the same flavor and we are studying a very rare process of the electron neutrino appearance.
 1030 That's why any confusion between muon and electron is extremely dangerous.

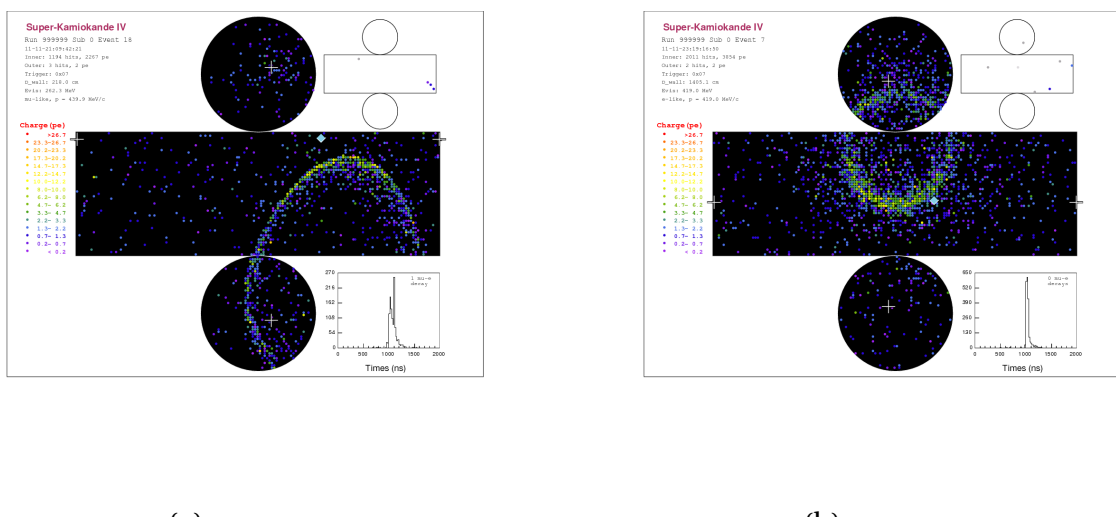


Figure 4.13: The event display of Cherenkov ring inside Super-Kamiokande detector: (a) ring from muon, (b) ring from electron.

1031 The Super-Kamiokande provides powerful shielding from the cosmic rays, but the atmospheric
 1032 neutrino could easily go through the rock and interacts inside the inner detector. That's how the
 1033 atmospheric studies are done, but for the T2K we need to distinguish neutrinos from the atmo-

1034 sphere and J-PARC accelerator. For this propose the timing information is the most useful one. As
 1035 mentioned in section 1 the beam is grouped in 8 bunches 19 ns width coming every 2 seconds.
 1036 The time synchronization between J-PARC and Super-Kamiokande allows us to select accurately
 1037 neutrinos that fall into bunches and suppress the atmospheric background that is uniform in time.
 1038 Thus the background is suppressed at the level of 8 orders.

1039

4

Analysis overview

1040

1041
1042**4.1**

Oscillation analysis

1043

1044
1045**a**

General overview

1046

1047

1048 As mentioned in the introduction the main goal of the T2K experiment is precise measure-
 1049 ments of the neutrino oscillation parameters and search for the CP-violation. This is done by
 1050 measuring the neutrino energy spectrum at the far detector and comparing it with the expecta-
 1051 tion without the oscillations. Spectra are divided into the neutrino flavor (muon and electron) and
 1052 sign, thus 4 spectra are the basic input for the oscillation analysis. Super-Kamiokande measures
 1053 neutrino energy in the assumption of the quasi-elastic interaction (Equation 4.5).

$$E_v^{rec} = \frac{m_f^2 - (m'_i)^2 - m_\ell^2 + 2m_i E_\ell}{2(m'_i - E_\ell + p_\ell \cos\theta_\ell)} \quad (4.5)$$

1054 where $E_b = 27$ MeV is binding energy for the Oxygen nucleus, $m'_i = m_i - E_b$, m_i and m_f are initial
 1055 and final nuclei mass respectively, m_ℓ , E_ℓ , p_ℓ , θ_ℓ are outgoing lepton mass, energy, momentum
 1056 and angle w.r.t neutrino beam respectively.

1057 Four neutrino spectra are essential for the minimal oscillation analysis, but the precision could
 1058 be dramatically improved with the near detector. ND280 is used for the constraints of the flux and
 1059 cross-section models.

1060 Despite neutrino production is well controlled the resulting flux could be slightly different from
 1061 the expectations. The possible reasons are not accurate predictions of the pion rescattering, meson
 1062 production multiplicity, interaction length, etc. The ND280 could constrain exactly the same off-
 1063 axis flux that will pass through Super-Kamiokande but before the oscillations. The measurements
 1064 are sampled in the neutrino flavor, sign and energy. The example of the prior and ND280 constrains
 1065 on the ν_μ flux are presented in Figure 4.14 (a).

1066 The neutrino interaction models are also tuned with the ND280 data. Different types of neu-
 1067 trino interactions are used for particular model parameters. For example, quasi-elastic interac-
 1068 tions (CCQE) are very sensitive to so-called axial quasi-elastic mass (M_A^{QE}), resonance produc-
 1069 tion (e.g. $\Delta^+ +$) is affected resonant axial mass (M_A^{RES}) so on. The detailed list of the various models used
 1070 and constrained is provided in [105]. The problem is that certain reactions could not be measured
 1071 independently. For example, neutrino could produce a resonance that will further decay into pion.
 1072 But the pion will be absorbed in the nucleus. Thus the reaction could not be distinguished from
 1073 the CCQE. To deal with this, we sample the neutrino interactions in ND280 not in the reactions
 1074 type, but in the “topologies”. Topology tells us what was observed in the detector, but not the ini-
 1075 tial neutrino reaction type. The observations in the ND280 are divided into CC interactions with

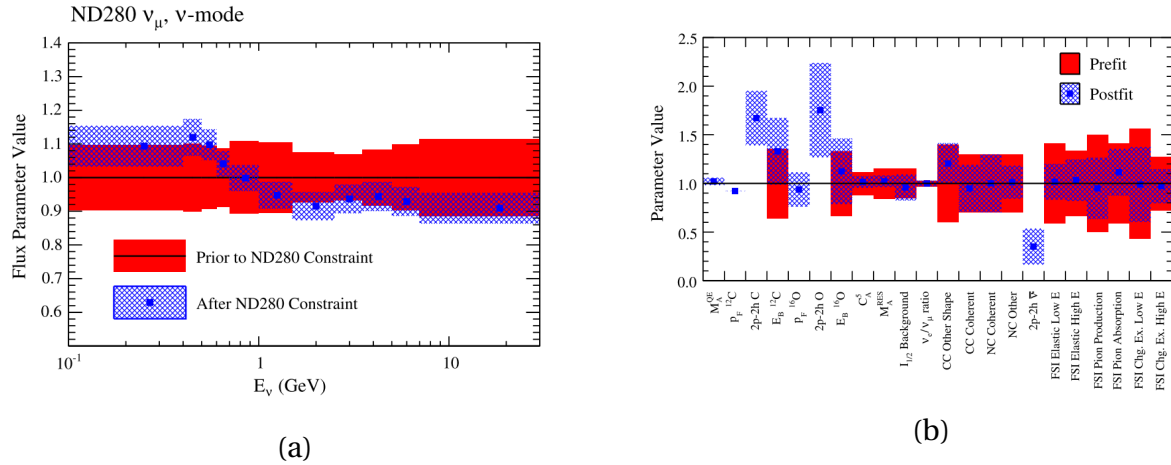


Figure 4.14: The priors (blue) and the results of the ND280 fit (red) for ν_μ (a) flux and (b) cross-section parameters. The T2K is operating in neutrino mode. Figure from [105].

no pions ($CC0\pi$), interactions with 1 pion ($CC1\pi$) and other CC ($CCOther$). The detection of the charged lepton is essential for all of these topologies as we are working with the charged current interactions. The examples of the $CC0\pi$ and $CC1\pi$ samples measured with ND280 are shown in Figure 4.15.

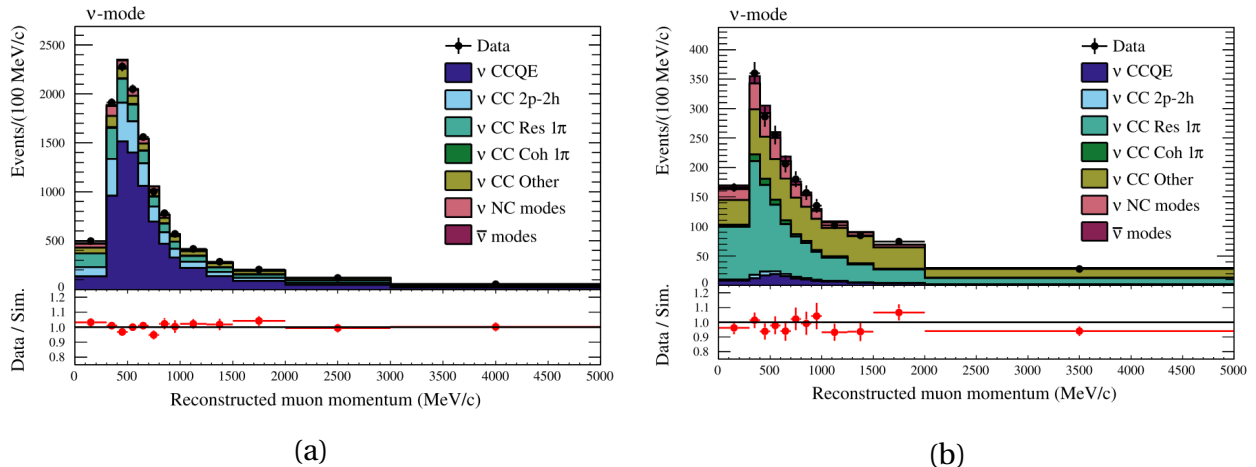


Figure 4.15: Data MC comparison for the (a) $CC0\pi$ and (b) $CC1\pi$ samples measured with the ND280 in the neutrino mode. Figure from [105].

The non-negligible contribution of the non-CCQE interactions in the $CC0\pi$ sample is extremely important. As mentioned above, SK reconstructs the neutrino energy in the CCQE assumption. There could be only lepton in the final state, but the reaction is not CCQE. It will lead to the completely wrong reconstructed neutrino energy and bias oscillation analysis a lot. That's why non-CCQE interactions should be precisely controlled. The $CC1\pi$ and $CCOther$ samples could help a lot with this, as they are dedicated to the detection of the non-elastic reactions.

b Analysis machinery

The scheme of the analysis workflow is presented in Figure 4.16. Different colors at the block-scheme represent the measurements (green), models (violet) and fit algorithms (blue).

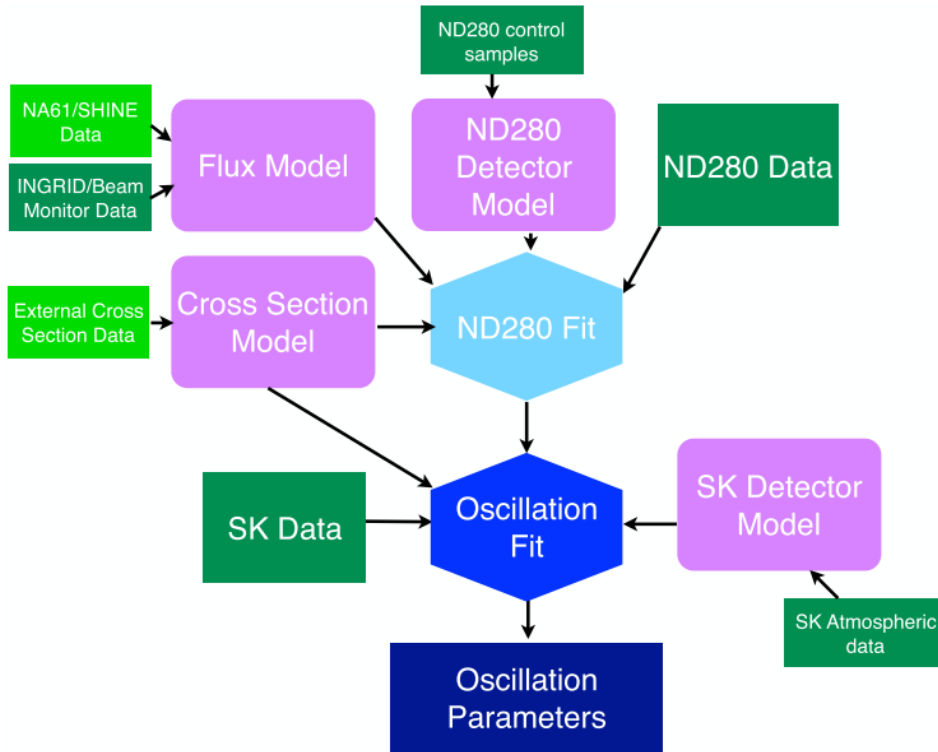


Figure 4.16: The scheme of the T2K oscillation analysis workflow. The measurements are presented in green (light — external, dark — T2K), the models are presented in violet and the fitter tools are presented in blue.

1091 The measurements start with the beamline monitors where the parameters of the proton beam
 1092 are estimated. Then the data from the NA61 experiment is used to estimate the meson production
 1093 in the target. The neutrino beam intensity and direction are monitored with the on-axis near de-
 1094 tector INGRID. All these results allow us to build the neutrino flux model.

1095 The near detector ND280 performs the measurements of the off-axis neutrino flux. The obser-
 1096 vations are sampled in the neutrino sign and the reaction topology: quasi-elastic, pion produc-
 1097 tion, deep inelastic. We use the results of other experiments as a prior estimation for the rate of
 1098 neutrino interactions. But there are plenty of the parameters in the model that could be tuned
 1099 precisely using all the samples collected in the ND280. Thus flux and the cross-section model are
 1100 tuned together with the ND280 control samples.

1101 The long history of the atmospheric neutrino measurements in Super-Kamiokande provides
 1102 accurate knowledge of the detector operation. This model is used together with the T2K events in
 1103 the SK for the final oscillation measurements. The spectrum of the observed electron neutrinos in
 1104 the far detector is presented in [Figure 4.17](#).

1105 As one could see the oscillation fit is the heart of the analysis. Three independent methods
 1106 were developed for the fit machinery.

- 1107 ➤ At the beginning, we perform the prefit using the data from both flux, near detector and
 1108 cross-section models to constrain the initial parameters of the neutrino beam before the
 1109 oscillations and precisely constrain the neutrino interactions model as well
- 1110 ➤ The first analysis is based on the Poisson statistics and constrains the oscillation parameters
 1111 with the likelihood minimization. It is using data binned in the lepton momentum and di-

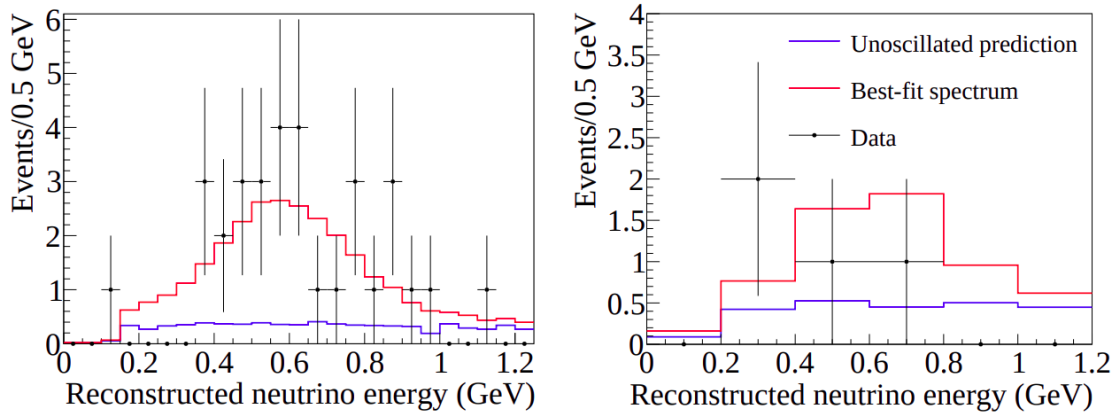


Figure 4.17: The spectrum of the electron neutrinos observed with the far detector comparing to the expectations without oscillation.

rection for the oscillation fit. This approach uses the prefit results and then fit the SK data to obtain the final result

- The second analysis although uses the minimization of the likelihood within Poisson statistics. But the samples are binned in the neutrino energy and lepton direction
- The final, Markov Chain approach is based on Bayesian statistics. Instead of using the near detector prefit and propagating it to the far detector the both detectors' samples are fit together. The oscillation parameters are estimated with a Markov chain method. The data samples are binned in the neutrino energy and lepton direction

The result is considered as robust only if all the methods are in a good agreement about the confidence/creditable intervals. The oscillation results are presented in Figure 4.18.

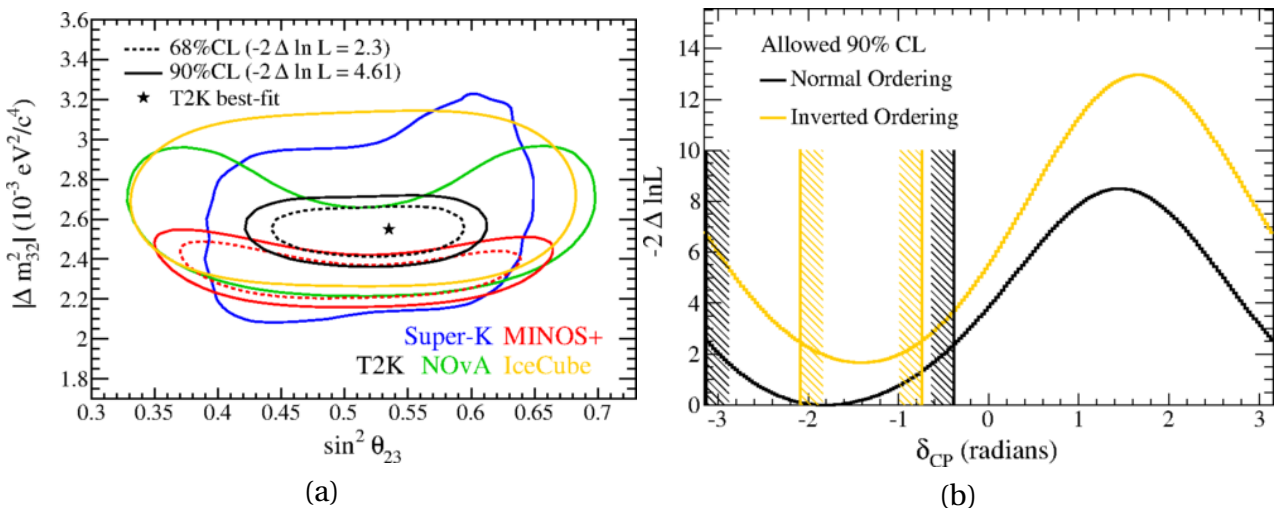


Figure 4.18: The oscillation results from the T2K experiment: (a) θ_{23} and Δm_{32}^2 constraints and (b) δ_{CP} constraints.

1122

1123

4.2 Neutrino cross-section measurements

1124 Alongside the oscillation analysis, T2K performs very precise measurements of the neutrino
 1125 cross-sections. The knowledge of the neutrino interactions' rates is essential for the oscillation
 1126 analysis as the most realistic theoretical model could be chosen. The ND280 provides an oppor-
 1127 tunity to study neutrino interaction with carbon, oxygen and iron with both neutrino and anti-
 1128 neutrino and with both flavors: muon and electron. The dominating sample in the ND280 is a
 1129 muon neutrino interaction with no pions in the final state. It's the main process for the T2K ener-
 1130 gies that's why it's studied pretty well [47]. Much more complicated analyzes are the interaction of
 1131 the electron neutrinos. The result of the comparison of the ν_e and $\bar{\nu}_e$ cross-section is presented in
 1132 Figure 4.19 [106].

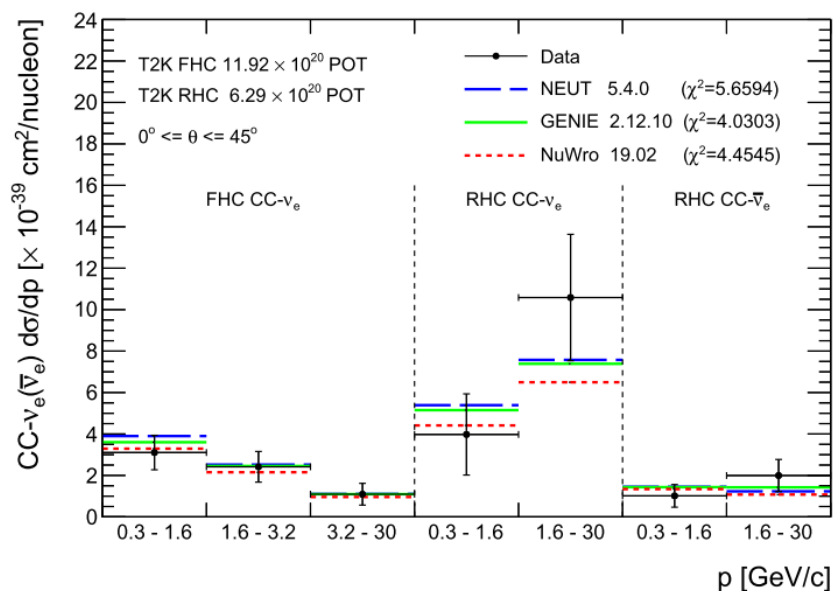


Figure 4.19: The result of the cross-section measurements in the ND280. Results for ν_e and $\bar{\nu}_e$ are compared against various theoretical models.

1134

Part II

1135

Heavy neutrino study

1136

1137

PROSPECTS IN T2K

1138 In the current work we study a possibility of the improvement of the constraints on the mixing
1139 elements of the HNL in the T2K experiment. The details about the experimental setup are de-
1140 scribed in the [chapter 4](#). The main feature of the experiment for the HNL search is very intensive
1141 proton beam providing by J-PARC accelerator. The beam operation is overviewed in the [section 1](#).
1142 The horn system allow to perform the analysis focusing positive or negative mesons from the pro-
1143 ton interactions. As mentioned in the [Neutrino mass](#), heavy neutrinos could be produced in the
1144 mesons decays. As a result there are two possible strategies of the HNL search:

- 1145 ➤ measurement of the meson decay kinematics. The effect is proportional to $|U_l|^2$;
1146 ➤ search for decay products of the heavy neutrino. As both HNL production and decay are
1147 proportional to $|U_l|^2$, the final effect $\propto |U_l|^4$.

1148 The schema of the T2K experiment is shown in [Figure 5.1](#). The muon monitor is the only in-
1149 strument that could measure the muons directly from the meson decay. In spite of its extreme
1150 usefulness for the neutrino beam intensity and direction measurements, it could not provide nec-
1151 essary precision for the search of the HNL through the detection of the muons from the meson
1152 decay. Thus the only way of the heavy neutrino study in the T2K is search for the HNL decays
1153 in the near detector complex. The near detector complex ([section 2](#)) consists of on-axis INGRID
1154 detector and off-axis ND280. The most precise analysis could be done with the the ND280's time
1155 projections chambers. As we are looking for the HNL decays in the neutrino beam the gaseous
1156 detectors will observe much less background from the neutrino interactions comparing to scin-
1157 tillators. There are phenomenological studies [107] that indicate the prospects of such analysis in
1158 the T2K experiment.

1159 With the 30 GeV proton beam mainly pions are produced with some fractions of kaons. The
1160 comparison of the neutrino flux from different parent particles are presented in [Figure 5.2](#). As
1161 we want to study the maximum range of the HNL mass we will concentrate on the kaon decays.
1162 Thus we will be able to study the mass region up to $493 \text{ MeV}/c^2$. The overview of the HNL nature
1163 including the relation with the Standard Model particles is presented in [chapter 2](#). The particular
1164 production and decay modes of the heavy neutrino masses that are available for the analysis in our
1165 experiment are summarized in the kinematic scheme in [Figure 5.3](#) with specific HNL mass region
1166 for each of them.

1167 As one can see from the scheme in our study we will concentrate on the two and tree body
1168 decays of the heavy neutrino.

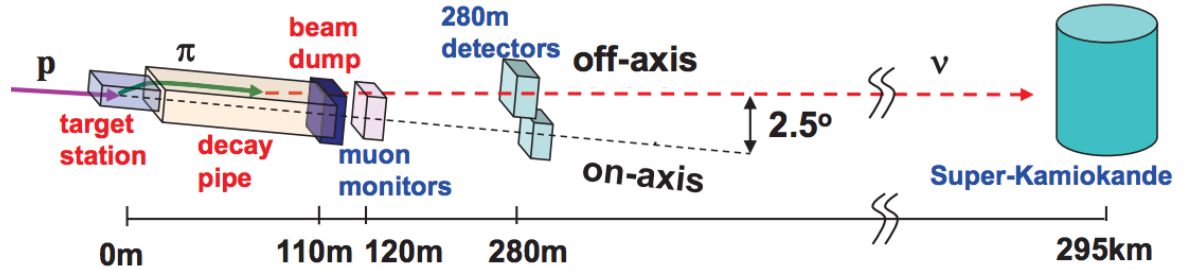


Figure 5.1: A schematic view of the neutrino beamline and the detectors in the T2K experiment.

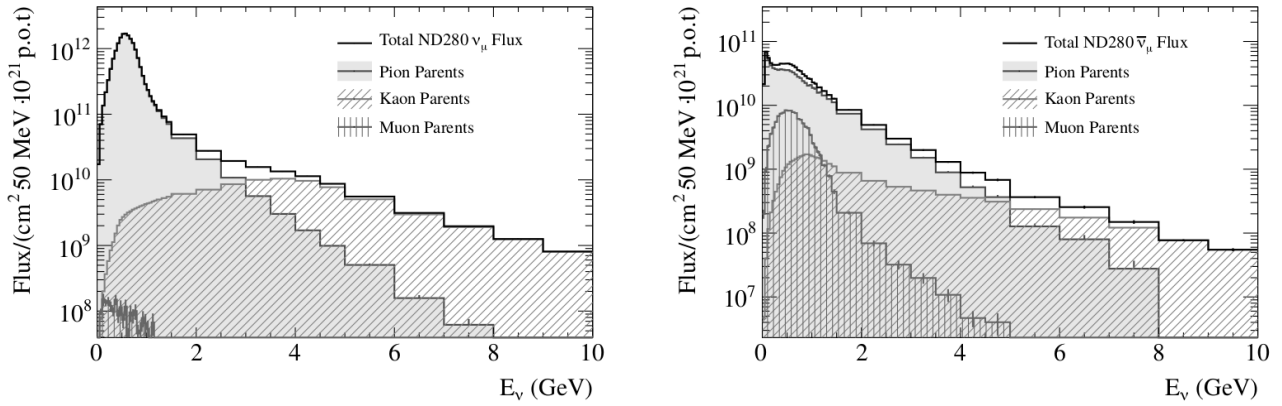


Figure 5.2: The muon neutrino and anti-neutrino flux prediction at the ND280 broken down by the neutrino parent particle type.

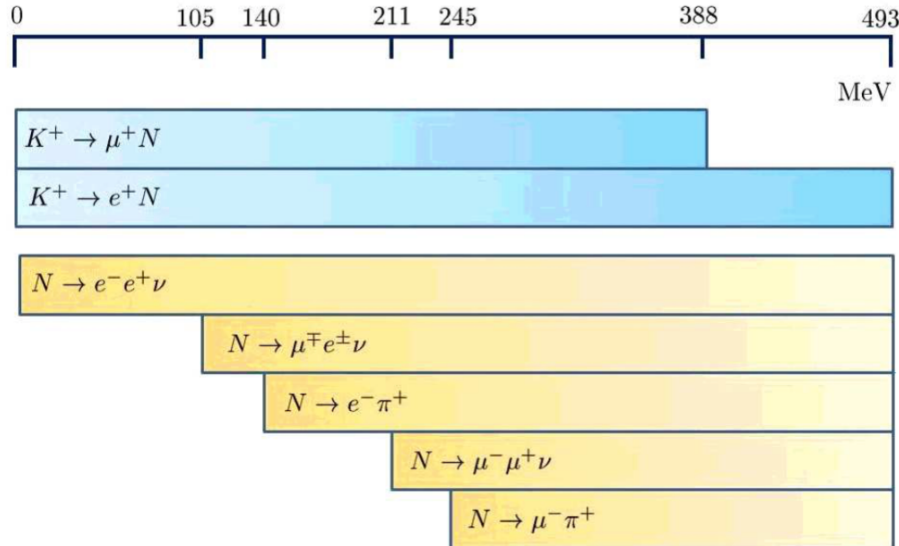


Figure 5.3: Summary of the production and detection processes of the heavy neutrino available for the analysis with the ND280. The horizontal axis corresponds to the HNL mass

$$N \rightarrow \ell^\pm \pi^\mp \quad (5.1)$$

$$N \rightarrow \ell^\pm \ell^\mp \nu \quad (5.2)$$

1169 We would like to highlight the importance of the study of a HNL dimuon decay mode: $N \rightarrow$
 1170 $\mu\mu\nu$. This decay has charge and neutral current contributions shown in Fig. 5.4 (from [108]).

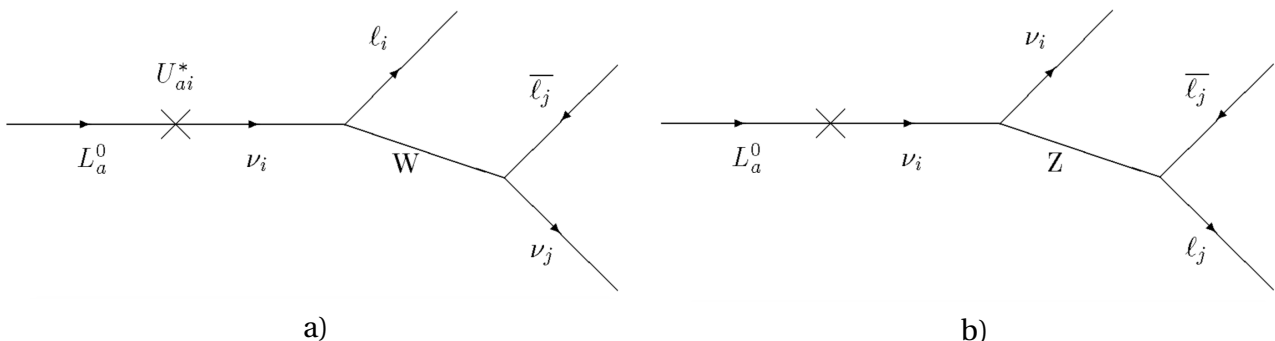


Figure 5.4: Feynman diagrams for the HNL decay $N \rightarrow \mu\mu\nu$ via charged (a) and neutral (b) current.

1171 If the HNL decays via NC, any type of the active neutrino could be produced (ν_e, ν_μ, ν_τ), so we
 1172 can study the mixing element including $|U\tau|$. This is interesting as the upper limits on this element
 1173 are rather high (Figure 2.6).

1174 The T2K experiment uses neutrino beam from π^\pm and K^\pm decays. In our study a search of HNL
 1175 from both K^+ and K^- decays is carried out in order to increase sensitivity because of the larger
 1176 statistics. We assume the Majorana nature of a HNL, this allows to study decays of K^+ , K^- and
 1177 both decay modes of a heavy neutrino to $\ell^\pm\pi^\mp$.

1178 As we focus on search of the HNL decay there are two analysis methods:

- 1179 ➤ search for a peak in the HNL candidate invariant mass spectrum
- 1180 ➤ search for a rare event in a low background environment

1181 The first one requires applying some simple cuts and then study difference between data and
 1182 MC estimation with a peak shape. We need a rather accurate background prediction for this method.
 1183 Also invariant mass resolution is one of the most important issue. We have studied the possible
 1184 resolution for the HNL signal samples. The events that pass all the cuts described in the section 2
 1185 give as the reconstructed mass distribution. The examples of such distribution are presented in
 1186 Figure 5.5. The resolution of the invariant mass reconstruction on the HNL mass is shown in Figure 5.6.
 1187 As one can see, RMS is quite large $\approx 70\text{MeV}$. The main background processes for the HNL
 1188 decay are interactions of the active neutrinos. In near detector there are three TPCs filled with
 1189 argon gas. The cross sections of the neutrino interactions in gas are not studied well. Studies of
 1190 these events were performed by ArgoNeuT group [109]. In our momentum region ($\approx 1\text{GeV}$) the
 1191 uncertainties are relatively large. Other background processes can be K^0, Λ, η decays, deep inelas-
 1192 tic neutrino scattering, etc. (subsection 2.3) that are also poorly studied. Because of this we can
 1193 not provide necessary accuracy of the background prediction and the method of the invariant
 1194 mass peak search can not be applied.

1195 The second method requires significant background suppression. Usage of the gaseous TPC
 1196 will provide very few neutrino interactions in the fiducial volume comparing to the scintillator
 1197 detectors. Also the reconstruction of the heavy neutrino momentum direction could help a lot
 1198 with the active neutrino events rejecting. We expect the HNL to be extremely collinear to the beam,
 1199 while $\mu\pi$ pairs from the neutrino interactions will be distributed in the much wider angle. The
 1200 details of the cut sequence are presented in the section 2.

1201 Thus we could perform a search of a few signal events in an extremely low background envi-
 1202 ronment (≈ 1). The details of the used statistical approach could be found in section 4.

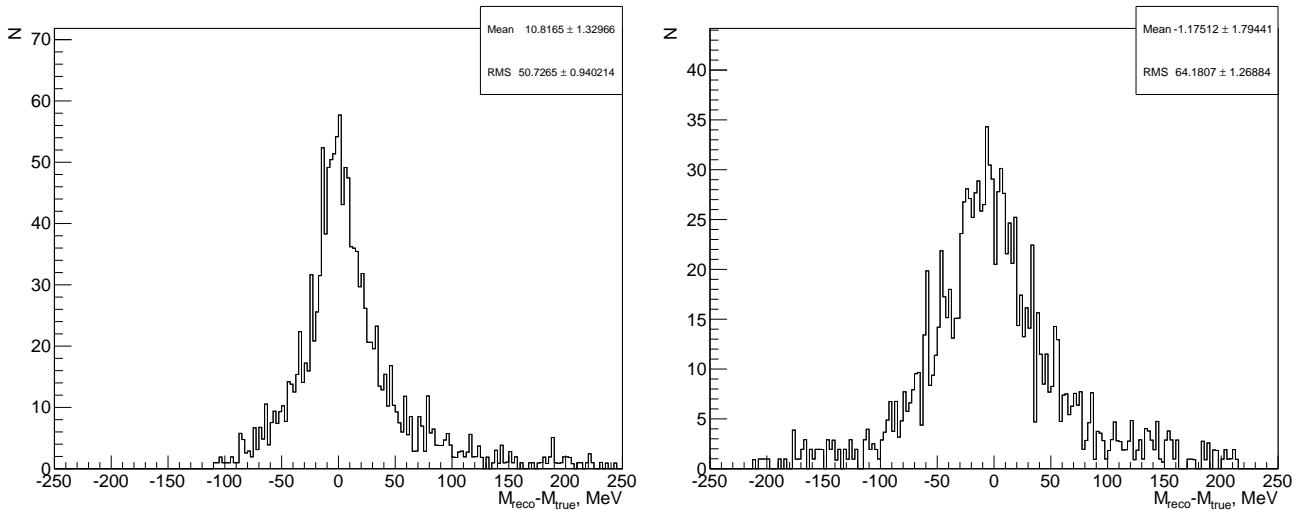


Figure 5.5: HNL invariant mass resolution. Left is for $M_{\text{HNL}} = 360$ MeV, right is for $M_{\text{HNL}} = 480$ MeV for the $\mu\pi$ mode.

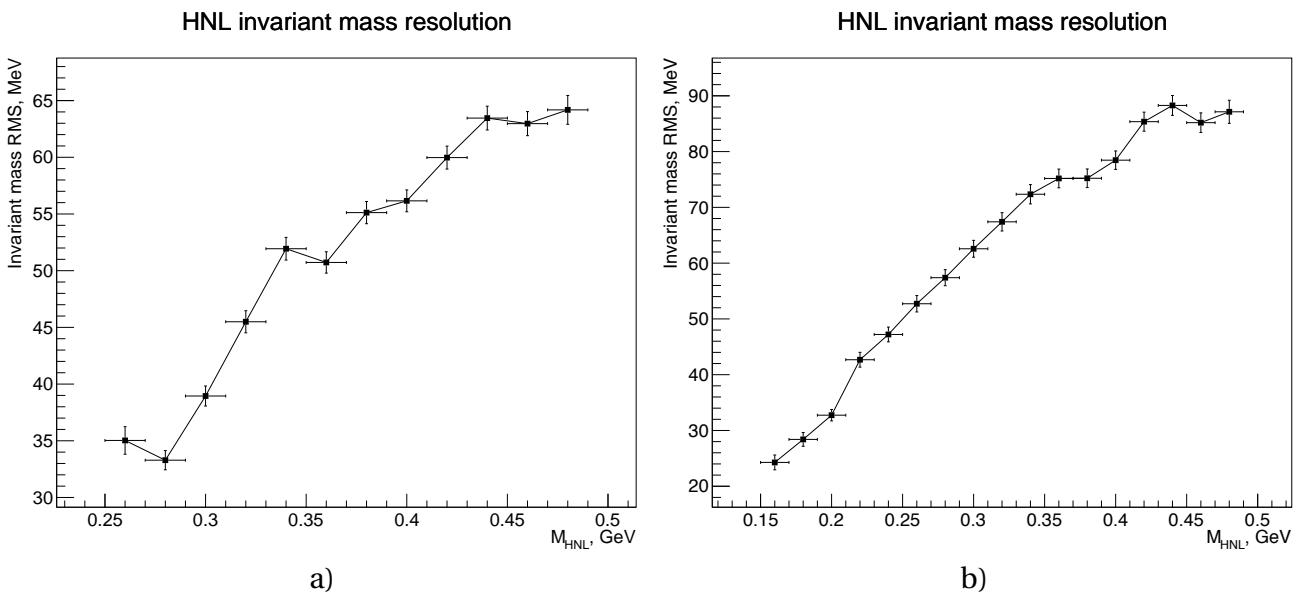


Figure 5.6: HNL invariant mass resolution (RMS) dependence on the HNL mass for (a) $N \rightarrow \mu\pi$ mode and (b) $N \rightarrow e\pi$ mode.

1203

1204

HNL FLUX SIMULATIONS

1205 First of all we need to estimate the sensitivity to the mixing elements in our experiment. So we need
1206 to evaluate the HNL flux at the ND280. We decided to use the results of the neutrino flux simulation
1207 that was developed for the oscillation analysis within the T2K experiment. With this simulation
1208 we have all the information about the neutrinos entering the ND280 and their parent particles.
1209 Because of the kinematics the phase space of the meson decay into HNL is more limited than
1210 the decay into massless neutrino. E.g. the maximum angle of the HNL direction with respect to the
1211 parent meson direction is lower comparing to the massless neutrino case. Thus if we consider only
1212 mesons that could produce neutrino entering ND280 and omit all the others, we will definitely take
1213 all the possible HNL parent particles.

1214 For the heavy neutrino simulation we take the particular meson decay and reweight is tak-
1215 ing into account new kinematic and the branching ratios. Thus we will obtain the heavy neutrino
1216 spectrum in our detector.

1217

1 T2K flux simulation

1218
1219 The accurate prediction of the neutrino flux is extremely important for the precise oscillation
1220 analysis. That's why the T2K collaboration have spent great effort on tuning the flux simulation
1221 in the most accurate way [101]. All the elements of the neutrino beamline (section 1) are taken
1222 into account. The most tricky part is the evaluation of the meson production through the proton
1223 interactions in the carbon target. To reduce the systematic uncertainties the measurements from
1224 the NA61/SHINE experiment are used [110].

NA61/SHINE experiment

The NA61/SHINE (SPS Heavy Ion and Neutrino Experiment) [111] is a multi-purpose facility at CERN that operates at Super Proton Synchrotron (SPS) in the North Area of CERN. The main physics goals are:

- study the properties of the onset of deconfinement and search for the critical point of strongly interacting matter which is pursued by investigating p+p, p+Pb and nucleus-nucleus collisions,
- precise hadron production measurements for improving calculations of the initial neutrino beam flux in the long-baseline neutrino oscillation experiments as well as for more reliable simulations of cosmic-ray air showers.

The detector operates at the fixed target made from different materials (carbon, beryllium, scandium). The detector scheme is presented in Figure 6.1. The setup consists of the trigger system, TPC tracking system with superconducting magnets, time of flight detectors and Projectile Spectator Detector (PSD).

For the T2K propose the experiment perform the measurements of the hadron interaction multiplicities with a proton beam and a carbon T2K-replica target. This data allows to constrain the neutrino production at the T2K much more precisely.

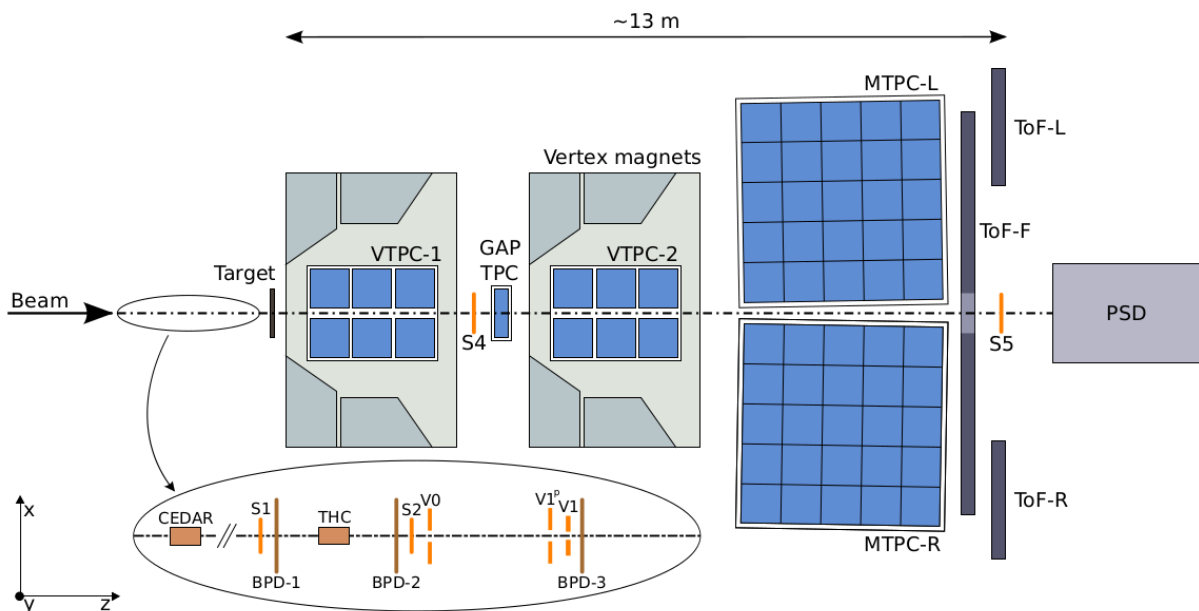


Figure 6.1: The scheme of the NA61/SHINE experiment.

1226 The flow diagram of the neutrino flux simulation is shown in Figure 6.2.

1227 The proton beam spatial distribution and divergence are measured in the beamline monitors.

1228 The FLUKA generator is used to perform the simulation of the hadron interaction with the target
1229 and a baffle. Incident protons are set at known position and with kinetic energy of 30 GeV. The
1230 information of the generated particles that exited the simulated volume is stored. The next step
1231 is a JNUBEAM generator that takes the information about the particles from the previous step
1232 and tracks them through the horns and helium vessel, decay volume and surrounding concrete
1233 until the decay or the kinetic energy drop down below the threshold (10 MeV). At this step π^\pm , K^\pm ,

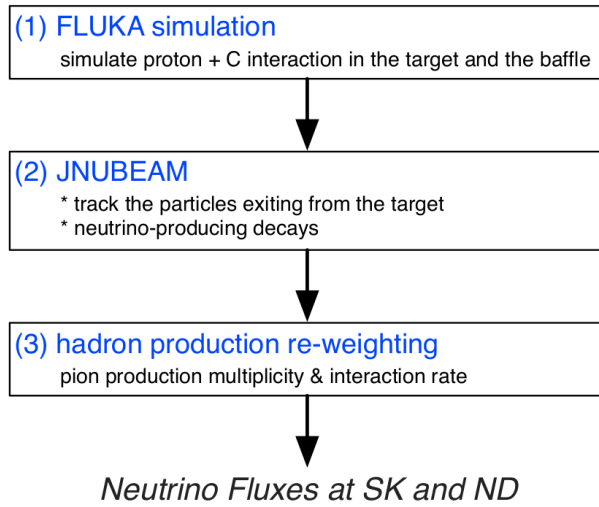


Figure 6.2: The neutrino flux prediction flow

1234 K_L^0 and μ^\pm decays are considered as neutrino sources. In order to save the computing time, the
 1235 daughter neutrino is pointing towards the detector plane and the appropriate kinematic weight is
 1236 assigned to the event.

1237 After such simulation chain is performed and the outgoing neutrino is saved the hadronic
 1238 chain in each event is reweighted based on the hadron interaction measurements. In our studies we are particularly interested in the kaon production. The generated kaon phase space and the
 1239 coverage of the NA61 measurements are presented in Figure 6.3.
 1240

1241 After the reweighing of the hadron chains the total accuracy of the prediction is evaluated [101].
 1242 The main systematic errors come from the hadronic interactions, primary beam alignment, horn
 1243 current and magnetic field. The resulting uncertainty of the neutrino flux predictions are shown in
 1244 Figure 6.4.

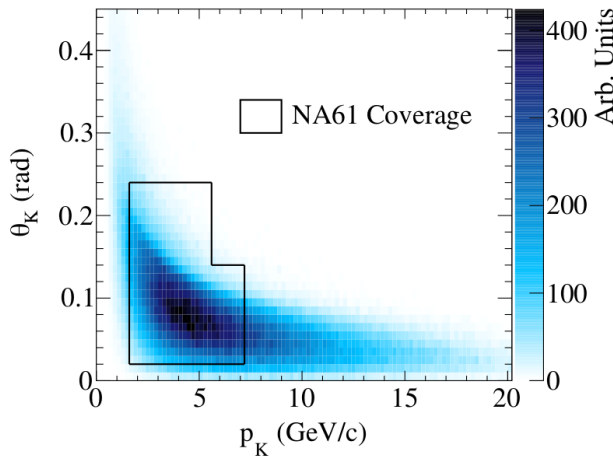


Figure 6.3: The phase space of positive kaons contributing to the predicted neutrino flux and the regions covered by the NA61/SHINE.

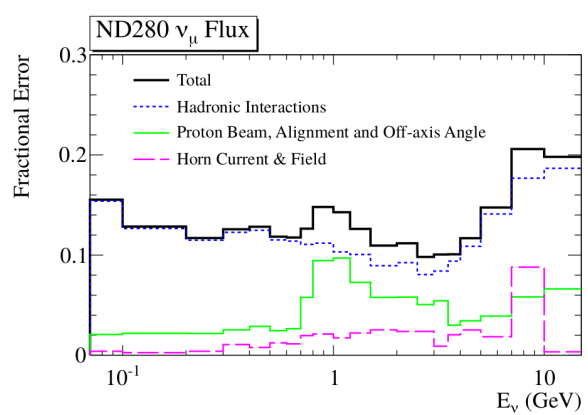


Figure 6.4: Fractional errors for the neutrino (left) and anti-neutrino (right).

1245

2 HNL production

1246

1247 For the propose of our study we would like to reweight the kaons decays based on the new
 1249 kinematics and branching ratios. But we want to keep all the fine-tuning described in the previous
 1250 section in order to keep the uncertainties as small as possible. Looking at the Figure 6.2, we would
 1251 like to change “(2) JNUBEAM: neutrino-producing decays”, but to keep everything else at place.
 1252

Every neutrino event in original files has a weight, which was calculated as

$$\text{weight}_{K\mu 2} = \text{scale}_{POT} \cdot \text{weight}_{geom} \cdot P_{\text{save}}^{-1} \cdot Br_{K\mu 2}, \quad (6.1)$$

1253 where

- 1254 ➤ scale_{POT} — 10^{21} POT normalization;
- 1255 ➤ weight_{geom} — probability of neutrino getting to the certain point of the detector plane,
 1256 which was selected randomly;
- 1257 ➤ P_{save}^{-1} — probability to save event. The energy spectrum has quite long tail and we want to
 1258 keep its shape precisely. For this we save relatively more events in the tail with respect to the
 1259 min peak. The appropriate weight is assigned to each event;
- 1260 ➤ $Br_{K\mu 2}$ — branching of $K \rightarrow \mu\nu_\mu$ decay.

1261 For the HNL we need to save scale_{POT} and P_{save}^{-1} but recalculate weight_{geom} and decay branch-
 1262 ing, so the weight of HNL event is

$$\text{weight}_{K \rightarrow \ell + N} = \text{weight}_{K\mu 2} \cdot \frac{\text{weight}_{geom,new}}{\text{weight}_{geom,old}} \cdot \frac{Br_{K \rightarrow \ell + N}}{Br_{K\mu 2}}, \quad (6.2)$$

1263 where $\text{weight}_{geom,old}$ is calculated applying $M_{HNL} = 0$ and $Br_{K \rightarrow \ell + N}$ is computed according
 1264 to [69]. The mixing element is just a multiplier and we assume it is equal to 1.

1265 The new branching ratio is calculated according to [69]:

$$Br(K \rightarrow \ell + N) = \frac{G_F^2 V_{us}^2 f_K^2 M_K M_{HNL}^2}{8\pi\hbar} \left(1 - \frac{M_{HNL}^2}{M_K^2} + \frac{2M_\ell^2}{M_K^2} + \frac{M_\ell^2}{M_{HNL}^2} \left(1 - \frac{M_\ell^2}{M_K^2} \right) \right) \\ \sqrt{\left(1 + \frac{M_{HNL}^2}{M_K^2} - \frac{M_\ell^2}{M_K^2} \right)^2 - \frac{4M_{HNL}^2}{M_K^2} \cdot \tau_K}, \quad (6.3)$$

1266 where

- 1267 ➤ G_F — Fermi constant,
- 1268 ➤ V_{us} — a CKM matrix element,
- 1269 ➤ M_ℓ and M_{HNL} — the lepton and the HNL masses,
- 1270 ➤ M_K, f_K, τ_K — kaon mass, form-factor, lifetime respectively.

1271 HNL enters the detector front plane randomly. The geometry weight is calculated as a probabil-
 1272 ity of a daughter particle to have a momentum with a certain angle θ w.r.t. the parent momentum.
 1273 Modifying

$$\text{weight}_{geom,new} = \text{weight}_{geom,lab} = \frac{p_{lab} E_{cm}}{p_{cm}^2} \cdot \text{weight}_{geom,cm} \\ \text{weight}_{geom,cm} = \frac{1}{4\pi} \delta(p - p_{cm}) \quad (6.4)$$

1274 we finally got

$$weight_{geom,lab} = \frac{1}{4\pi} \frac{p_{lab}E_{cm}}{p_{cm}^2} \frac{\cos\theta_{lab} \left(\beta/\beta_{lab} \pm \sqrt{1 + \gamma^2 \left(1 - (\beta/\beta_{lab})^2 \right) \tan^2\theta_{lab}} \right)}{\gamma \left(1 - \beta^2 \cos^2\theta_{lab} \right)}. \quad (6.5)$$

1275 Here we assume that the HNL's lifetime is rather large enough to reach the ND280. There are
1276 two reasons for such assumption:

- 1277 ➤ if the HNL mean free path is shorter, it will dramatically reduce the HNL flux at ND280 and
1278 the sensitivity will be rather poor;
- 1279 ➤ short lifetime doesn't allow to calculate probability of the HNL decay in TPC like [Equation 6.7](#)
1280 and make study more complicated, because life time τ depends on mixing element

1281 From the cosmology [69] we have an upper bound on the HNL lifetime $\tau < 0.1s$, which is mainly
1282 based on the baryogenesis models. So for the current analysis we have the HNL lifetime region
1283 $1\mu s < \tau < 0.1s$ which is wide enough. An estimation of the corresponding mean free path of the
1284 HNL gives $\Lambda_{HNL} = c\beta\gamma\tau \gg 280m$.

1285 To cross-check our kinematic model we compare the HNL spectra for $M_{HNL} = 0$ with the active
1286 neutrino spectrum from $K\mu 2$ and make sure that they are identical. After performing modeling of
all kaon decays we get the HNL spectra at the ND280 entrance plane ([Figure 6.5](#)).

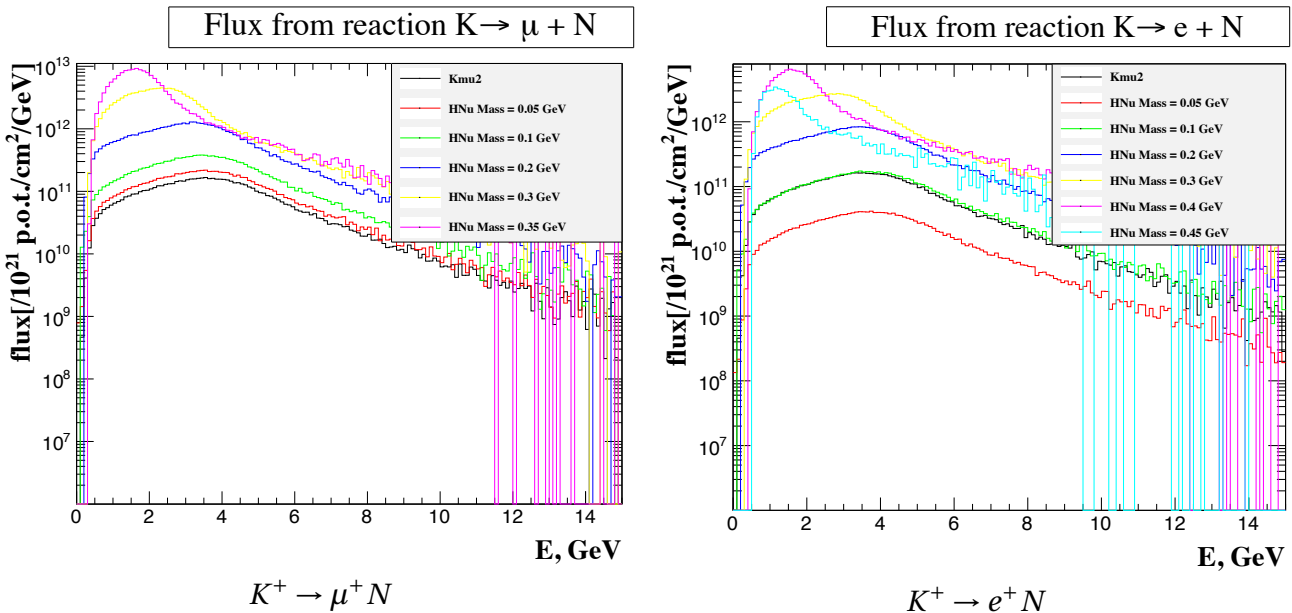


Figure 6.5: HNL energy spectra at the ND280 front plane for two modes: $K^+ \rightarrow \mu^+ N$ and $K^+ \rightarrow e^+ N$ for the different HNL masses.

1287 There are two effects, that cause the flux difference comparing to the active neutrino flux
1288 (Equation 6.2). The first one is “massive” kinematic of the parent meson decay. This correction
1289 is calculated according to [Equation 6.5](#). This impact is shown in [Figure 6.6](#). The branching ratio is
1290 assumed equal to 1.

1292 The second effect is the modification of the branching ratio of the kaon decay. It is calculated
1293 according to [Equation 6.3](#). The branching ratio dependence is shown in [Figure 6.7](#). Notice that it
1294 could be larger than 1 as the mixing element is considered 1, in reality it will reduce the branching
1295 ratio below the level of one.

1296 The difference of the time of flight for the active neutrino and HNL is described in the analysis
1297 section 1 chapter 7.

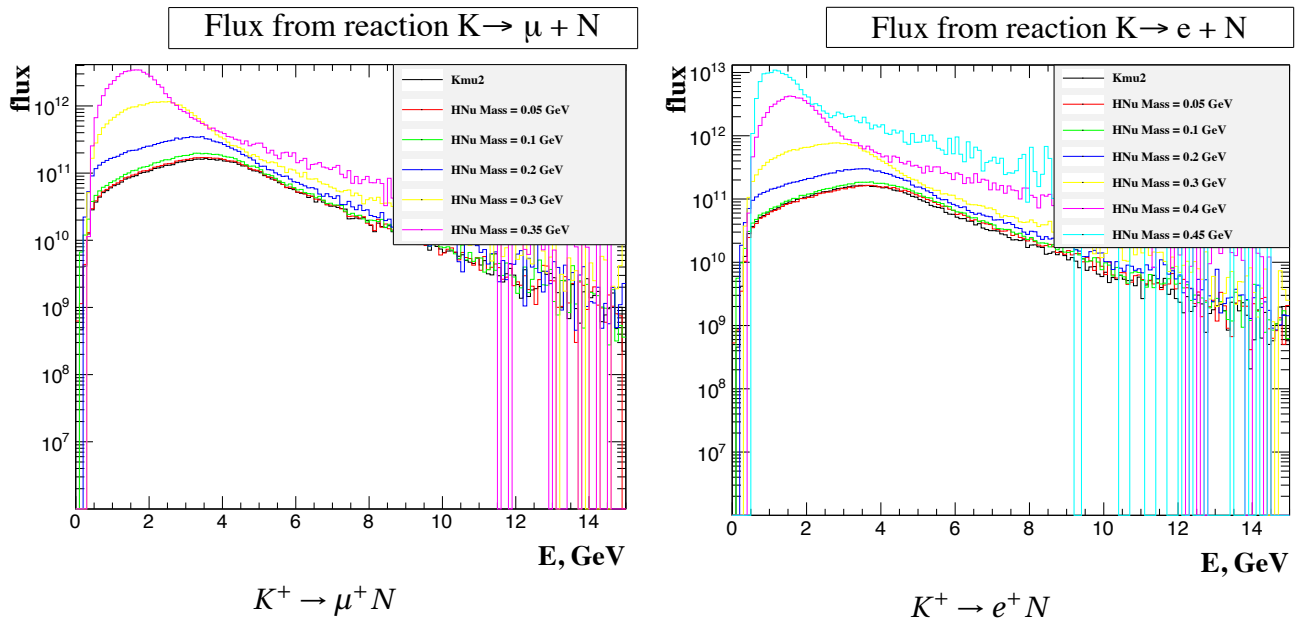


Figure 6.6: HNL spectra at the ND280 front plane for two modes and for the different HNL masses assuming the branching ratios equal to 1.

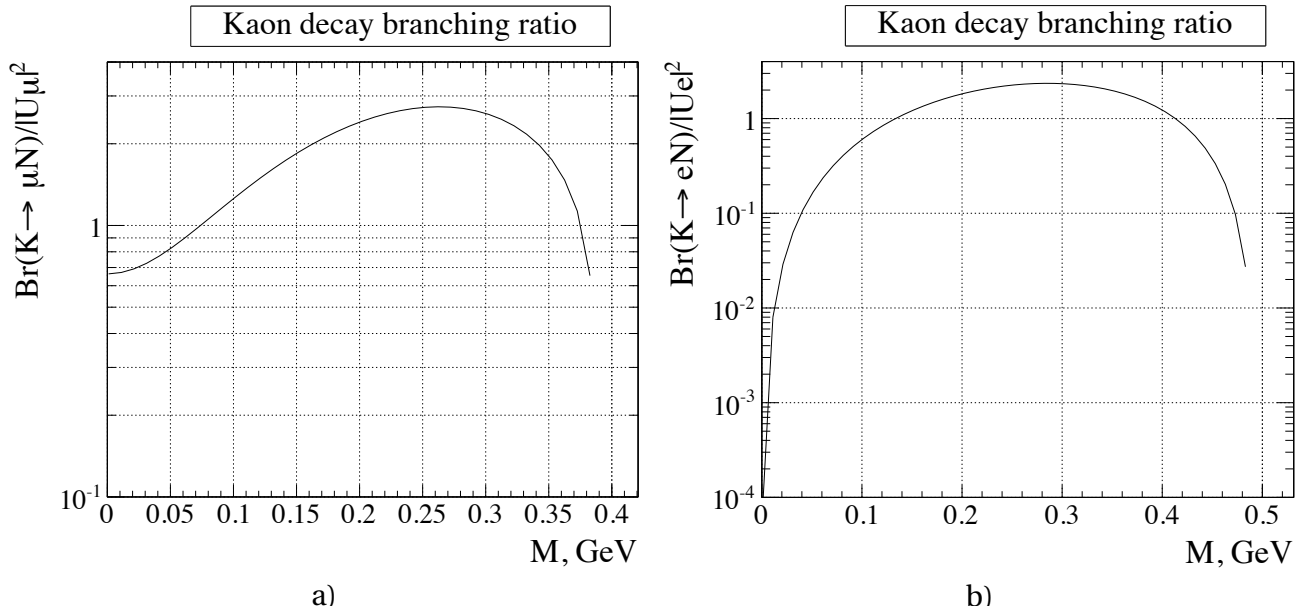


Figure 6.7: Kaon decay branching ratio divided into the mixing element for two modes: (a) $K \rightarrow \mu N$ and (b) $K \rightarrow e N$.

1298 Since we study both K^+ and K^- modes we compare HNL fluxes from both parent particles. The
 1299 flux of HNL from K^- decays is nearly three times lower than one from K^+ decays. It was expected
 1300 since the cross section of K^- production is approximately tree times lower.

1301

3 HNL decays

1302 From the spectra of the heavy neutrinos, we can estimate the number of events from HNLs'
 1303 decays and a sensitivity to mixing elements. As already described we just need the number of ex-

1306 pected signal events. Number of HNL decays is

$$N_{decays} = \phi(HNL/10^{21} p.o.t./cm^2) \cdot S_{det} \cdot P_{decay}^{TPC} \cdot Br_{mode}, \quad (6.6)$$

1307 where

1308 ➤ $\phi(HNL/10^{21} p.o.t./cm^2)$ — the HNL flux per $10^{21} POT$ per cm^2 ;

1309 ➤ S_{det} — area of the ND280 front plane;

1310 ➤ P_{decay}^{TPC} — the probability of a HNL decay in one of 3 TPCs;

1311 ➤ Br_{mode} — branching of a current decay mode.

1312 The decay probability between two points with coordinates z_1 and z_2 , assuming large mean free
1313 path, is

$$P_{decay}(z_2 - z_1) = \exp\left(-\frac{z_1}{c\beta\gamma\tau}\right) - \exp\left(-\frac{z_2}{c\beta\gamma\tau}\right) \approx \frac{z_2 - z_1}{c\beta\gamma\tau} \quad (6.7)$$

1314 where τ is HNL lifetime. Taking into account that

$$Br_{mode} = \frac{\Gamma_{mode}}{\Gamma_{total}} = \Gamma_{mode} \cdot \tau, \quad (6.8)$$

1315 finally have

$$N_{decays} = \phi(HNL/10^{21} p.o.t./cm^2) \cdot \frac{V_{FV}}{c\beta\gamma} \cdot \Gamma_{mode}, \quad (6.9)$$

1316 where V_{FV} is a sum of the fiducial volumes of 3 TPC's. The decay width is calculated according
1317 to [108, 69]. For 2-body decay we have

$$\begin{aligned} \Gamma(N \rightarrow \pi^+ \ell_\alpha^-) &= \frac{|U_\alpha|^2}{16\pi} G_F^2 |V_{ud}|^2 f_\pi^2 M_{HNL}^3 \left(\left(1 - \frac{M_\ell^2}{M_{HNL}^2}\right)^2 - \frac{M_\pi^2}{M_{HNL}^2} \left(1 + \frac{M_\ell^2}{M_{HNL}^2}\right) \right) \\ &\times \sqrt{\left(1 - \frac{(M_\pi - M_\ell)^2}{M_{HNL}^2}\right) \left(1 - \frac{(M_\pi + M_\ell)^2}{M_{HNL}^2}\right)} \end{aligned} \quad (6.10)$$

1318 where

1319 ➤ ℓ means lepton,

1320 ➤ G_F — Fermi constant,

1321 ➤ f_π — pion form-factor,

1322 ➤ V — CKM matrix element.

1323 The dependence of the decay width on the HNL mass is shown in Figure 6.8.

1324 Based on the known number of expected decays we could evaluate the sensitivity of our exper-
1325 iment to the mixing elements. This estimation will be done for the optimistic scenario of the 100%
1326 efficiency, no background and no systematic uncertainties. According to [112] the 90% C.L. could
1327 be set with 0 events observed and 2.3 events expected. As the HNL flux $\phi \propto |U|^2$ and the decay
1328 width $\Gamma_{mode} \propto |U|^2$:

$$|U|_{limit}^4 \times N_{decays} = 2.3 \quad (6.11)$$

1329 Thus the limit on the squared mixing element will be put with:

$$|U|_{limit}^2 = \sqrt{\frac{2.3}{N_{decays}}}, \quad (6.12)$$

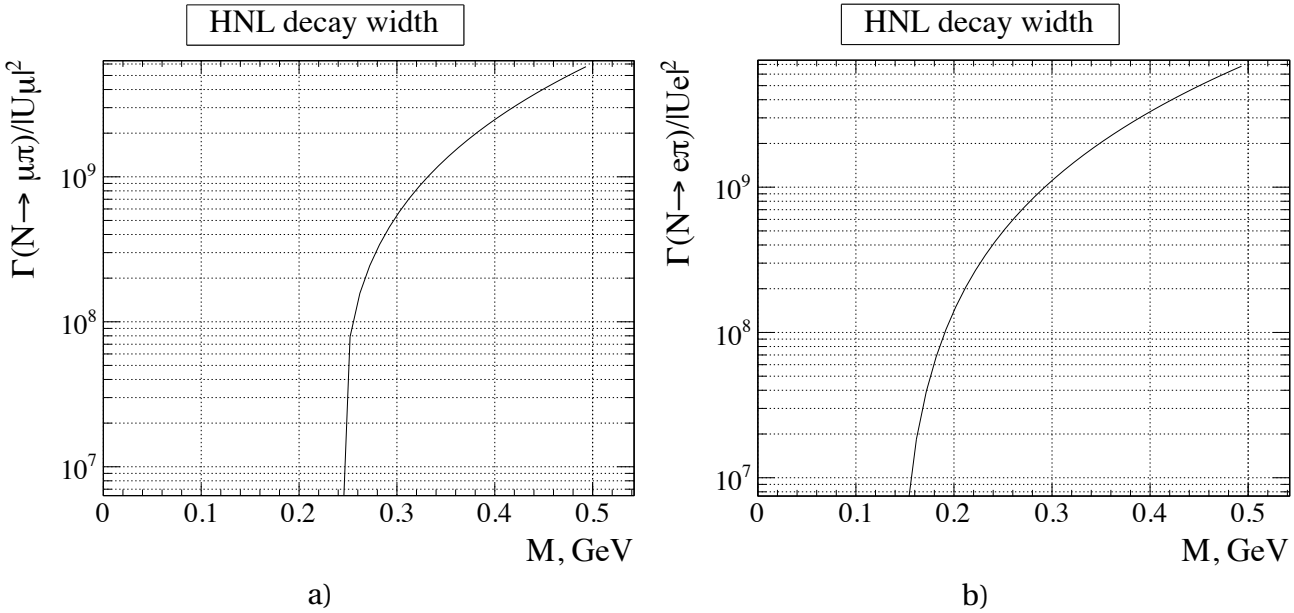


Figure 6.8: HNL decay width for two modes: (a) $N \rightarrow \mu\pi$ and (b) $N \rightarrow e\pi$ divided into the mixing element.

1330 The sensitivity of our experiment for two body decays is shown in Figure 6.9, Figure 6.10, in green.
 1331 It's compared with current limits from PS191 [80] (in red) and Asaka et al prediction [107] (in blue).

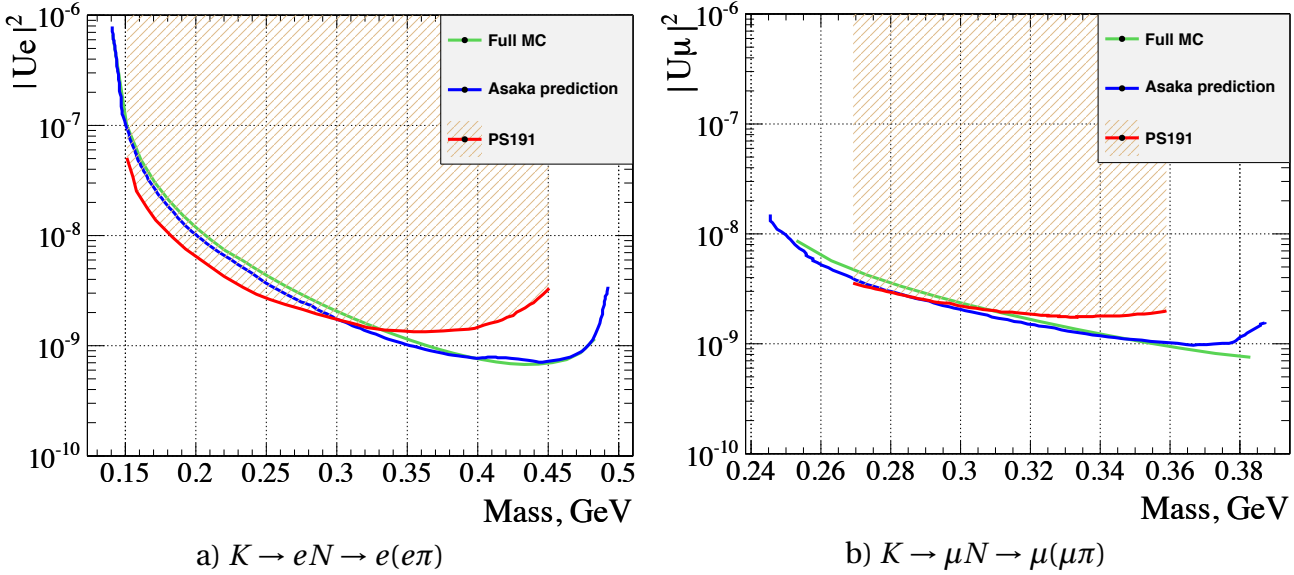


Figure 6.9: Sensitivity of T2K to mixing element for two body decay modes for $10^{21} POT$. The detection efficiency of 100% and no background are assumed.

1332
 1333 Three body decays of HNL were also studied. Possible improvement over the PS191 results is
 1334 worse than for 2-body modes, the background for such events seems to be much larger due to
 1335 the isotropic distribution of the charged daughter particles. In our study we will concentrate on
 1336 2-body decays and $N \rightarrow \mu\mu\nu$ mode. Three body sensitivity is shown in Figure 6.11 and Figure 6.12.
 1337 An important 3-body mode is $K^+ \rightarrow e(\mu^-\mu^+\nu_{e,\mu,\tau})$ because $\ell\bar{\ell}$ pairs can be produced together
 1338 with any kind of the active neutrino due to the NC process [108]. The mixing element for this
 1339 process looks like $|U_e| \sqrt{|U_e|^2 + |U_\mu|^2 + |U_\tau|^2}$. Assuming $|U_e|^2 \gg |U_\mu|^2$, we can get some constraints

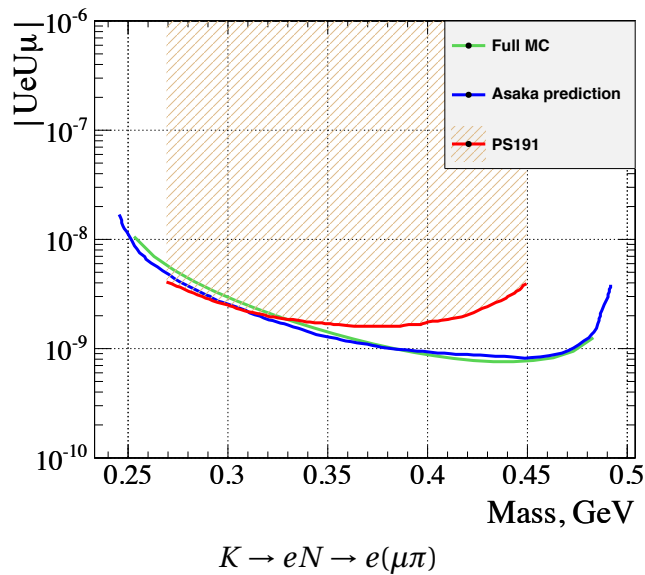


Figure 6.10: Sensitivity of T2K to mixing element for two body decay modes for $10^{21} POT$. The detection efficiency of 100% and no background are assumed.

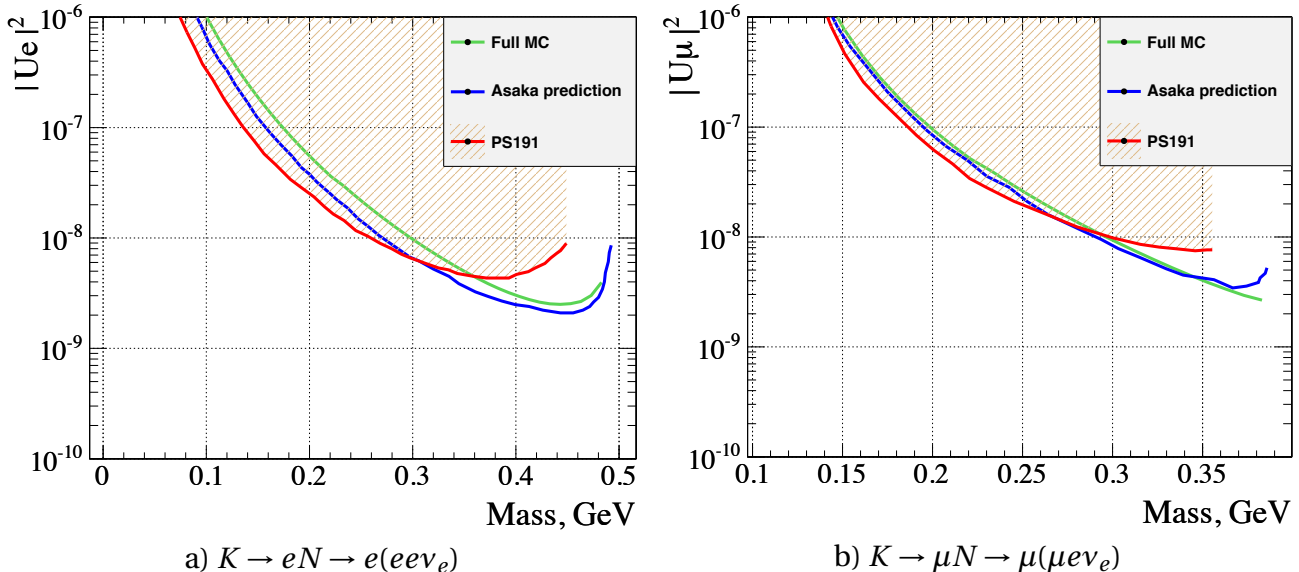


Figure 6.11: Sensitivity of T2K to mixing element for three body decay modes for $10^{21} POT$. The detection efficiency of 100% and no background are assumed.

1340 on $|U_e| \sqrt{|U_e|^2 + |U_\tau|^2}$ that wasn't obtained before in PS191 and limits on $|U_\tau|$ are also rather poor.
 1341 Results for this decay mode are shown in Figure 6.12 b.

1342 As one can see, all our results are close to the estimation made by Asaka et al.
 1343

3.1 HNL daughter particles

1345 Now we have all the information about the HNLs that enter ND280. Thus we could generate
 1346 the secondary particles that will be born in the heavy neutrino decay. The decay itself is simulated
 1347 in the HNL rest frame. Then the boost is applied towards the heavy neutrino initial direction. The
 1348 decay points are randomly generated along the HNL tracks inside the TPC volume. So the decay
 1349 positions are expected to be uniformly distributed in this volume. Cross-check (Figure 6.13) shows
 1350

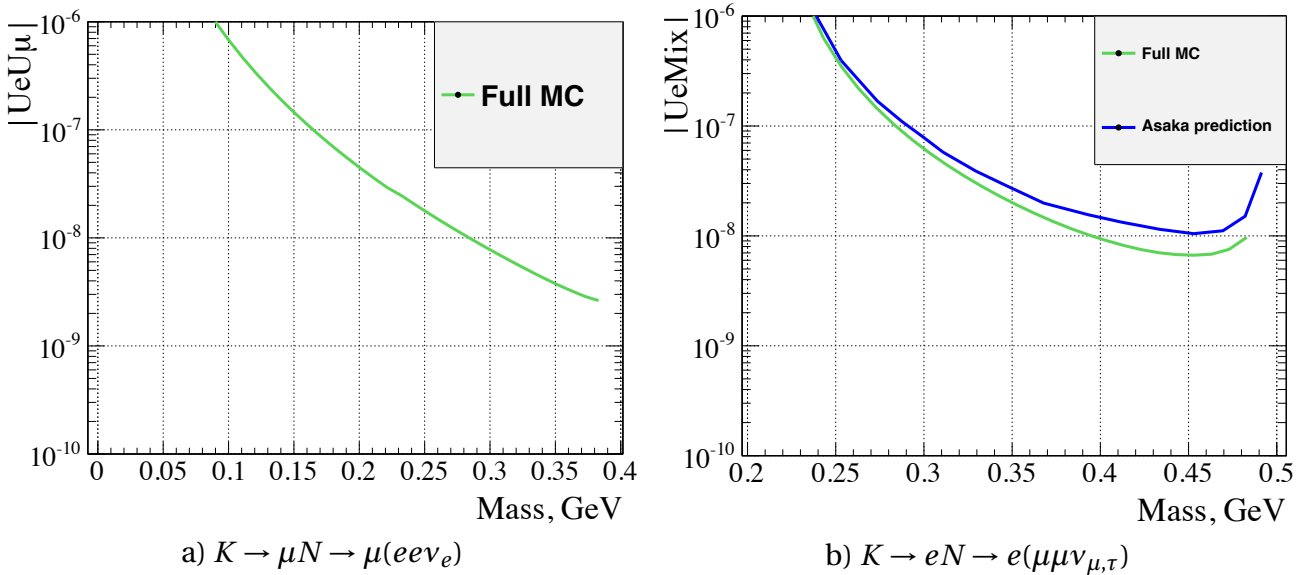


Figure 6.12: Sensitivity of T2K to mixing elements in tree body decay modes: (a) for $|UeU\mu|$ and (b) for $|U_e| \sqrt{|U_e|^2 + |U_\tau|^2}$. The detection efficiency of 100% and no background are assumed.

1351 some deviations at the upper and bottom edges for the large HNL mass but it was also expected
 1352 due to the off-axis flux.

1353 The simulation of the 2-body decay is straight forward. The direction of the first particle is
 1354 thrown isotropically. Then base on both momentum and energy conservation laws whole the de-
 1355 cay is parametrized in the HNL rest frame. We will obtain the final kinematics of the daughters
 1356 with the boost along the heavy neutrino momentum. The kinematic evaluation is covered in [113],
 1357 chapter 2. For the each event the following weight is assigned:

$$weight_{2-body} = weight_{K \rightarrow \ell N} \cdot \frac{L}{\beta \gamma c} \cdot \Gamma_{2-body}, \quad (6.13)$$

1358 The 3-body decay case is a bit more complicated. For this case we can't just throw all the di-
 1359 rections as we have one degree of freedom in the decay. To deal with it we used the normalization
 1360 with the maximum width of the decay. For each event the following weight is assigned:

$$weight_{3-body} = weight_{K \rightarrow \ell N} \cdot \frac{L}{\beta \gamma c} \cdot \frac{\frac{d\Gamma(p_1, p_2)}{dp_1 dp_2}}{\max\left(\frac{d\Gamma(p_1, p_2)}{dp_1 dp_2}\right)} \cdot P, \quad (6.14)$$

1361 where L is total length of HNL path in three TPCs. We normalize the weight of each particular
 1362 decay with respect to the maximum possible value. This will make the absolute number of the
 1363 events smaller, but as we use the signal sample only for the efficiency evoluation the effect will be
 1364 compensated. That's important as the selection probability could depend on the kinematics and
 1365 we need to assign proper weight to each generated event for proper efficiency treatment.

1366 The polarization of the HNL is taken into account in the simulation according to the calcula-
 1367 tions from [111]. The HNL polarization during its production is given by:

$$\vec{\Pi} = \frac{(\delta_\ell - \delta_N) \lambda^{1/2} (1, \delta_\ell, \delta_N)}{\delta_\ell + \delta_N - (\delta_N - \delta_\ell)^2} \vec{n} \quad (6.15)$$

1368 where

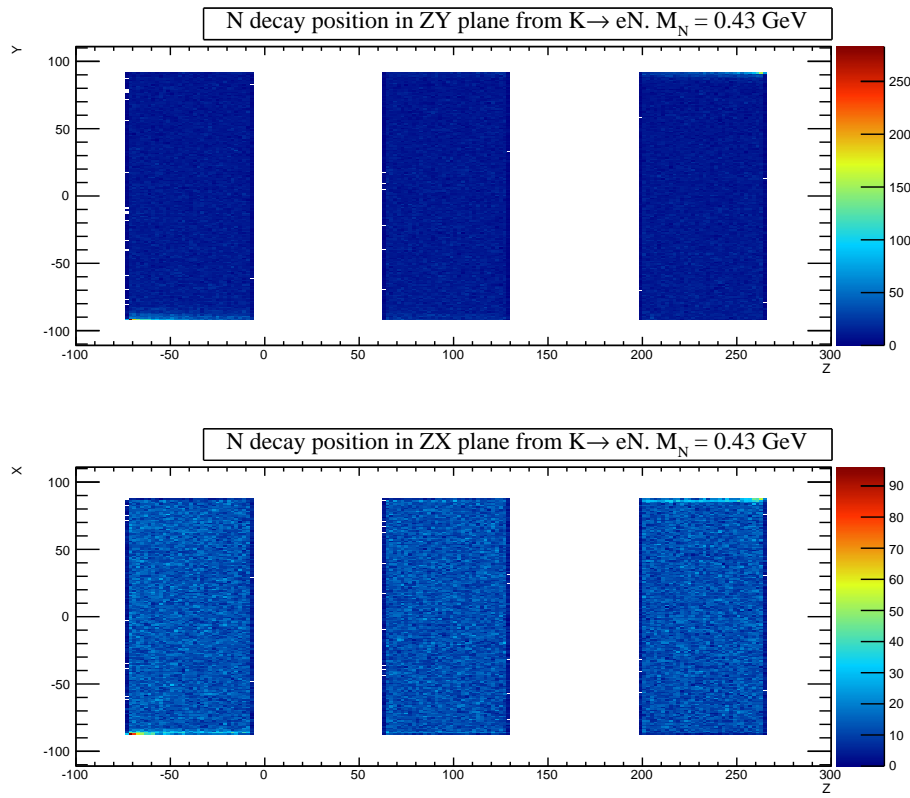


Figure 6.13: Distribution of HNL decay positions over 3 TPCs. The decay position is in the detector coordinate system in mm.

1369 ➤ $\delta_N = (M_N/m_K)^2$

1370 ➤ $\delta_\ell = (m_\ell/m_K)^2$

1371 ➤ $\lambda(x, y, z) = x^2 + y^2 + z^2 - (xy + yz + xz)$

1372 ➤ \vec{n} is the kaon direction in the heavy neutrino rest frame

1373 The polarization of the HNL as a function of its mass in the decay $K \rightarrow \mu + N$ is shown in
 1374 Figure 6.14. One could see that in the limit $M_N \rightarrow 0$ the heavy neutrino behaves exactly as a mass-
 1375 less neutrino and becomes a left-handed. Also it's interesting to see that the polarization vanishes
 1376 when the HNL mass is equal to the muon one.

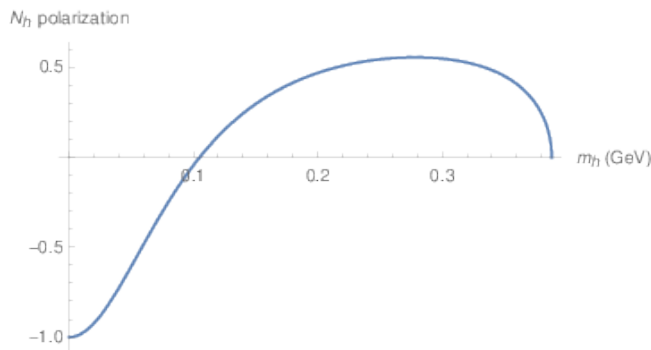


Figure 6.14: The polarization of the HNL as a function of its mass in the decay $K \rightarrow \mu + N$ [111].

1377 The polarization of the beam ($\vec{\Pi}$) is a statistical effect. As the HNL is a fermion it could take only
 1378 discrete polarization: -1 or 1. In the simulation for each decay the polarization value is computed
 1379 and then the random value is thrown in the range (-1; 1) to determine if the HNL is left-handed
 1380 or right-handed. Then this characteristic is taken into account during the heavy neutrino decay
 1381 simulation with:

$$\frac{dN}{d\cos\theta} (N \rightarrow \ell\pi) \propto (1 - \delta'_\ell)^2 - \delta'_\pi (1 + \delta'_\ell) - \frac{\sqrt{\lambda'}}{2} (1 - \delta'_\ell) \prod \cos\theta \quad (6.16)$$

1382 where:

1383 ➤ $\delta'_\ell = (m_\ell/M_N)^2$

1384 ➤ $\delta_\pi = (m_\pi/M_N)^2$

1385 ➤ $\lambda' = \lambda(1, \delta'_\ell, \delta'_\pi)$

1386 ➤ θ is an angle between the outgoing lepton and the parent meson (kaon) in the HNL rest
 1387 frame

1388 After simulation of the HNL decays we have all information about kinematics of their daugh-
 1389 ter particles, i.e. momentum, direction, opening angles. This characteristics are presented in [Fig-](#)
 1390 ure 6.15 and [Figure 6.16](#). It's important to note that most of the particles have momentum below
 2 GeV. Our TPCs was designed to reconstruct events in this energy region. The heavy neutrino

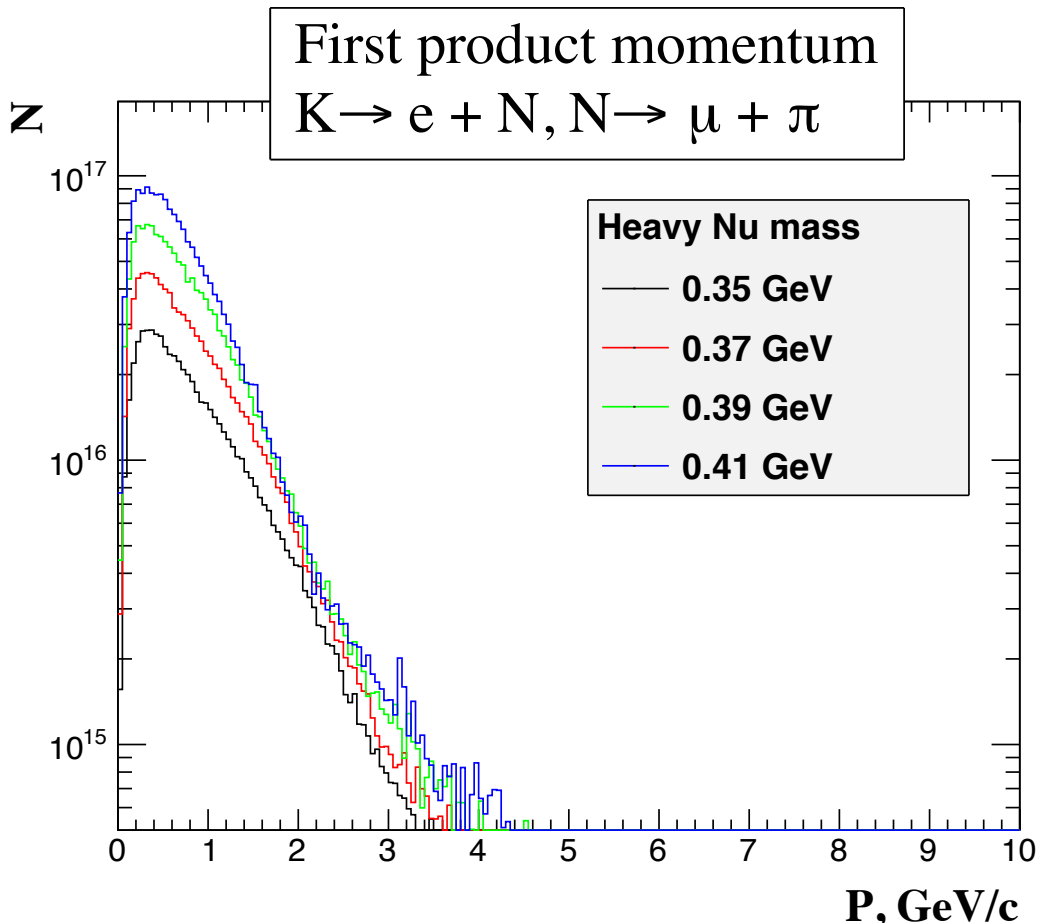


Figure 6.15: Energy spectra of HNL daughter particles.

1391

1392 daughter particles are propagated through the detector with the help of the Geant4 package [114].

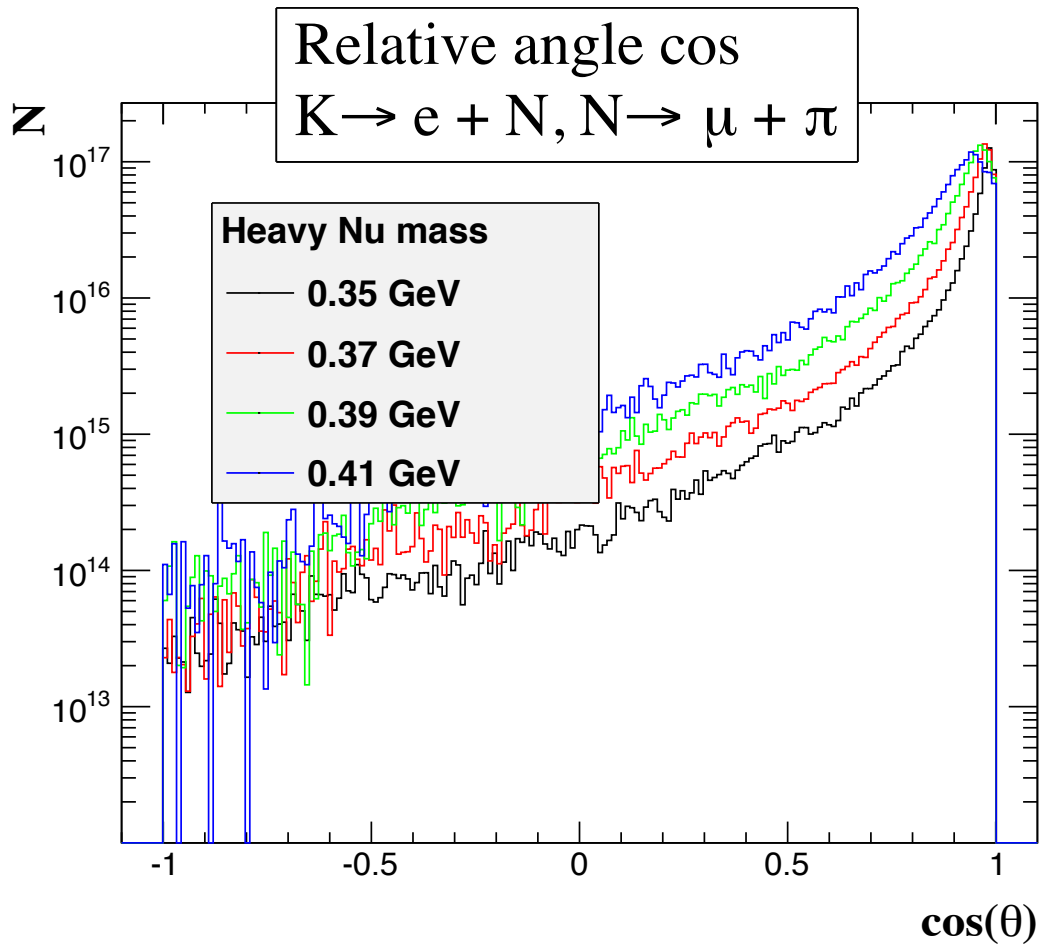


Figure 6.16: Opening angle spectra of HNL daughter particles.

1393 All the secondary interactions, decays, etc. are considered. The example of a “good” MC event with
 1394 the HNL decay in the first TPC and further evolution of a daughter muon and a pion is shown in
 1395 [Figure 6.17](#). The detector response is fully simulated from the initial ionization until the readout
 1396 signal from the electronics. Thus we could develop the event selection and estimate its efficiency
 1397 with the MC generated signal sample.

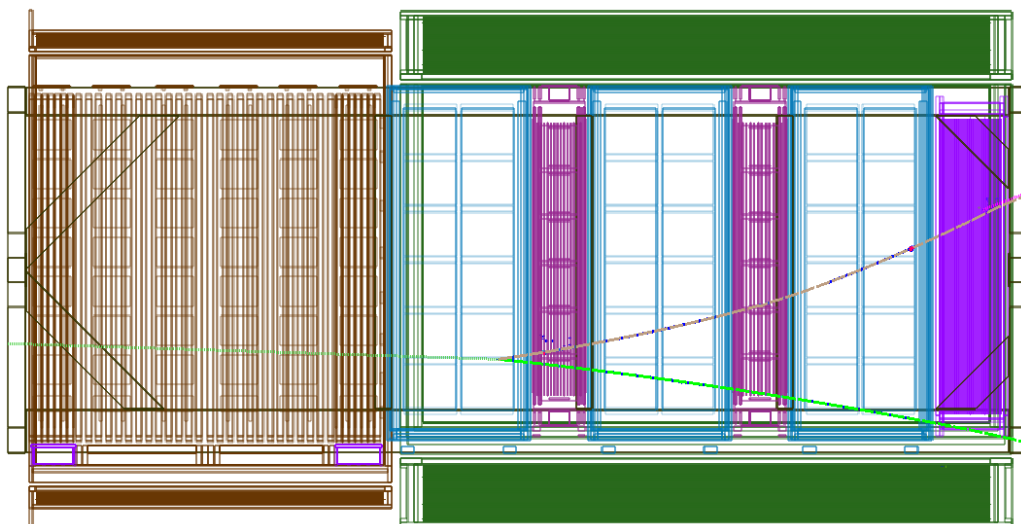


Figure 6.17: Example of simulated event from HNL decay in the first TPC. Dashed green line corresponds to HNL track, green line to the muon track, brown line to the pion track.

1398

1399

HNL ANALYSIS

1400 The search for heavy neutrino consists of several parts. At the first step we apply the time correc-
 1401 tion to the signal sample. The correction is related to the time delay of the HNL with respect to the
 1402 neutrino bunch. The details are presented in the [section 1](#). Then the cut sequence was developed
 1403 in order to select signal and suppress the background events. The details about the selection are
 1404 described in the [section 2](#). Controlling the uncertainties is an important part of any analysis. In our
 1405 case the uncertainties will come from the detector response simulation and flux prediction ([sec-](#)
 1406 [tion 3](#)). Finally we choose the appropriate statistical method for the results treatment ([section 4](#)).

1407

1 Time of flight correction

1408

1409 Heavy neutrino time of flight is different from the active neutrino. The difference is calculated
 1410 according to Eq. [7.1](#).

$$\delta T = \frac{d}{\beta c} - \frac{d}{c} = \frac{d}{c} \left(\frac{1}{\beta} - 1 \right), \quad (7.1)$$

1412 where d is a distance between the HNL production and decay points, $\beta = v/c$ is a kinematic pa-
 1413 rameter of the HNL. The ToF modeling is not performed during the HNL simulation. So we apply
 1414 the correction $T' = T + \delta T$ in the analysis, shifting all timestamps in the event by the δT . In the T2K
 1415 the neutrino beam repeats the proton beam spill structure with 8 bunches. The bunches are Gaus-
 1416 sian with $\sigma \approx 19\text{ns}$ ([section 1](#)). Due to the ToF correction the HNL bunch will change its shape. The
 1417 new bunch structure is shown in [Figure 7.1](#).

1418 For active neutrino analysis the standard time gate is $|T_{\text{event}} - T_{\text{bunch}}| < 60\text{ns}$. By the T_{bunch}
 1419 the mean value of the Gaussian distribution is considered. In our analysis we should widen the
 1420 time window in order to increase the efficiency of the selection. Since the shape of the HNL bunch
 1421 is asymmetric, we applied different cuts value for upper and lower boundaries of the time window.
 1422 For the bounds we are limited by the electronics time gate. As the experimental setup was origi-
 1423 nally designed to deal with neutrino bunches the data recording time was limited. We widen the
 1424 cut values as much as the data acquisition allow us to do it and put the limits to

$$-100\text{ns} < T_{\text{vertex}} - T_{\text{bunch}} < 300\text{ns} \quad (7.2)$$

1425 We do not apply any additional time of flight cut to separate interactions of the active neutrinos
 1426 and the HNLs decays as the bunches have a strong time overlap especially for low masses. Any

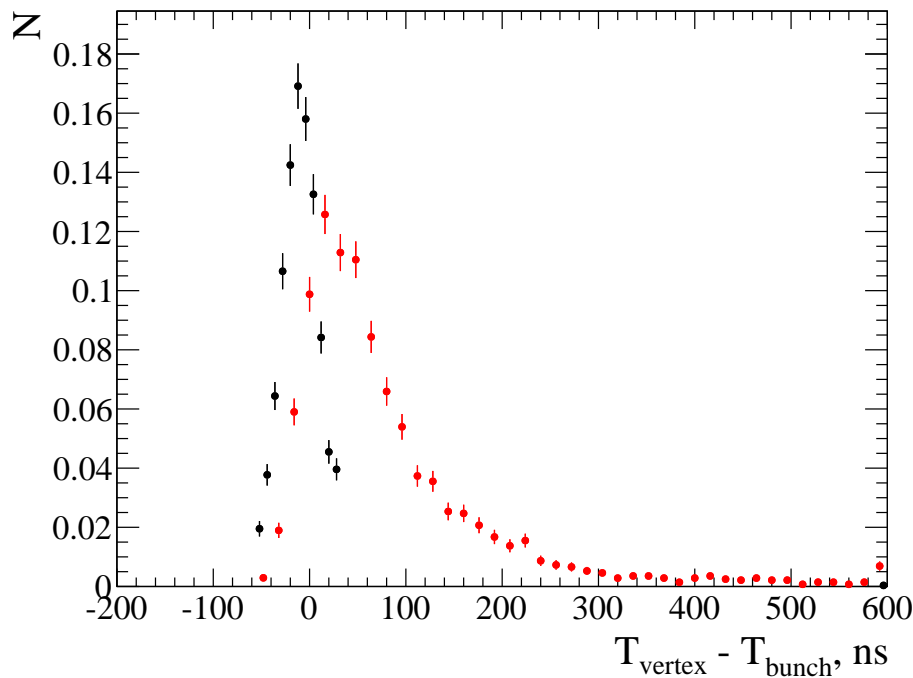


Figure 7.1: The active neutrino bunch (in black) and the HNL bunch (in red) for $M_{HNL} = 480\text{MeV}$.

1427 attempts to suppress the active neutrinos by the ToF will cause the significant reduction of the
 1428 HNL selection efficiency which is already small.

1429

2 Event selection

1430

1431 The next step is developing cut sequence for proper selection of the signal events and reduc-
 1432 tion of background. For selection of the HNL candidates decay we apply the following criteria:

- 1433
1. Global vertex in the TPC fiducial volume. Vertex should be “good”, that means it should be
 1434 reconstructed with $\chi^2 < 1000$, Position variance $< 500 \text{ mm}$;
 2. Two different charged “good” tracks associated with this vertex;
 3. One of the tracks use the same TPC as vertex. This was made to prevent vertex migration
 1435 from the active neutrino interactions in the FGD;
 4. No activity in the upstream detector;
 5. No other tracks start in the same TPC;
 6. Proper particle identification as $e\pi$ or $\mu\pi$ using dE/dx in the TPC;
 7. Invariant mass cut: $140\text{MeV} < M_{HNL} < 850\text{MeV}$ for the $e\pi$ mode and $250\text{MeV} < M_{HNL} <$
 1442 750MeV for the $\mu\pi$ mode;
 8. Polar angle for HNL candidate $\theta < 8.0^\circ$ for the $e\pi$ mode and $\theta < 3.7^\circ$ for the $\mu\pi$ mode, since
 1443 the HNL direction should be extremely collinear to the neutrino beam;
 9. Kinematic cut on the opening angle between daughter particles $\cos\theta > 0.00$;

1444

1447 For the dimuon mode we apply additional cuts to select only muon tracks:

1448 10. Both tracks have the subtracks in ECal;

1449 11. Both subtracks in ECal are MIP like (not electromagnetic shower);

1450

2.1 Cuts description

1453 In this section the main cuts for the signal event selection and background reduction will be
 1454 briefly overviewed. Many of the cuts were inherited from the existing T2K analysis, e.g. the distin-
 1455 guishing the particle type was studied very carefully for the oscillation analysis. We checked that
 1456 the cut values are suitable for the case of the HNL selection and developed several analysis specific
 1457 cuts.

1458

a Quality and fiducial cut

1460

1461 The basic idea of the current study is to search for heavy neutrino decays only in the TPC vol-
 1462 ume filled with argon. In this case we can avoid large amount of background from the active neu-
 1463 trino interactions. The limits of the fiducial volume were inherited from the study of the active
 1464 neutrino interactions in argon. The volume doesn't contain the walls and the central cathode, so
 1465 only argon gas is expected as a target.

1466 The density difference between gas (TPC) and polystyrene and water (FGD) is about 3 orders,
 1467 that gives about the same reduction of the background. As we search for two or three body decays,
 1468 the selection can be easily implemented with the global vertex approach. In the current ND280
 1469 reconstruction the global vertex analysis is performed with the Kalman filter. The main idea is
 1470 to search for tracks with close start/end positions and then perform some iterations of filter to
 1471 make fit more accurate and define χ^2 and position uncertainties of the vertex reconstruction. As
 1472 already described, in our study the vertex should be inside the TPC fiducial volume. Studying MC
 1473 background, we found that the vertex association is completely wrong in some cases, i.e. two tracks
 1474 from different origins are associated into one vertex or a broken track gives a vertex with two tracks.
 1475 All these errors are often characterized with a large χ^2 value or a position variance at the level of
 1476 the detector length. To avoid misidentifying these events as a HNL candidate we added the "vertex
 1477 quality cut" which requires $\chi^2 < 1000$ and the position variance < 500 mm.



VerteXing with Kalman filter

The Kalman filter is a recursive filter that estimates the internal state of a dynamic system from number of noisy measurements. Originally was developed for the rocket science and is still actively used in this field. The flow of the method is shown in [Figure 7.2](#). As one could see we start with the prior measurements, make a prediction about the next step based on the model, then correct the prediction with the actual measurement.

In the case of the vertex finding in the detector the model is the track propagation through the detector in magnetic field. For the prior we extrapolate the reconstructed tracks to the closest intersection point. Then we go through several iterations using the observed detector hits as a data. At the end we come to the precise reconstruction of the vertex position with the know uncertainty and the quality of the fit.

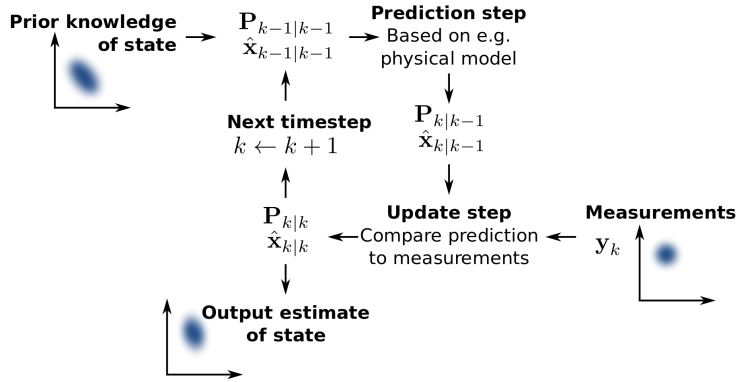


Figure 7.2: The flow of the Kalman filter usage.

1478 The next question is the efficiency of global vertex algorithm. We tested this method on our
 1479 signal samples and found that only $\approx 32\%$ of events pass first two cuts (“good” vertex and two
 1480 different charge “good” tracks. There are two possible reasons:

- 1481 ➤ the problem is in the bad vertex association algorithm. In this case we need to develop our
 1482 own method of tracks association, i.e. look at the tracks with close start positions;
- 1483 ➤ pure efficiency was caused by bad quality of the reconstructed tracks. This problem is un-
 1484 avoidable as we can't rewrite the whole reconstruction.

1485 To check both possibilities we looked at the fraction of the good reconstructed tracks. Our study
 1486 demonstrates that only for 50% of the events we have successfully reconstructed two different
 1487 charged “good quality” tracks. “Good tracks” means that the track has more than 18 nodes in its
 1488 longest segment in TPC. It is the standard cut for proper dE/dx particle identification. For
 1489 the active neutrino interaction studies one requests > 18 nodes in the most upstream TPC. In our
 1490 study we expect the vertices inside TPC FV, so the track length in the upstream TPC may not be
 1491 long enough. In this case we use the same cut value but not for the most upstream segment of the
 1492 track, but for the longest one among all TPCs. Applying the PID cut reduce this amount to 34%. So
 1493 the problem is not in the global vertex algorithm, but in the current tracks reconstruction. In this
 1494 case we can't significantly increase the efficiency of our selection because we are limited by the
 1495 track reconstruction performance. The main reasons of the drop of efficiency are:

- 1496 ➤ TPC edge reconstruction failure. If the track has < 10 hits in TPC, the current TPC segment
 1497 will not be added to the global track. It will start in the next detector and can be treated as a
 1498 background;
- 1499 ➤ Pion scattering/showering. If a pion interacts in a scintillator (FGD), its TPC track can be not
 1500 long enough for proper reconstruction;
- 1501 ➤ Tracks separation. As two tracks can be extremely collinear they may be not separated in a
 1502 TPC.

1503 Z position for the reconstructed vertices is presented in [Figure 7.3](#). All the reconstructed ver-
 1504 tices before fiducial cut are shown. The Z vertex distribution is not uniformed at the boundaries
 1505 of the TPCs due to the edge reconstruction failure. Also we can conclude that the probability for
 1506 location of vertex outside the TPC is rather small.

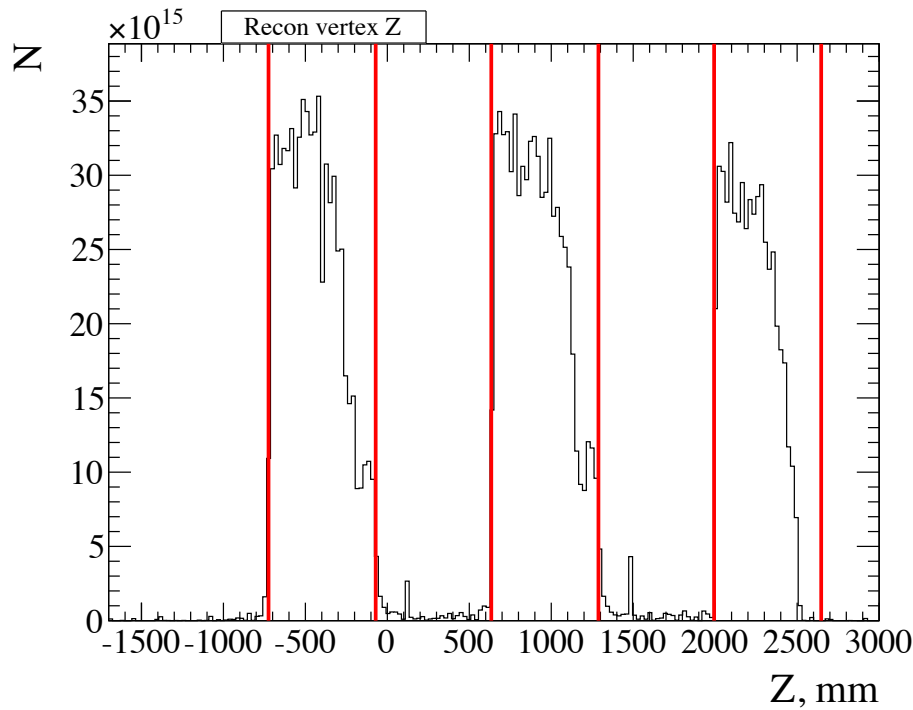


Figure 7.3: Vertex position for signal samples before the FV cut. Red lines are TPC bounds.

1507

b HNL daughter-tracks start position

1508

1509

1510 Some cases of the vertex migration were found in the background analysis (subsection 2.3). An
 1511 active neutrino can interact in the FGD and all tracks of this event start in the FGD, but because of
 1512 the errors of the reconstruction algorithm the vertex is extrapolated into the TPC FV. We can easily
 1513 avoid such background with checking the activity in the TPC with vertex. If there are no tracks the
 1514 event will be rejected.

1515

c Veto cuts

1516

1517

1518 Signal events from the HNL decay can't have any activity in the upstream detector. But there are
 1519 some background events from a neutral particle decay or interaction. For example, π^0 decay into
 1520 to photons and further production of the electron-positron pair. Also some mesons or baryons that
 1521 can be produced in the active neutrino interactions and can cause production signal-like events.
 1522 To suppress such events we should apply some constraints on the upstream activity. There is a
 1523 possibility of electronics noises in the detector. Also there can be some activity after the previous
 1524 bunch. To reduce event pile up we didn't constrict all the upstream activity. We developed the veto
 1525 cut only for the first upstream detector. For the TPC1, we look for the P0D tracks which start or
 1526 ends in the last P0D layers (100 mm). For the TPC2 and the TPC3, we look at the FGD time bins.
 1527 We are interested only in the bins that have a time signature near the center of bunch as this is only
 1528 possibility to cause the vertex with two tracks in current bunch. Possible time gates are defined as
 1529 4σ , where $\sigma = 50\text{ ns}$. The "4 sigma" is inherited from the default beam bunching procedure but the
 1530 sigma value was increased as the bunch size for the massive neutrinos is larger (section 1).

1531

d TPC additional activity cut

1532

1533

1534 Some process with more than two daughter particles can take place in the TPC. If only two of
 1535 them are associated into the vertex the event will be signal-like. To prevent such background we
 1536 apply the cut on the TPC activity. Only the HNL candidate daughters should start in the TPC with
 1537 the vertex. If there is any additional track's start point the event is rejected.

1538

e Particle identification

1539

1540

1541 We study the heavy neutrino decay into the charged lepton and pion. For the particle iden-
 1542 tification the standard TPC dE/dx methods were applied [103]. For the analysis we choose the
 1543 longest TPC segment as containing the most reliable information. Then the likelihood is build for
 1544 each of the considered particle option: electron, muon, pion, proton. For particular particle selec-
 1545 tion we are constraining its likelihood and also limiting other hypothesis likelihoods to stay at the
 1546 low value.

1547

f Invariant mass cut

1548

1549

1550 As we search a decay of a massive particle into two charged particles, the invariant mass can
 1551 be calculated. The upper bound on the mass of the HNL produced from the kaon decay is $M_{HNL} <$
 1552 $M_K \approx 500\text{ MeV}$ and the lower bound is $M_{HNL} > M_\ell + M_\pi$. But the resolution of the invariant mass
 1553 reconstruction should be taken into account. The resolution of our detector is shown in Figure 5.5.
 1554 We accept 4σ difference from the true value and assume cut value 750 MeV for the $\mu\pi$ mode and
 1555 850 MeV for the $e\pi$ mode. The lower bound is strictly defined by the invariant mass calculation
 1556 method ($M_\ell + M_\pi$). The cut value is set to 250 MeV for the $\mu\pi$ and 140 MeV for the $e\pi$. This cut help
 1557 to reject the events from active neutrino interactions with high reconstructed invariant mass that
 1558 certainly can not be the HNL decays.

1559

g Kinematic cuts

1560

1561

1562 The heavy neutrinos from the kaon decays in the decay volume have a momentum collinear
 1563 to the beam axis. So the momenta of the reconstructed HNL candidate should have rather small
 1564 polar angle. This constraint can significantly reduce the background because the direction of the
 1565 charged particles from the active neutrino interactions is quite isotropic. Since the HNL is a rather
 1566 massive particle its daughter particles shouldn't have large opening angle. We have studied angular
 1567 distribution for both the background and the signal samples. Firstly we studied the distribution of
 1568 the polar angle of the HNL candidate for events that passed all previous cuts, as it is the most
 1569 strict kinematic cut. Then we looked at the opening angle of the HNL candidate daughters. The
 1570 results are presented in Figure 7.4, Figure 7.5 and Figure 7.6. For this plots we use the NEUT MC
 1571 results with a statistics $6.5 \cdot 10^{21}\text{ POT}$. On these plots the background is normalized to 10^{21} POT .
 1572 The total signal is normalized to 1, only the shape of the signal distribution is important. It can't
 1573 be normalized to any POT as it is proportional to mixing element. The cut value were set in order
 1574 to maximize the sensitivity.

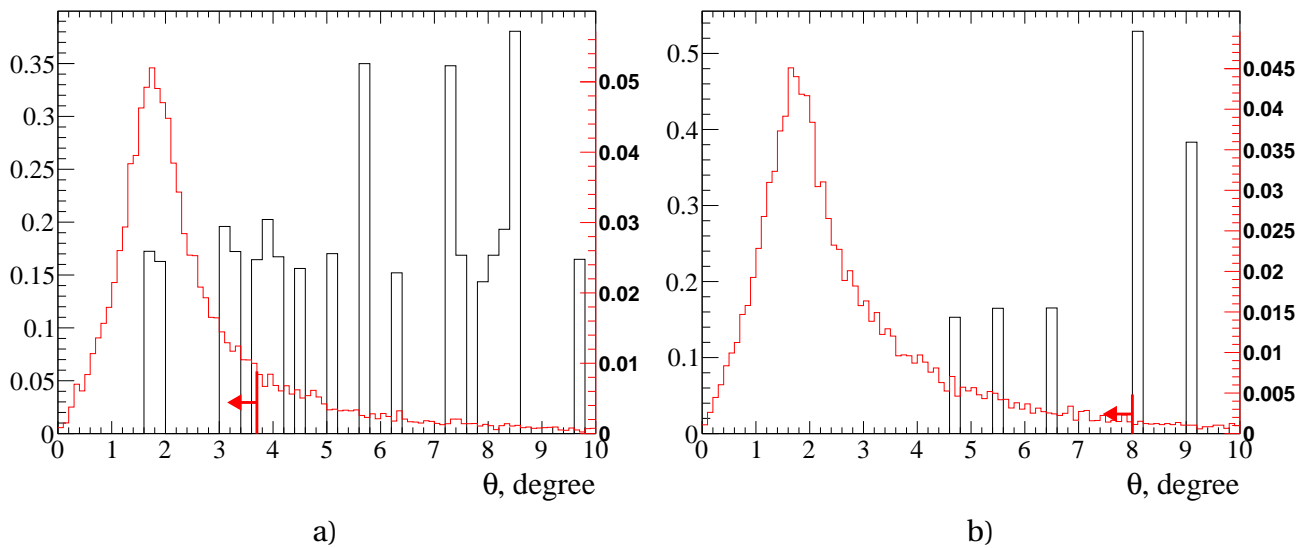


Figure 7.4: Angular distribution of the HNL candidate events (a) for $\mu\pi$ mode and (b) for $e\pi$. Red is the signal samples, black is the BG and vertical line is a cut value. BG is normalized to $10^{21} POT$, signal is normalized to 1.

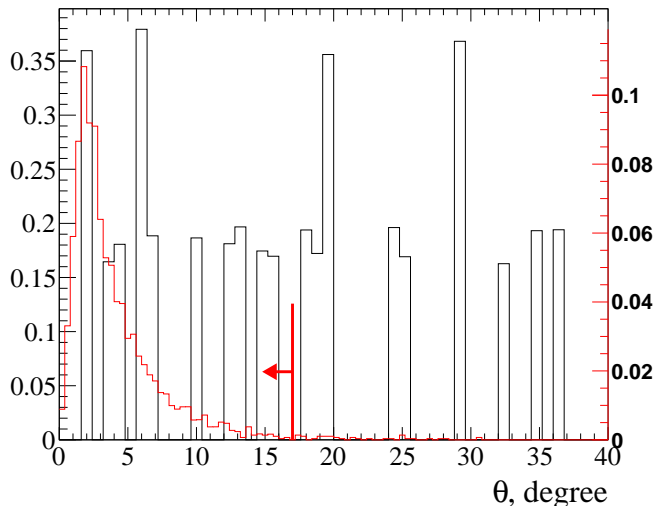


Figure 7.5: Angular distribution of the HNL candidate events for $\mu\mu\nu$ mode. Red is the signal samples, black is the BG and vertical line is a cut value. BG is normalized to $10^{21} POT$, signal is normalized to 1.

1575

h $N \rightarrow \mu\mu\nu$ mode cuts

1576

1577

1578 As we need to select only two muons, we should determine the particle type very accurately.
 1579 The main problem is muon/pion separation in the TPC. Also some protons can be identified as a
 1580 muon with the dE/dx method. As a muon has a high penetration ability, it is expected to reach the
 1581 detectors outside the tracker. The protons have a very low probability to leave the tracker, so they
 1582 will be rejected. The pions can leave the tracker but they will cause a shower in the ECal. For the
 1583 pion/proton misidentification as a muon we select only events in which both muons' tracks have
 1584 the subtracks in the ECal and these subtracks should be identified as MIP, but not as EM shower.

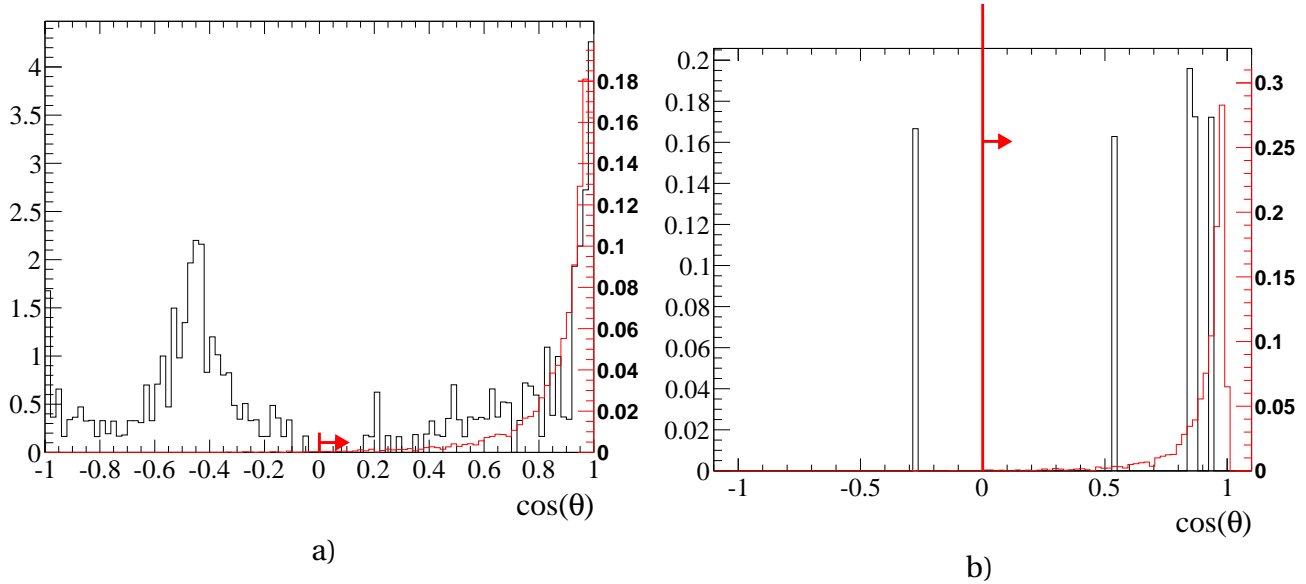


Figure 7.6: An opening angle for the HNL daughter particles for the $\mu\pi$ mode (a) before the polar angle cut was applied and (b) after. Red is the signal samples, black is the BG and vertical line is a cut value. BG is normalized to $10^{21} POT$, signal is normalized to 1.

1585

2.2 Signal selection efficiency

1586

1587 Applying all these cuts to the signal samples give us the total selection efficiency (Figure 7.7,
 1588 [Figure 7.8](#)). The efficiency of the HNL selection in our TN is defined as a ratio of the number of the
 1589 selected events to the number of the generated HNL events inside the TPCs FV. The main reason
 1590 for the dependence of the efficiency on the HNL mass is the track reconstruction. For the large
 1591 HNL mass we have more events with successfully reconstructed “good quality” tracks associated
 1592 into the vertex.
 1593

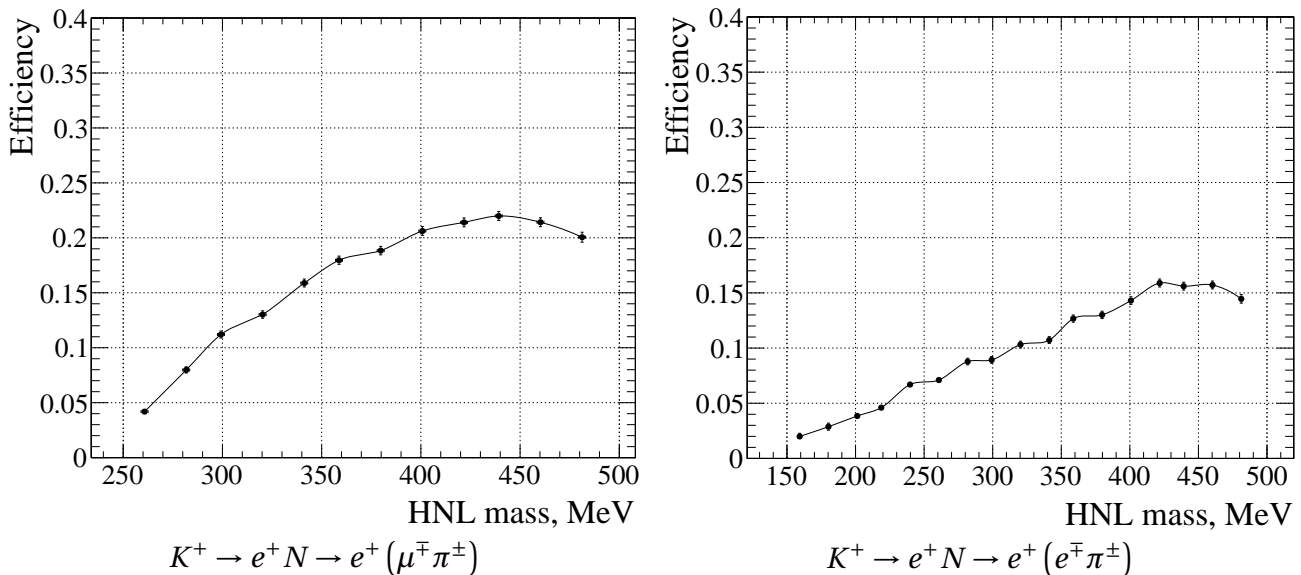


Figure 7.7: Selection efficiency for two body decays of HNL.

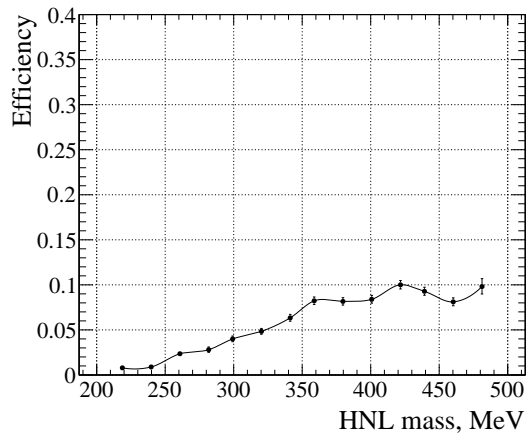


Figure 7.8: Selection efficiency for HNL decay mode $N \rightarrow \mu\mu\nu$.

1594 The efficiency dependence on different cuts is shown in Figure 7.9. The main reason for the
 1595 efficiency drop is “quality and fiducial cut” which is described in details in the subsubsection 2.1.a.

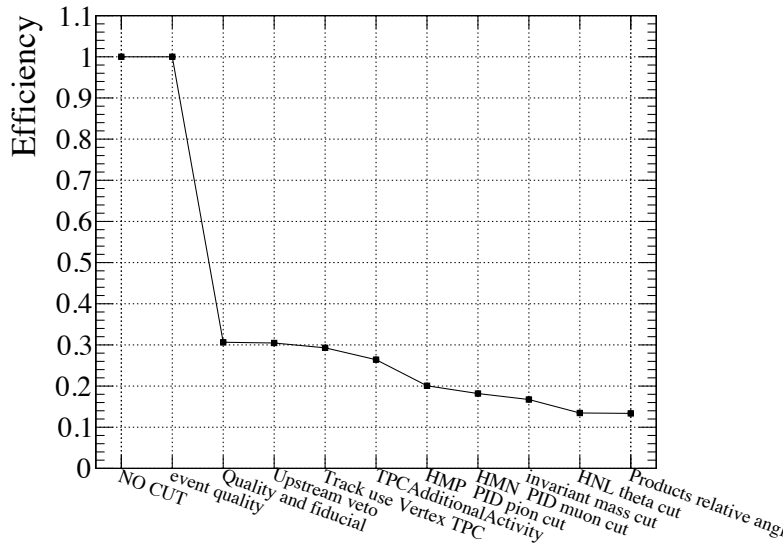


Figure 7.9: Efficiency dependence on the applied cuts for mode $N \rightarrow \mu^\pm + \pi^\pm$ for all HNL masses.

1596
 1597 The dependence of the efficiency on the HNL momentum and opening angle of the daughter
 1598 particles is shown in Figure 7.10. As expected the maximum efficiency is for HNL with momentum
 1599 below 2 GeV. The TPCs were designed for the event reconstruction in this energy region.

1600 Since we study the HNL production from K^+ , K^- and their decays into $\ell^\pm h^\mp$, the efficiency
 1601 should be evaluated for each of them. Such result is presented in Fig. 7.11. We can see the agree-
 1602 ment of the efficiency study for the different modes. The only difference is that the $\mu^-\pi^+$ selection
 1603 efficiency is a bit higher than the $\mu^+\pi^-$ one.
 1604

2.3 Background suppression

1605
 1606 Applying the same selection cuts to MC data from the different generators NEUT [115], GE-
 1608 NIE [116] and NuWro [117], we can estimate the background. We use different generators for the
 1609 cross-check as they use slightly different neutrino interactions parameters. For example, Genie is

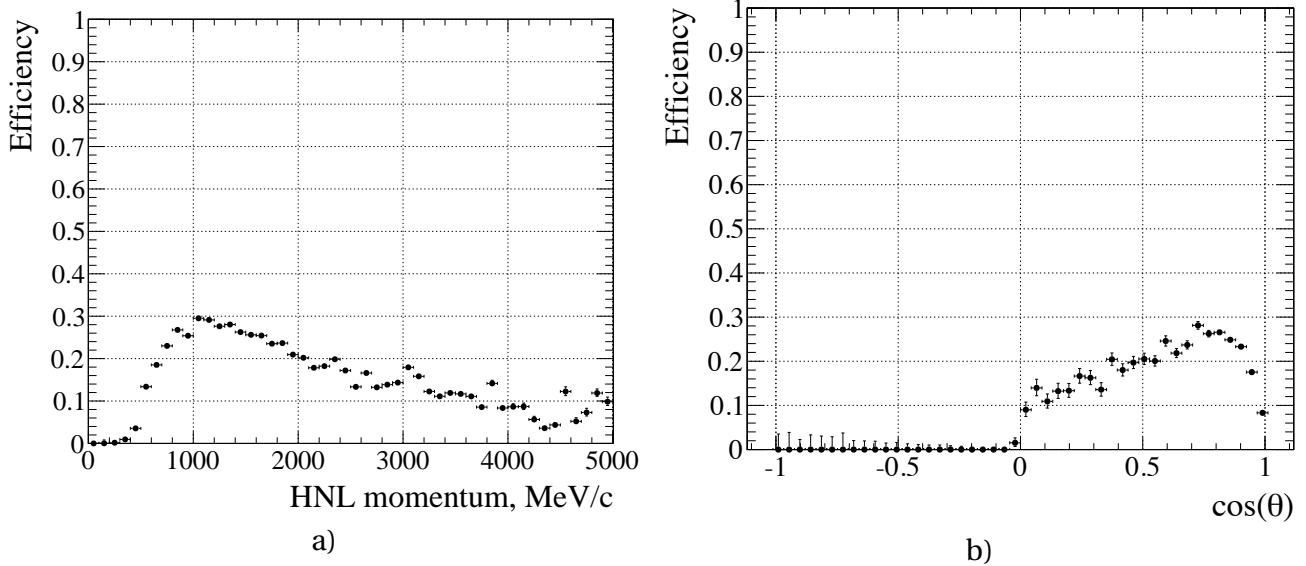


Figure 7.10: The dependence of efficiency for mode $N \rightarrow \mu\pi$: (a) on the HNL momentum and (b) opening angle of daughter particles.

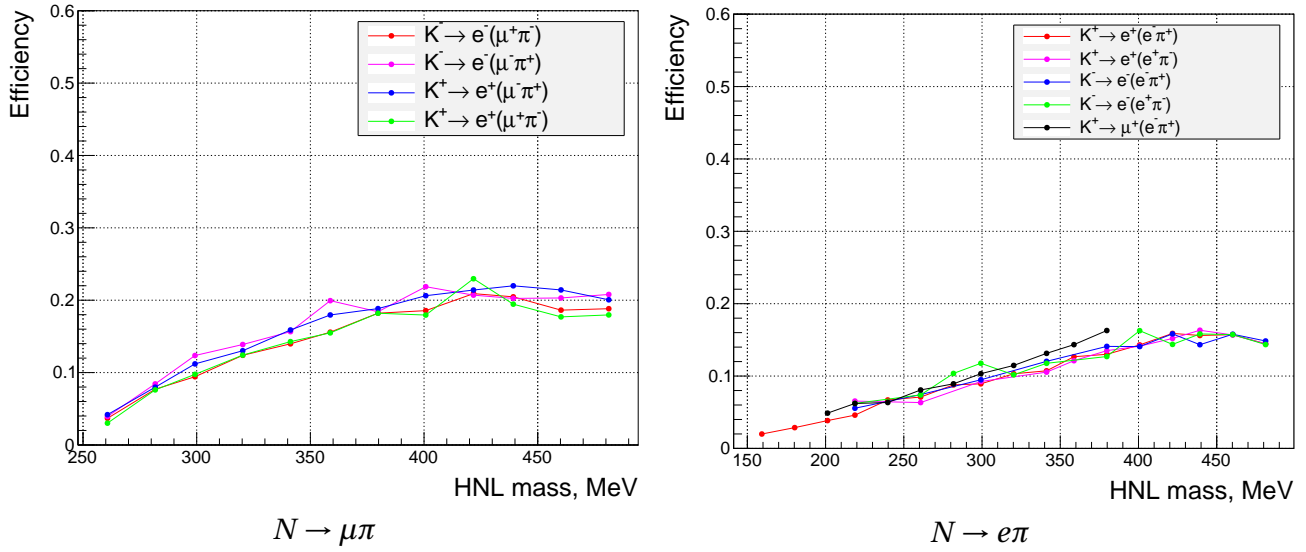


Figure 7.11: HNL selection efficiencies for several production and decay modes.

more common for the kaon analysis (we can expect BG from K^0); NuWro gives a large statistic for the TPC volume. Following statistics was studied, for NEUT $6.5 \cdot 10^{21} POT$, for GENIE $5 \cdot 10^{21} POT$, for $\bar{\nu}$ mode with NEUT $5.8 \cdot 10^{21}$. We studied the MC data from interaction in the magnet volume for NEUT and GENIE. NuWro provides data with neutrino interactions only in TPC volume with statistics $4.7 \cdot 10^{22}$ POT. OOFV (Out Of Fiducial Volume) processes are not simulated with the NuWro and few events identified as OOFV have true vertices in TPC but not in FV. For comparison of the background all the results were normalized to $10^{21} POT$. The efficiency of signal event selection and the background reduction for the different reaction types of active neutrino interactions based on run 2-6 from the NEUT generator are shown in [Table 7.1](#), [Table 7.2](#), [Table 7.3](#). The efficiency is equal for the same modes as we use our own HNL generator and the result does not depend on the neutrino generator. For more detailed cut description see [section 2](#). The relative angle cut (kinematic) is shown in the table only if it reduces the number of the background events comparing to the polar angle cut. We start with the “Quality and fiducial” cut which requires vertex

1623 with two different charge tracks in the TPC fiducial volume. Here we have the main efficiency drop
 1624 down to 50% ([subsubsection 2.1.a](#)).

N	Cut	CCQE	RES	DIS	COH	NC	2P2H	OOFV	$\bar{\nu}_\mu$	ν_e	Total	Eff
1	Vertex	140.11	30.88	20.34	4.57	8.48	1.65	647.31	2.39	3.63	859.34	44.0
2	Veto	136.47	27.86	17.58	4.25	8.15	1.65	514.72	2.10	3.45	716.23	43.9
3	Use TPC	135.77	27.31	17.19	4.25	8.15	1.48	505.18	2.10	3.45	704.88	41.9
4	TPC act.	122.44	21.24	10.75	3.89	6.55	0.82	281.47	1.80	2.43	451.39	39.1
5	PID 1	99.68	16.10	8.47	3.39	4.84	0.66	130.92	1.65	0.36	266.06	37.2
6	PID 2	5.08	5.51	5.60	2.03	1.25	0.00	48.64	1.37	0.19	69.66	31.3
7	Inv mass	0.83	3.52	2.17	1.67	0.90	0.00	43.17	0.92	0.00	53.18	29.2
8	θ cut	0.00	0.17	0.36	0.34	0.00	0.00	0.00	0.00	0.00	0.87	21.3
9	Kinematic	0.00	0.17	0.20	0.34	0.00	0.00	0.00	0.00	0.00	0.70	21.1

Table 7.1: The number of MC background events after every cut for $10^{21} POT$ from NEUT for $\mu\pi$ mode.

N	Cut	CCQE	RES	DIS	COH	NC	2P2H	OOFV	$\bar{\nu}_\mu$	ν_e	Total	Eff
1	Vertex	140.11	30.88	20.34	4.57	8.48	1.65	647.31	2.39	3.63	859.34	34.5
2	Veto	136.47	27.86	17.58	4.25	8.15	1.65	514.72	2.10	3.45	716.23	34.4
3	Use TPC	135.77	27.31	17.19	4.25	8.15	1.48	505.18	2.10	3.45	704.88	33.6
4	TPC act.	122.44	21.24	10.75	3.89	6.55	0.82	281.47	1.80	2.43	451.39	31.1
5	PID 1	99.68	16.10	8.47	3.39	4.84	0.66	130.92	1.65	0.36	266.06	24.8
6	PID 2	5.74	0.17	0.92	0.17	0.20	0.00	13.91	0.00	0.00	21.11	17.8
7	Inv mass	0.66	0.17	0.37	0.17	0.20	0.00	13.32	0.00	0.00	14.87	17.1
8	θ cut	0.00	0.00	0.00	0.17	0.00	0.00	0.32	0.00	0.00	0.48	15.2
9	Kinematic	0.00	0.00	0.00	0.17	0.00	0.00	0.32	0.00	0.00	0.48	14.8

Table 7.2: The number of MC background events after every cut for $10^{21} POT$ from NEUT for $e\pi$ mode.

N	Cut	CCQE	RES	DIS	COH	NC	2P2H	OOFV	$\bar{\nu}_\mu$	ν_e	Total	Eff
1	Vertex	140.11	30.88	20.34	4.57	8.48	1.65	647.31	2.39	3.63	859.34	42.1
2	Veto	136.47	27.86	17.58	4.25	8.15	1.65	514.72	2.10	3.45	716.23	42.0
3	Use TPC	135.77	27.31	17.19	4.25	8.15	1.48	505.18	2.10	3.45	704.88	40.5
4	TPC act.	122.44	21.24	10.75	3.89	6.55	0.82	281.47	1.80	2.43	451.39	38.2
5	PID 1	121.90	17.97	9.27	3.54	4.19	0.82	134.29	1.36	0.54	284.87	33.6
6	PID 2	4.38	5.01	5.22	1.70	0.91	0.00	27.59	1.08	0.91	46.09	22.5
7	Use ECal	2.12	1.79	1.89	0.68	0.34	0.00	2.56	0.33	0.00	9.72	9.9
8	ECal MIP	1.09	0.55	1.31	0.51	0.00	0.00	1.08	0.16	0.00	4.71	9.3
9	θ cut	0.93	0.36	0.39	0.51	0.00	0.00	0.00	0.00	0.00	2.18	9.1

Table 7.3: The number of MC background events after every cut for $10^{21} POT$ from NEUT for $\mu\mu\nu$ mode.

1625 Finally we have:

1626 As one can see, the different generators give nearly the same results. The reduction of back-
 1627 ground for mode $e\pi$ with NuWro generator caused by the lack of the data with neutrino events

	NEUT	GENIE	NuWro	NEUT $\bar{\nu}$
$\mu\pi$	0.79	0.69	0.85	0.91
$e\pi$	0.69	0.95	0.38	0.23
$\mu\mu\nu$	1.81	1.63	2.10	0.98

Table 7.4: The total number of MC background events for $10^{21} POT$.

1628 outside TPC — one of the most influential BG process. For our estimations we take the worse result
 1629 — the maximum background.

1630 The statistics accumulated in the T2K experiment is divided into 8 runs. The total good quality
 1631 data available for analysis is $(10.23\nu + 6.29\bar{\nu}) \cdot 10^{20} POT$. Scaling of the MC backgrounds to the real
 1632 data, collected at ND280, gives us the expected number of the background events (Table 7.5).

	run 2-8
$\mu\pi$	1.44
$e\pi$	1.12
$\mu\mu\nu$	2.85

Table 7.5: The total number of MC background events scaled to real data statistics.

1633 The origin of the backgrounds for $N \rightarrow \mu\pi$ mode is interactions in gas, mainly coherent and
 1634 resonance pion production. For the $N \rightarrow e\pi$ mode the main background process is π^0 decay into
 1635 two gammas and further electron positron pair production and misreconstruction one of the pair
 1636 component as a pion. For the $\mu\mu\nu$ mode the main background is CCQE. We select tracks for the
 1637 muon candidates with ECal. The candidate should be MIP like so pions from the COH and RES
 1638 processes are suppressed. But the protons that were misidentified as a muon in TPC can give a
 1639 track in ECal. Such tracks can be reconstructed as MIP in some cases.

1640 Neutrino interactions in gas were not well studied and it leads to the large uncertainties of the
 1641 background estimation. So, we are going this MC data only for comparison with the real data, but
 1642 not for the final result estimation. This strategy was described in section 4.

1643

3 Systematic uncertainties

1644 In general case the systematic uncertainty will come both from the signal expectations and
 1645 from the estimations background. In our case (section 4) the background estimations are not af-
 1646 fecting the final sensitivity result. Thus their systematics could be omitted.

1647 In this case we have the systematic uncertainties only from the number of predicted events.
 1648 Assuming $|U|^2 = 1$ we calculated the events number according to Equation 6.6

$$N_{events} = \phi(HNL/10^{21} p.o.t./cm^2) \cdot \frac{V_{FV}}{c\beta\gamma} \cdot \Gamma_{mode} \cdot Eff, \quad (7.3)$$

1651 where Eff is the selection efficiency. Possible uncertainties sources are:

- 1652 ➤ $\phi(HNL/10^{21} p.o.t./cm^2)$ - a HNL flux. As it is calculated based on the kaon flux, the uncer-
 1653 tainties of the kaon flux modeling should be included here,
- 1654 ➤ Eff - a selection efficiency uncertainties, the detector systematics should be included here.

1655

3.1 Detector systematics

1657 To study detector uncertainties, we can use the results of the same study for the active neutrino
 1659 interactions. But some changes should be applied as we use TPC instead of FGD. We consider the
 1660 following systematics:

- 1661 ➤ Magnetic Field distortions. Uncertainties in magnetic field map,
- 1662 ➤ TPC momentum scale,
- 1663 ➤ TPC momentum resolution,
- 1664 ➤ TPC PID. Uncertainties in particle identification,
- 1665 ➤ TPC tracking efficiency,
- 1666 ➤ TPC charge ID efficiency. Uncertainties of charge identification,
- 1667 ➤ TPC-FGD matching efficiency,
- 1668 ➤ TPC cluster efficiency. Additional inefficiency of TPC cluster reconstruction,
- 1669 ➤ Pion secondary interactions,
- 1670 ➤ Global vertex association

1671 For the mode $N \rightarrow \mu\mu\nu$ we should consider additional ECal systematics as we use this detector
 1672 in our cut sequence:

- 1673 ➤ TPC-ECal track clustering and matching efficiency,
- 1674 ➤ ECal Particle Identification



Systematic evaluation in the ND280

The systematic uncertainties are estimated in the ND280 detector with two methods:

- Observable-variation systematic
- Efficiency-like systematic

The variation systematic is applied for all variables that are reconstructed quantities on which we have an uncertainty. The method of propagation includes varying the observable, applying all the selection cuts and study the selected event number variation. This variation will be the uncertainty estimation of the analysis result.

The efficiency-like (weight) systematic concerns all the variables that correspond to a reconstruction/detection probability. For example the probably to have or not to have the reconstructed track. The uncertainty estimation starts from choosing the appropriate control samples with lots of events with and without successful detection. Then we study the difference between MC and data samples. The mean of the difference will be used as the correction for the MC, while the variation will be used as the uncertainty of the value. This method is much faster from the computing point of view, as do not require to run the selection many times.

1675 The systematic that was estimated by ourselves for this particular analysis is the uncertainty of
 1676 the track association into the global vertex (GV). We look at the GV in the TPC fiducial volume. So
 1677 we should estimate the vertex association systematics. It's impossible for neutrino interactions in
 1678 the TPC FV because of the lack of the statistics, so the FGD FV was chosen for this study.

1679 We check the efficiency of the successful association of the "suitable" tracks in vertex. Two
 1680 samples are defined for the FGD1 and FGD2 respectively. "Suitable" means that the tracks should
 1681 pass the following cuts:

- 1682 ➤ both start in the FGD1/2 FV;
- 1683 ➤ different charge;
- 1684 ➤ close start position 50 mm for X and Y axis and 100 mm for Z axis;
- 1685 ➤ only one sample (FGD1 or FGD2) was filled with tracks that passed upper cuts.

1686 The efficiency of the vertex merger is defined as the ratio of the number of the tracks' pairs as-
 1687 sociated in vertex to tracks' pairs that passed the cuts that were listed above. We should check if
 1688 this efficiency depends on the tracks parameters i.e. momentum, opening angle. The results are
 presented in [Figure 7.12](#)

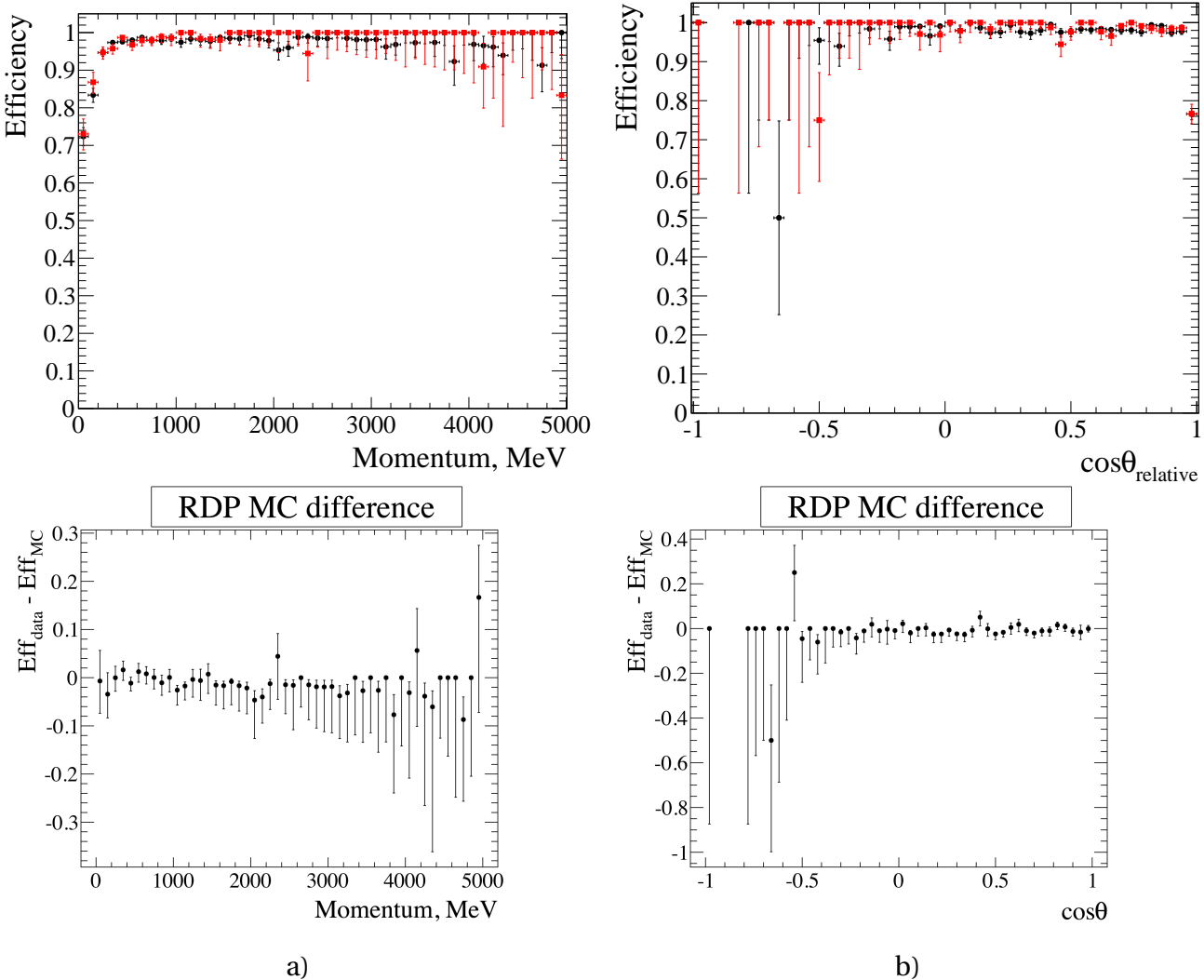


Figure 7.12: Dependence of the global vertex association systematics on the track momentum (a) and on the opening angle (b) for FGD1 sample in black for DATA and in red for MC.

1690 We conclude that there is neither angular nor momentum systematics dependence. The efficiency
 1691 for MC and DATA are presented in [Table 7.6](#). The systematics for the HNL study was estimated
 using these efficiency differences with weight-like method. One more check is the spatial

	FGD1	FGD2
DATA	$0.958^{+0.0023}_{-0.0024}$	$0.944^{+0.0027}_{-0.0026}$
MC	$0.962^{+0.0036}_{-0.0038}$	$0.952^{+0.004}_{-0.0042}$
Systematic uncertainty for $N \rightarrow \mu\pi$	0.58%	0.46%
Systematic uncertainty for $N \rightarrow e\pi$	0.51%	0.4%

Table 7.6: Global vertex association efficiency and systematics.

1692
 1693 resolution comparison between the data and MC. We checked the difference between the track
 1694 start position and the vertex position. The results are shown in [Figure 7.13](#), the statistics is sum-
 1695 marized in [Table 7.7](#). As we can see the mean value for MC and data are rather close, the difference
 between them is near fit error and much less than RMS.

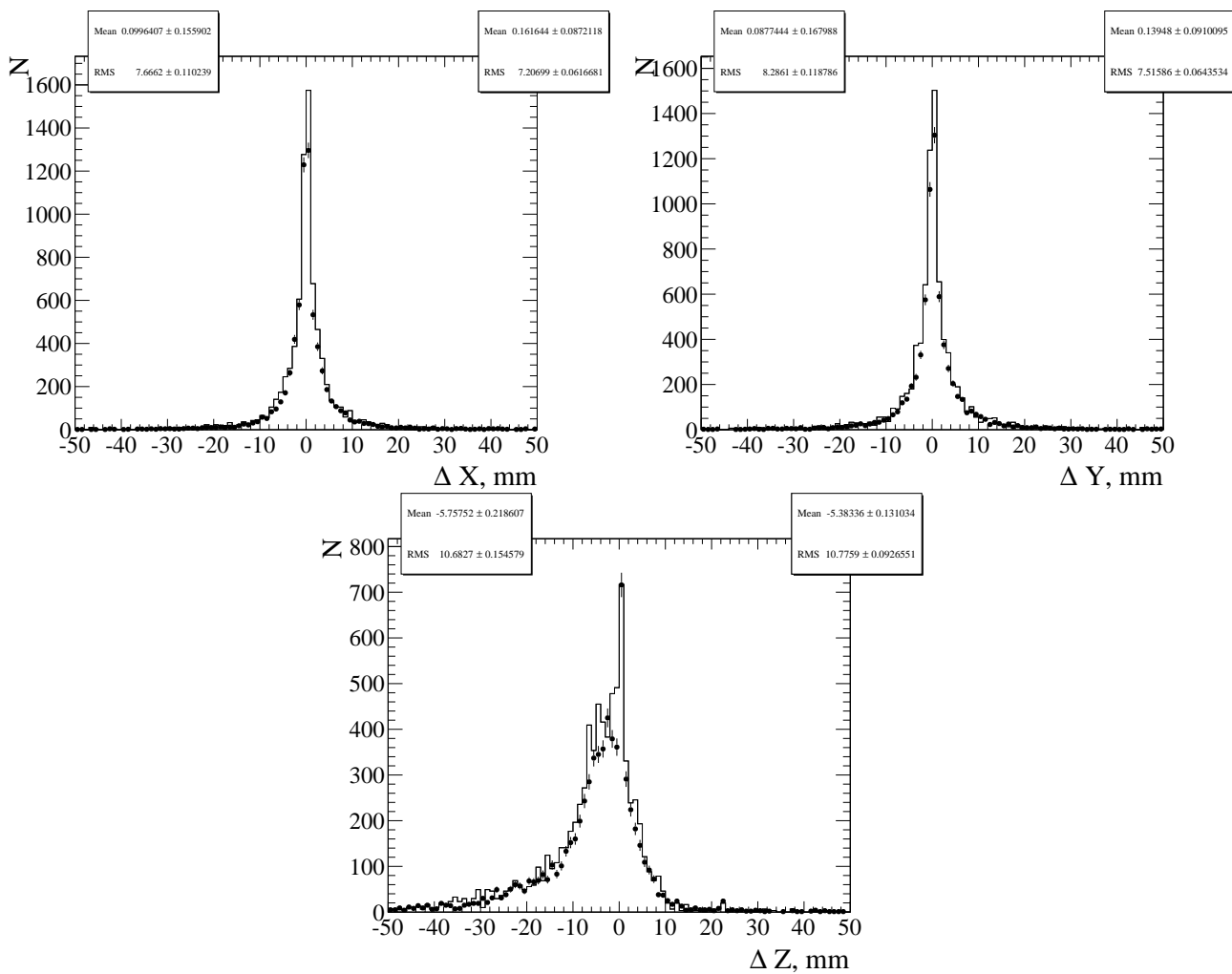


Figure 7.13: Global vertex spatial resolution for experimental and MC data. Dots and left statistic
 box are experimental data, histograms and right statistic box is MC data.

1696
 1697 The global vertex systematics can be obtained only for the FGD but tracks from HNL decays
 1698 start in TPC. So the following strategy was used: for the TPC1 tracks we consider systematics from

Axis		Mean	RMS
X	MC	0.16 ± 0.09	7.20 ± 0.06
	DATA	0.1 ± 0.16	7.67 ± 0.11
Y	MC	0.09 ± 0.17	8.29 ± 0.12
	DATA	0.14 ± 0.09	7.5 ± 0.06
Z	MC	-5.76 ± 0.22	10.68 ± 0.15
	DATA	-5.38 ± 0.13	10.78 ± 0.09

Table 7.7: Summary of the statistics for spatial resolution for experimental and MC data presented in [Figure 7.13](#).

1699 the FGD1 sample, for the TPC2 and TPC3 tracks we apply the FGD2 sample results. This method
 1700 gives the uncertainties at level 0.5%.

The results of all the systematic study are presented in [Table 7.8](#).

	$\mu\pi$	$e\pi$	$\mu\mu\nu$
Variation-like			
B Field distortions	0.48%	0.37%	0.02%
TPC momentum scale	0.03%	0.01%	0.04%
TPC momentum resolution	2.34%	0.78%	0.46%
TPC PID	0.41%	0.75%	1%
Efficiency-like			
TPC cluster efficiency	$\ll 1\%$	$\ll 1\%$	0.01%
TPC tracking efficiency	0.44%	0.34 %	0.46%
TPC charge ID efficiency	0.04%	0.21%	0.76%
TPC-FGD matching	0.27%	$\ll 1\%$	0.03%
Pion secondary interactions	3.88%	2.91%	-
Global vertex combining	0.58%	0.52%	0.48%
ECal PID	-	-	0.27%
ECal TPC matching	-	-	0.01%
Total	4.64%	3.20%	1.51%

Table 7.8: Detector systematics summary.

1701
 1702 The detector systematic dependence on HNL mass is shown in [Figure 7.14](#) and [Figure 7.15](#). As
 1703 one could see the most critical uncertainty comes from the pion secondary interactions for the
 1704 modes $e\pi$ and $\mu\pi$. As the dimuon mode $\mu\mu\nu$ doesn't produce pions in the final state it's free from
 1705 that uncertainty and the total error is much smaller.
 1706

3.2 Flux systematics

1708 Heavy neutrino flux in the ND280 is calculated based on the kaon flux in the decay volume
 1710 ([chapter 6](#)). Because of this, uncertainties in the kaon flux will affect the number of events. The
 1711 total flux error consists of the meson multiplicities, pion rescatter, interaction length, focusing
 1712 and other errors [101]. These fractional errors and the total flux uncertainty are presented on the
 1713 [Figure 7.16](#). In the active neutrino studies the meson multiplicity uncertainty is dominated by
 1714 the pion multiplicities. In our analysis we are sensitive only to kaon multiplicity errors. For the

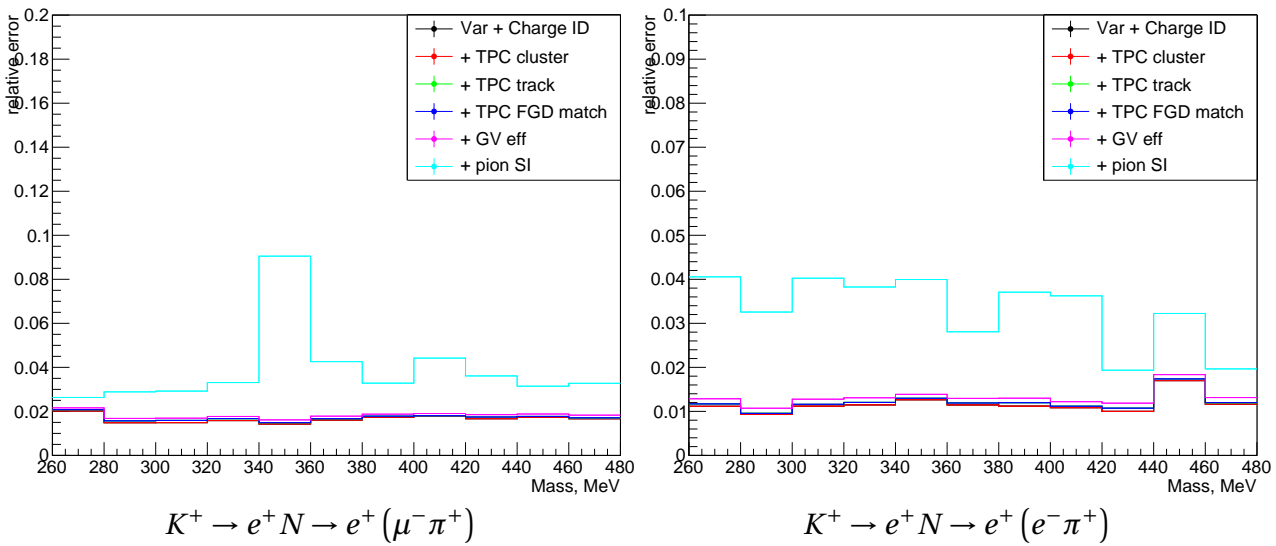


Figure 7.14: Detector systematics dependence on HNL mass

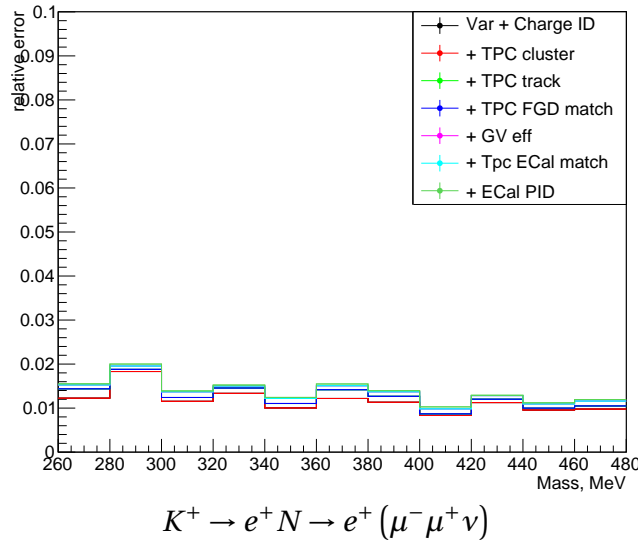


Figure 7.15: Detector systematics dependence on HNL mass

1715 HNL analysis we consider all the uncertainties except meson multiplicities are the same as for the
 1716 active neutrino flux. Thus to estimate kaon flux errors we take total neutrino flux error subtract
 1717 meson multiplicity error and add kaon multiplicity uncertainty.

1718 To estimate the kaon multiplicity errors we use data from NA61. Relative uncertainties on the
 1719 K multiplicities are presented on the [Figure 7.17](#). For HNL analysis we deal mainly with the kaons
 1720 collinear to beam axis. We consider a conservative estimation of the kaon multiplicity uncertainty
 1721 as 20%. For all the other sources of the flux errors we take the maximum value among all energy
 1722 bins – 11%.

1723 The additional source of uncertainties is the flux reweight. For the HNL simulation we take so
 1724 called “nominal” flux. It is the average neutrino flux. The real flux changes a bit from run to run.
 1725 The run change is realized with the help of the renormalization of the event weight for every run.
 1726 We used the reweight files and checked that the run differences affect on our result in order $\ll 1\%$.
 1727 The error from this effect was summarized in quadrature with all other flux errors.

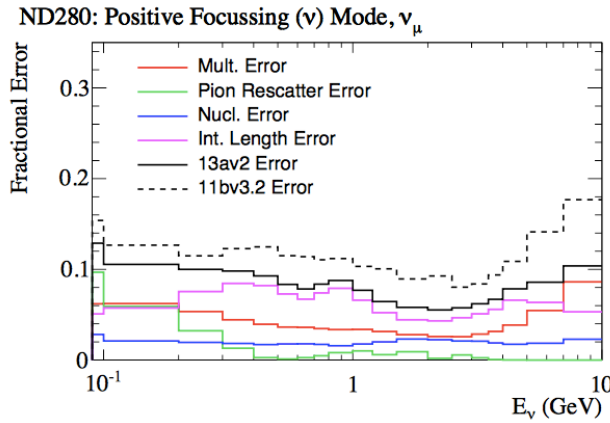
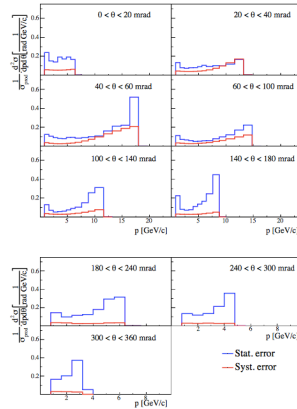
Figure 7.16: ν_μ Flux uncertainties.

Figure 7.17: Kaon multiplicity uncertainties.

1728 The results of the systematics study are presented on the Figure 7.18. The detector systematics
 1729 is widely described in previous subsection. As we analyze all charge conjugated modes together
 1730 we take the highest systematics uncertainties among them.
 1731

3.3 Pile up

1734 For the veto cuts we look for the activity in the upstream detector. Also we reject the events
 1735 that have tracks in the TPC with HNL candidate that doesn't correspond to the HNL daughters.
 1736 These are possible sources for the pile ups. The percentages of such events in the real data are
 1737 summarized in Table 7.9. In the table we use symbol "A" to mark the run period when P0D was
 1738 filled with air and "W" when it was filled with water. The content of the P0D may have influence
 1739 on the result of applying our veto cut. We have studied both ν and $\bar{\nu}$ runs as the pile ups can
 1740 be different for them. Also the two main sources of pile ups are separated for each TPC. For the
 1741 correction we use the maximum pile up value from all the runs in the each TPC which is shown in
 1742 red. In fact with this method effect of the pileups is overestimated.
 1743

4 Statistical methods

1745 The statistical approach to the low level signal analysis is described in the Highland and Cousins
 1746 work [112]. As number of the HNL decay events is proportional to the forth power of the mixing
 1748 element (chapter 6), constraints on $|U_i|^2$ without systematics looks like:

$$|U_i|_{limit}^2 = \sqrt{\frac{U_n}{N_{events}}} \quad (7.4)$$

1749 where

- 1750 ➤ $i = e, \mu$ is a lepton flavor,
- 1751 ➤ U_n is 90% C.L. Poisson limit for n observed events,
- 1752 ➤ N_{events} is expected number of signal events assuming $|U|^2 = 1$.

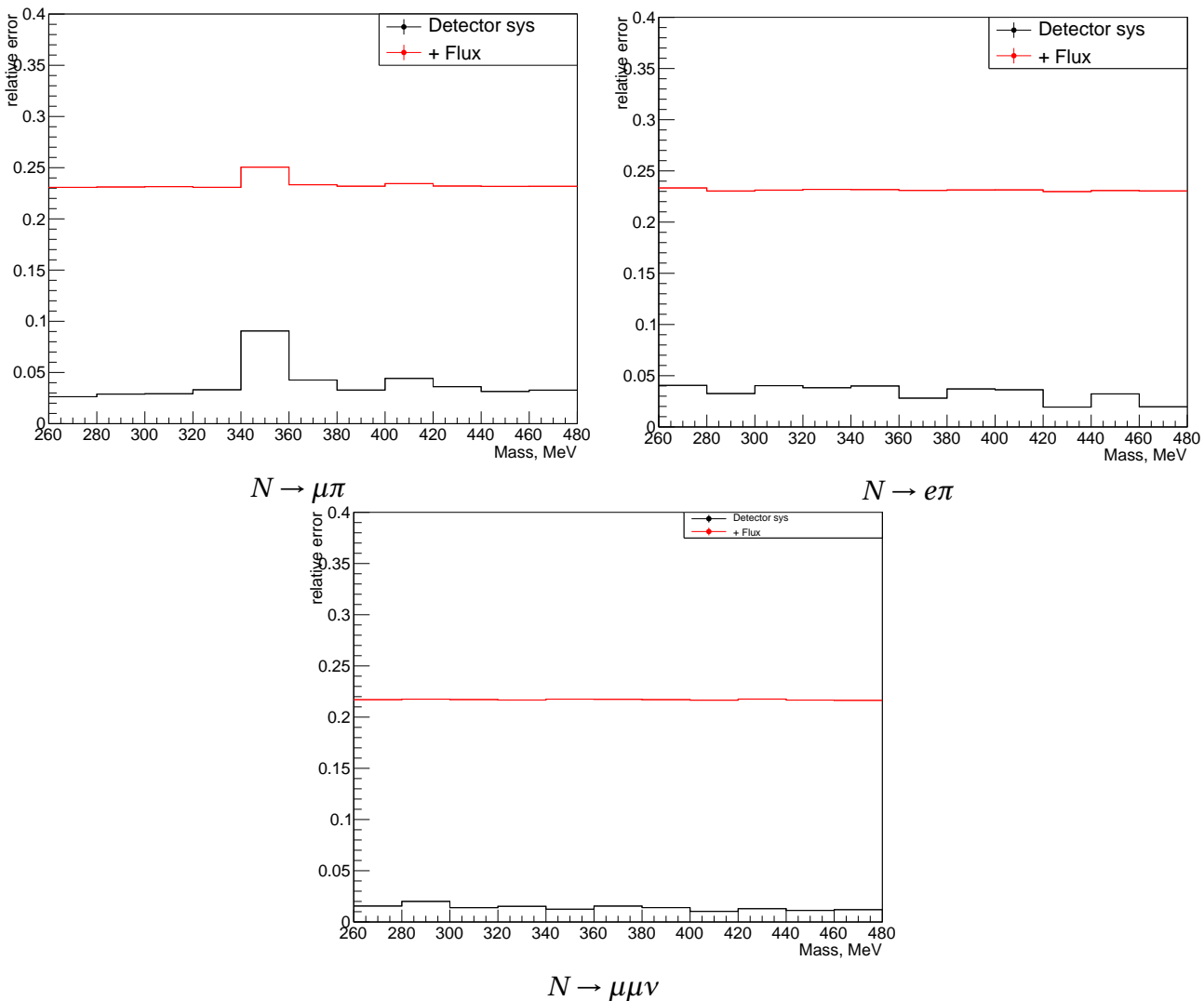


Figure 7.18: Detector and flux systematic errors for different modes.

1753 If we take into account the detector acceptance uncertainty, the result can be calculated according
 1754 to [112]:

$$U_n = U_{n0} \left\{ 1 + E_n \frac{\sigma_{Acc}^2}{2} \left(1 + \left(\frac{E_n \sigma_{Acc}}{2} \right)^2 \right) \right\} \quad (7.5)$$

1755 where

1756 ➤ U_{n0} is 90% C.L. Poisson limit for n observed events,

1757 ➤ σ_{Acc} is the acceptance error,

1758 ➤ $E_n = U_{n0} - n$ represents the excess of the upper limit of a Poisson parameter over the number
 1759 n of observed events, for a specified confidence level.

1760 This approach can be applied only while $\sigma_{Acc} < 1/E_n$. We already showed that in our study $\sigma_{Acc} \approx$
 1761 0.3 and $1/E_n > 0.5$ (this values are described in the section 3). So this method could be applied for
 1762 the analysis.

1763 One more important feature of the current analysis is that we don't consider the background
 1764 and its uncertainty. We used the background estimations to tune our selection. For the final result
 1765 we will treat all the observed events as a signal and then put a conservative limit on the mixing

Cut	Run 1W	Run 2W	Run 2A	Run 3b A	Run 3c A
TPC1 start	0.3%	0.61%	0.69%	0.64%	0.75%
TPC1 veto	0.32%	0.43%	0.49%	1.83%	2.15%
TPC1 all	0.57%	0.96%	1.00%	1.08%	2.75%
TPC2 start	0.25%	0.48%	0.55%	0.52%	0.6%
TPC2 veto	1.03%	1.73%	2%	1.83%	2.18%
TPC2 all	1.19%	2.05%	2.36%	2.18%	2.57%
TPC3 start	0.26%	0.46%	0.53%	0.48%	0.57%
TPC3 veto	0.93%	1.56%	1.78%	1.64%	1.95%
TPC3 all	1.1%	1.85%	2.11%	1.95%	2.3%
	Run 4W	Run 4A	Run 5W	Run 5W $\bar{\nu}$	Run 6A $\bar{\nu}$
TPC1 start	0.89%	0.95%	0.7%	0.35%	0.45%
TPC1 veto	2.55%	2.76%	1.95%	0.96%	1.26%
TPC1 all	3.25%	3.45%	2.51%	1.25%	1.62%
TPC2 start	0.71%	0.76%	0.55%	0.29%	0.38%
TPC2 veto	2.65%	2.76%	2.03%	1.15%	1.47%
TPC2 all	3.1%	3.24%	2.39%	1.34%	1.71%
TPC3 start	0.68%	0.72%	0.53%	0.28%	0.35%
TPC3 veto	2.34%	2.46%	1.81%	1.02%	1.31%
TPC3 all	2.75%	2.89%	2.15%	1.2%	1.54%
	Run 7b	Run 7c	Run 8A	Run 8A	
TPC1 start	0.62%	1.74%	1.76%	1.27%	
TPC1 veto	0.55%	1.46%	1.26%	0.93%	
TPC1 all	1.07%	2.93%	2.77%	2.02%	
TPC2 start	0.52%	2.30%	1.37%	0.99%	
TPC2 veto	2.03%	4.73%	4.63%	3.42%	
TPC2 all	2.35%	5.53%	5.43%	2.83%	
TPC3 start	0.49%	1.30%	1.33%	0.96%	
TPC3 veto	1.81%	4.23%	4.14%	3.06%	
TPC3 all	2.11%	4.94%	4.84%	3.57%	

Table 7.9: Event pile up in real data.

elements. Such approach will be indeed conservative, but the pros is that we are free from the background uncertainty at all. If during the unblinding plenty of events was found we would put the worse limits on the mixing. Such method could be improved in the future (see section 3).

1769

1770

1771

1 MC sensitivity estimations

1773 After studying the MC efficiency (subsection 2.2), background processes (subsection 2.3), sys-
 1775 tematics (section 3) and pile ups (subsection 3.3), sensitivity to the mixing elements based on MC
 1776 could be estimated according to Equation 7.5). The results are shown in Figure 8.1 and Figure 8.2.
 1777 Because of the small background the acceptance uncertainties have a small effect on the sensitiv-
 1778 ity.

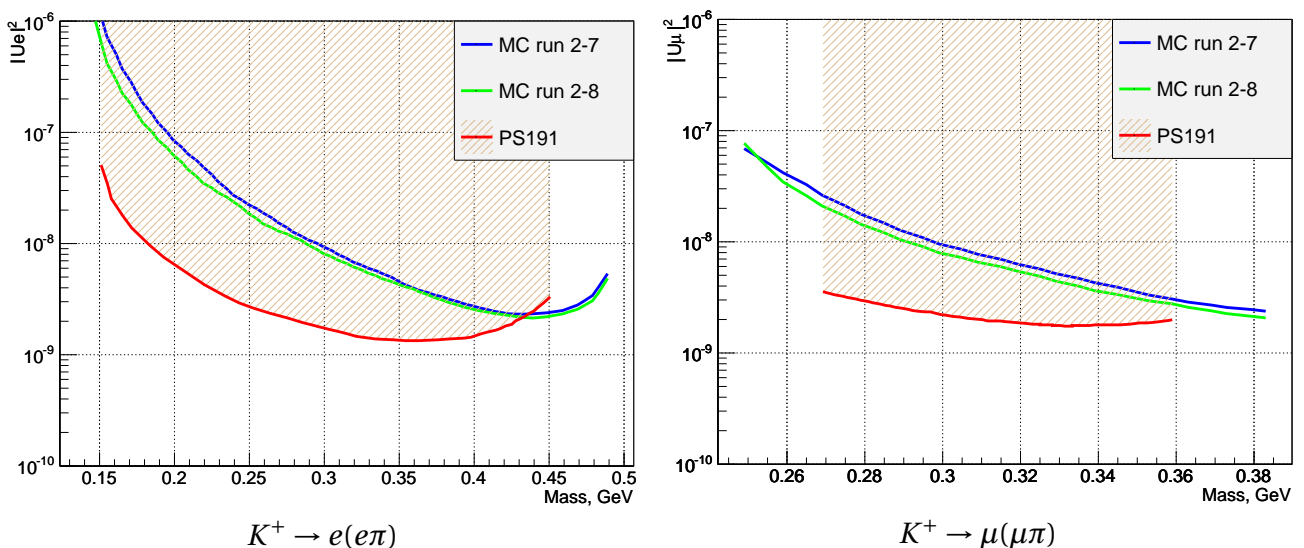


Figure 8.1: Sensitivity to mixing elements $|Ue|^2, |U\mu|^2$ based on MC samples analysis

1779 As one can see the improvements of PS191 limits can be obtained with the current statistics.

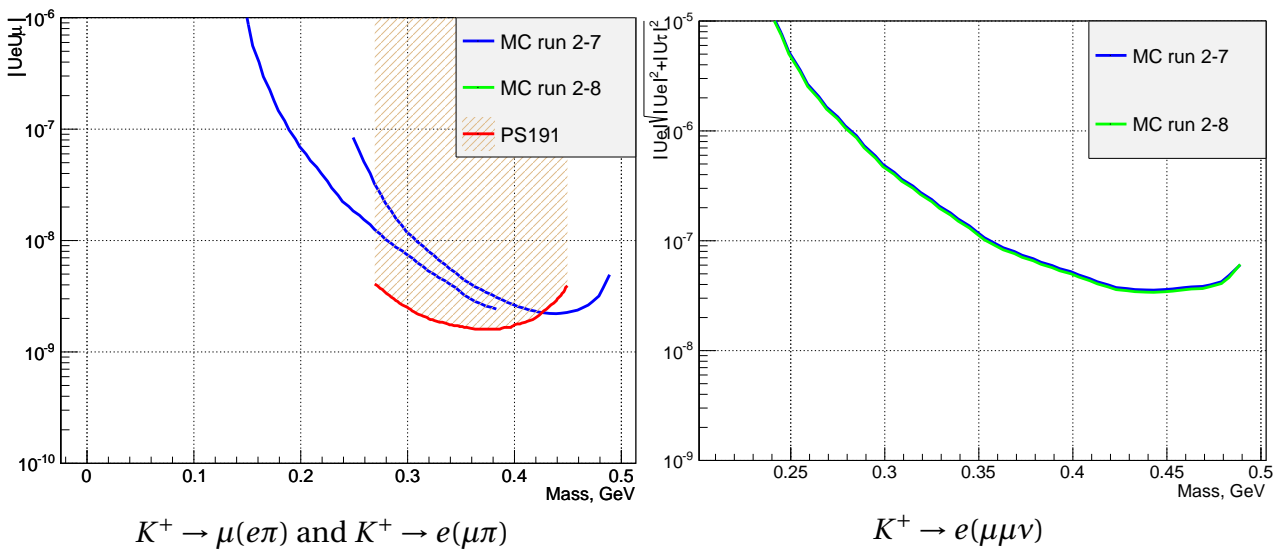


Figure 8.2: Sensitivity to mixing elements $|UeU\mu|$ and $|U_e| \sqrt{|U_e|^2 + |U_\tau|^2}$ based on MC samples analysis.

1780

1781

2 Data unblinding

1782 The current analysis was approved for the data unblinding. The numbers of observed events
 1784 in data are presented in the [Table 8.1](#). All the results are presented for full ND280 data set (run 2-8).

	Events in data
$\mu\pi$	0
$e\pi$	0
$\mu\mu\nu$	1

Table 8.1: The total number of events observed in data.

1785 One event for the $N \rightarrow \mu\mu\nu$ mode was observed. It happened in the TPC3 and looks like the
 1786 signal event: two muon-like tracks with the direction extremely collinear to beam axis. The event
 1787 display for this event is presented in [Figure 8.3](#).

1788 More accurate study shows that the invariant mass of this muon pair is too high for the heavy
 1789 neutrino decay $M_{inv} \approx \text{GeV}$. But based on blind analysis method and our analysis strategy this
 1790 event will be treated as a signal and appropriate upper limit on the mixing element will be set.

1791 Based on this numbers final sensitivity to mixing elements based on our analysis can be esti-
 1792 mated. The results are presented in [Figure 8.4](#) and [Figure 8.5](#). The data statistics $(10.23\nu + 6.29\bar{\nu}) \cdot$
 1793 $10^{20} POT$ was used.

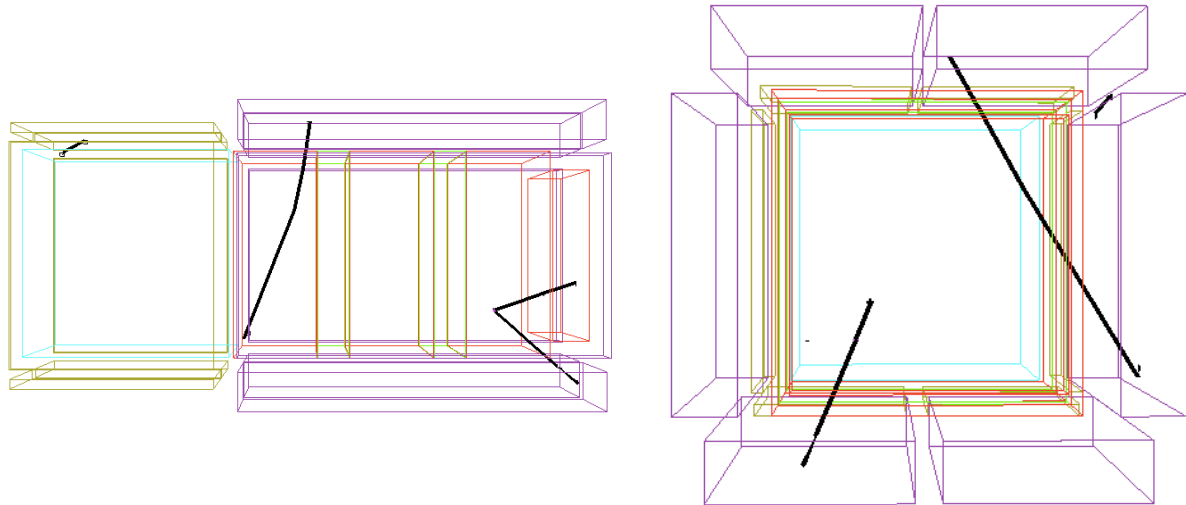


Figure 8.3: Event observed in the $N \rightarrow \mu\mu\nu$ mode in the data sample in the TPC3.

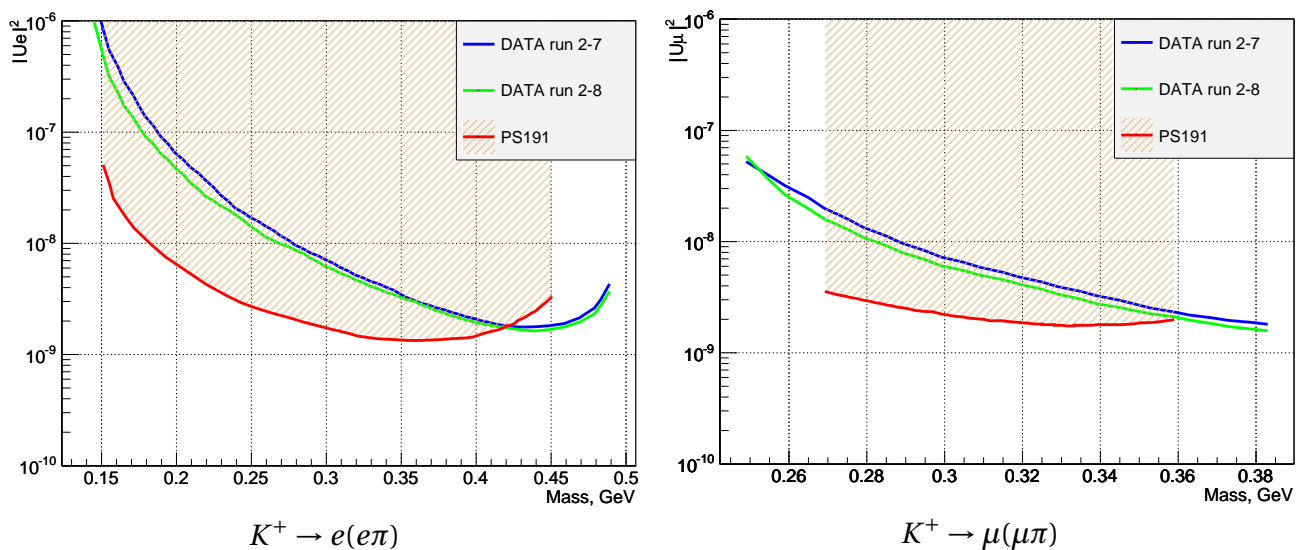


Figure 8.4: Sensitivity to mixing elements $|Ue|^2, |Um|^2$ based on the data samples analysis.

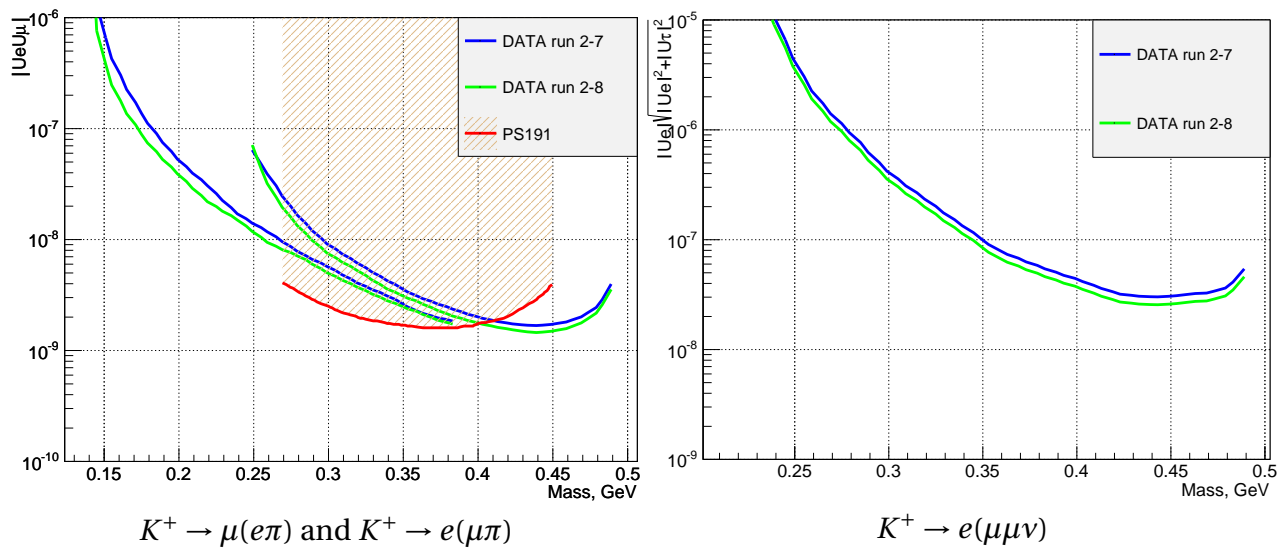


Figure 8.5: Sensitivity to mixing elements $|U_{e\mu}|$ and $|U_{el}|\sqrt{|U_{el}|^2 + |U_\tau|^2}$ based on the data samples analysis.

1794

3 Prospects

1795

1796 The current study put a conservative limit on the mixing elements of the heavy neutrino. The
1798 more accurate result could be obtained with the precise background estimations

1799 This work was continued by other collaborators and other methods were used for the data
1800 treatment. The accurate background estimations were developed and a new Markov Chain Monte
1801 Carlo method was used for the mixing elements limitation. All the production and decay modes of
1802 the heavy neutrino are analyzed together and the solid final result is obtained. The joint analysis
1803 including all the methods was published [118].

1804 The T2K experiment will continue taking data. The preliminary plan is to accumulate 20×10^{21}
1805 POT [91]. With larger statistics (x11 to current) we will obviously be more sensitive to the HNL
1806 mixing elements. As the result is proportional to square root from the expected events number the
1807 limits could be improved by the factor of 3.

1808 The upgrade of the near detector complex is ongoing now [119] (also Part III). Two additional
1809 TPC will be installed. For the current study it means that the fiducial volume will be extended by
1810 $\approx 10\%$. That will also slightly improve the final result.

1811

Part III

1812

ND280 upgrade

1813

1814

INTRODUCTION

1815 As mentioned in [chapter 4](#), the first goal of the T2K experiment was to measure the θ_{13} mixing angle. The non-zero value of this angle would open a road towards the CP-violation in the neutrino
1816 oscillations. After the successful discovery of the θ_{13} , T2K entered a phase of the precise measure-
1817 ment of the neutrino oscillation parameters. The experiment provides the most precise estima-
1818 tions for the θ_{23} and also very accurate measurements of the Δm_{23} and θ_{13} . The big progress was
1819 obtained in the search for the CP-violation with the determination of the 3σ confidence level on
1820 the possible values of the δ_{CP} [120]. The δ_{CP} measurement became the main goal of the experi-
1821 ment.

1823 The next-generation experiments like DUNE [93] and Hyper-Kamiokande [92] will be able to
1824 achieve 3σ sensitivity to the CP-violation across the wide range of the δ_{CP} values but on the time
1825 scale 2026 and beyond. The T2K experiment can probe this effect with less sensitivity but much
1826 earlier. The sensitivity of the T2K experiment with the total statistics of 20×10^{21} POT is shown in
1827 [Figure 9.1](#).

1828 More statistics is necessary to determine the neutrino/anti-neutrino asymmetry more pre-
1829 cisely and to justify if the effect takes place. The improvement of the sensitivity versus the col-
1830 lected data is shown in [Figure 9.1](#) b. Initially, the T2K was supposed to collect the total statistics
1831 of 7.8×10^{21} POT. The extended run of the T2K experiment aiming at the total statistics 20×20^{21}
1832 POT was proposed [91]. This additional period of data collection was called T2K-II. The beamline
1833 will be upgraded to provide a more intensive neutrino beam ([section 1](#)). Thus the data statistics
1834 accumulation will go faster.

1835 There is a room for further improvement of the sensitivity with the reduction of the system-
1836 atic uncertainty. [Figure 9.1](#) presents the sensitivity of the T2K experiment with different assump-
1837 tions: current systematic uncertainties (in blue), improved systematics by factor 2/3 (in orange),
1838 only statistical uncertainty (in black). With the improved systematics, the desired sensitivity will
1839 be reached faster, and finally, the wider range of the δ_{CP} could be studied. The budget of the sys-
1840 tematic uncertainties of the T2K experiment is described in [105]. The main sources in decreasing
1841 order are neutrino cross-sections, flux, secondary interactions in the SK, SK detector. The system-
1842 atics related to the SK is very hard to reduce and it is going to be extremely expensive. Also, it gives
1843 a minor impact. The systematic uncertainty related to the neutrino cross-section and flux could
1844 be better constrained with the upgrade of the near detector.

1845 T2K near detector provides superior systematics reduction. It decreases the uncertainty of the
1846 oscillation analysis from 12% down to 6%. But for the T2K-II the further systematics reduction is re-

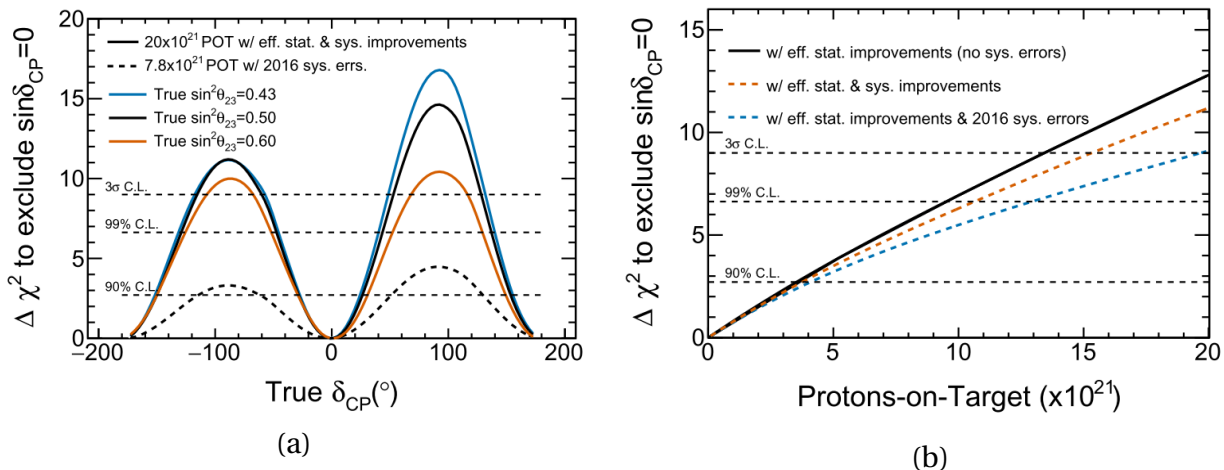


Figure 9.1: An expected sensitivity of the T2K experiment to the CP-violation in the neutrino oscillations. The known mass order is assumed. Three systematic uncertainties estimations are used: (blue) 2016 value, (orange) with improvements by factor 2/3 and (black) only stat. uncertainties. (a) shows the sensitivity over the δ_{CP} value and (b) shows the sensitivity evolution over the collected statistics for $\delta_{CP} = -\pi/2$.

1847 quired. The acceptance of the near detector is known to be limited. Originally ND280 was designed
1848 for the reconstruction of the forward-going particles, while the far detector Super-Kamiokande
1849 detects the particles in the 4π phase space. Also, ND280 is not able to detect low energy nucleons
1850 produced in the neutrino interactions that make the neutrino energy reconstruction inaccurate.
1851 The upgrade of the near detector is proposed (section 2). The idea is to use a highly granulated
1852 target to reduce the threshold of particle detection. Above and below this target two new TPCs
1853 will be placed. Thus the phase space acceptance will be enlarged and include particles pointed in
1854 the perpendicular direction with respect to the incoming neutrino. With the improvements men-
1855 tioned above the systematic uncertainty of the oscillation analysis will go below 4%. The present
1856 value is about 6%. Hence the improvement of the sensitivity illustrated in Figure 9.1 is possible.

1857

1 Beamline upgrade

1858

1859 The neutrino interactions are extremely rare processes. The natural way to gain statistics in the
1860 experiment is to use a very intensive beam. The T2K experiment uses the beam produced by the
1861 J-PARC accelerator complex. After the few upgrades, the power of the beam in the main ring of the
1862 accelerator reached 500 kW. As a result, the J-PARC complex provides one of the most intensive
1863 neutrino beams in the world. It was proved that T2K could obtain better physics results with the
1864 statistics extension to 20×10^{21} POT [91]. For these propose the J-PARC accelerator will be upgraded
1865 to provide even more intensive beam with the power of 1.3 MW.

1866 The beamline power upgrade schedule is shown in Figure 9.2. The accelerator will be stopped
1867 for one year for the major hardware improvement. In the following years, the intensity will slightly
1868 grow alongside the data collection. The target power 1.3 MW is planned to be reached by 2028.
1869 This is beyond T2K. The Hyper-Kamiokande experiment is going to use the same beamline and
1870 use all the benefits from the power upgrade after the T2K. The details about the beamline upgrade
1871 are widely described in [121].

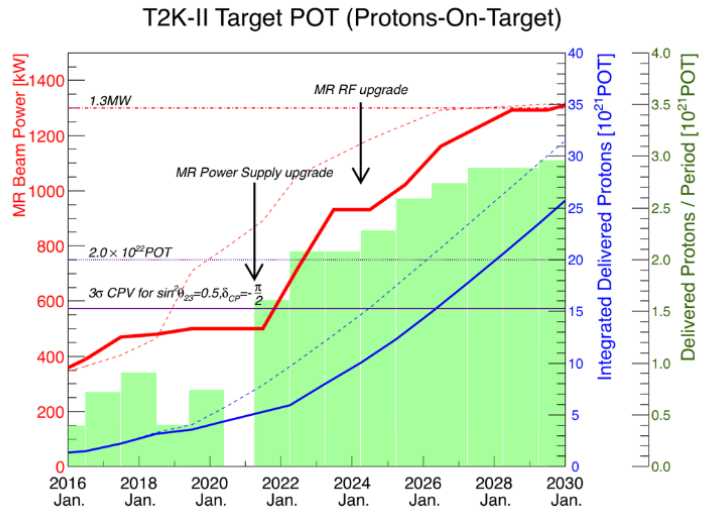


Figure 9.2: Target J-PARC beam power (red) and the expected total accumulated statistics (blue) as a function of the year. Two possible schedules are considered shown with solid and dashed lines.

1873

2 Detector overview

1874

1875

1876

1877

2.1 Current detector limitations

1878 The T2K off-axis near detector is widely described in subsection 2.2 of chapter 4. The schematic
 1880 view of the setup is presented in Figure 4.8 (b). There are plenty of known problems that limit the
 1881 performance of the ND280. As a result, the total T2K systematics is dominated by the neutrino
 1882 cross-section and flux uncertainty. These uncertainties could be reduced with better constraints
 1883 with the upgraded ND280.

1884 One of the main limitations is caused by restrictive phase-space coverage. The event display
 1885 of the neutrino interaction in the ND280 as well as the detector layout is shown in Figure 9.3. The
 1886 scintillator neutrino targets (Fine Grained Detectors) are shown in violet. They are alternated with
 1887 3 TPCs shown in blue. Such a setup is perfect for the reconstruction of the forward and backward
 1888 going particles. But if the lepton from the neutrino interaction goes at a high angle w.r.t. the beam
 1889 (up/down in Figure 9.3) we will not be able to perform accurate measurements. It will not leave
 1890 a long enough track in the TPCs, hence we could not estimate the momentum with the curvature
 1891 and the particle type with the energy loss. It is even possible that the particle goes alone the single
 1892 vertical bar in FGD. In this case, even tracking with the scintillator detector is impossible. The
 1893 efficiency of the muon selection from the $\nu_\mu CC$ interactions in the FGD1 over the outgoing lepton
 1894 angle is shown in Figure 9.4.

1895 The far detector can detect the outgoing lepton with uniform efficiency over the 4π phase-
 1896 space. But the near detector could measure only neutrino interactions producing forward going
 1897 leptons. The comparison of the detectors' acceptance and the expected lepton phase space are
 1898 shown in Figure 9.5. To extend the constraints from the ND280 to the full phase-space various
 1899 models of the neutrino interactions are used. But the uncertainties of such models are quite high.
 1900 The direct measurements of the leptons in 4π angle in the near detector will dramatically reduce
 1901 the systematic uncertainty.

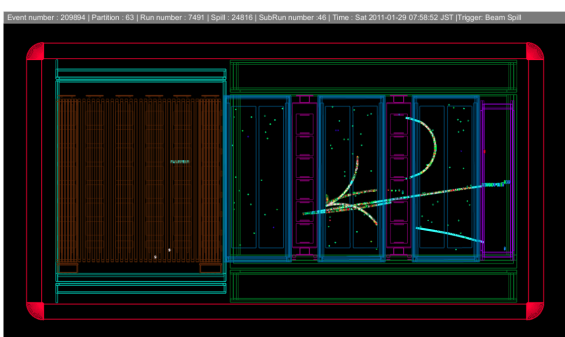


Figure 9.3: The event display of the neutrino interaction in the FGD1 in the ND280. The beam is coming from the left.

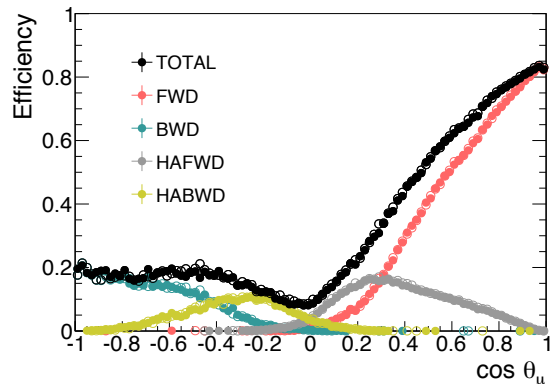


Figure 9.4: Muon selection efficiency from the $\nu_\mu CC$ interactions in the FGD1 as a function of the lepton angle w.r.t. Z axis.

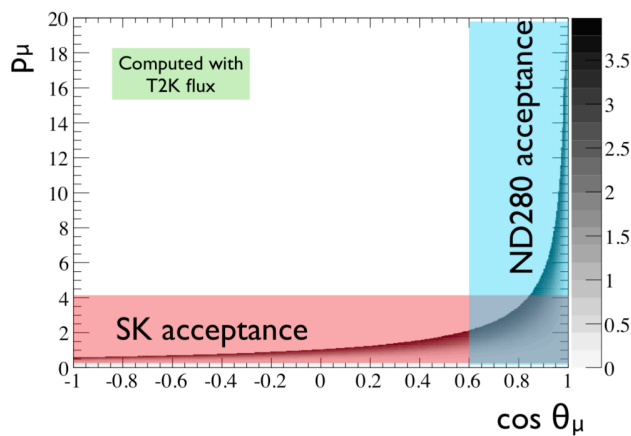


Figure 9.5: The acceptance of both near and far detectors of the T2K experiment over the expected lepton phase space.

1902 The other subject of concern is the threshold of particle detection. Thanks to muon penetration
 1903 ability, they are leaving a long track and could be easily detected. But protons from the neutrino
 1904 interactions are mostly low energetic and travel a short distance. It's pretty tricky to detect
 1905 them with the sandwich detector like FGD. The proton should go through at least q few layers
 1906 for robust detection. If it is pointing at a high angle w.r.t. beam the situation is even worse. The
 1907 current threshold of the proton detection in FGDs is around 500 MeV, while the proton spectrum
 1908 starts from 200 MeV. Nucleon detection from the neutrino interaction is extremely important in
 1909 the T2K. As mentioned in [chapter 4](#), Super-Kamiokande uses CCQE interaction assumption to re-
 1910 construct the neutrino energy. But in reality, neutrino interacts not with the free nucleon but with
 1911 the Oxygen in SK and with Carbon and Oxygen in ND280. The nuclear effects ([subsubsection 1.4.b](#)
 1912 of [chapter 1](#)) are biasing the neutrino energy measurements. They could even change the event
 1913 topology. For example, after neutrino interacts with pion production, the pion could be absorbed
 1914 in the nuclei and the event will look like the CCQE interaction. That's why nuclear effects should
 1915 be precisely constrained. It could be done with the precise measurement of both outgoing lepton
 1916 and nucleon kinematics. The detection of short pion tracks will also, help a lot with the proper
 1917 reconstruction of the interaction topology and will gain the neutrino energy estimation accuracy
 1918 as well.

1919

2.2 New design proposal

To improve the performance of the near detector its upgrade was proposed [119]. The ND280 tracker (2 FGDs and 3 TPCs) will be kept in place and will continue operation. Thus the data from both T2K-I and T2K-II could be analyzed together. The π^0 detector will be replaced with the new neutrino target and 2 horizontal TPCs. The upstream part will be surrounded by the time of flight (ToF) detectors. The various CAD models are presented in Figure 9.6 and Figure 9.7.

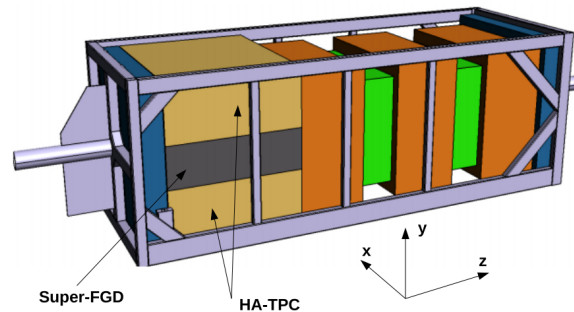


Figure 9.6: The scheme of the upgraded near detector. The downstream part is kept as it is. The new horizontal target and two high angle TPCs are put in the upstream part,

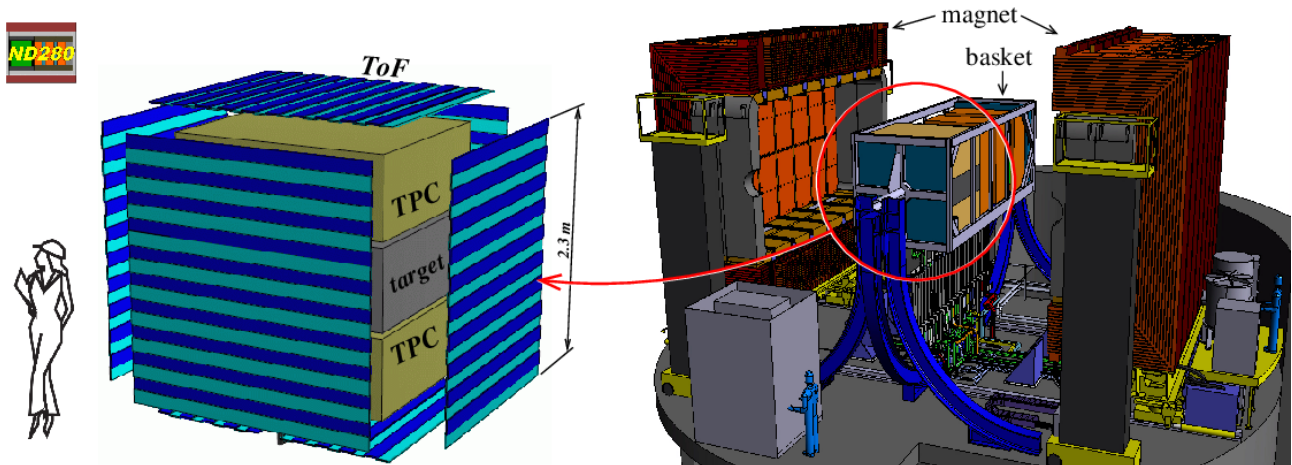


Figure 9.7: The CAD model of the whole upgraded detector setup and the inset of the mostly affected by the modifications upstream part.

The new neutrino target Super-FGD (SFGD) will be composed of small plastic scintillator cubes. The cube edge is set to 1 cm providing fine granularity. Three orthogonal holes are drilled in the cube for the light readout with the WLS fibers. Thus the Super-FGD could reconstruct the tracks in 3D. High granularity significantly reduces the threshold of particle tracking. Also, such a structure will improve the separation between gamma conversion and electron neutrino CC interaction resulting in more precise ν_e cross-section measurements. The dimensions of the new target are $182 \times 184 \times 56 \text{ cm}^3$ giving the total mass close to 2 tonnes. The total fiducial mass of the ND280 will be nearly doubled. The large size of the target allows detecting the secondary interactions of

1935 the neutrons from the anti-neutrino CCQE interactions $\bar{\nu} + p \rightarrow \ell + n$. As mentioned in the [Introduction](#)
1936 measurement of the outgoing nucleons are critical for the precise neutrino energy recon-
1937 struction and probing neutrino interactions models. The details of the neutron detection proposal
1938 are presented in [chapter 13](#). More details about SFGD detector will be provided in [chapter 12](#).

1939 Two atmospheric pressure High angle TPCs (HATPC) will be put above and below Super-FGD.
1940 They will enlarge the phase space to the full coverage. The readout will be organized by the mi-
1941 cromegas as for the current TPC, but the new technology will be implemented. The detectors will
1942 be covered with the resistive foil resulting in the charge spreading over the pads. Thus the spatial
1943 resolution could be improved with the same pad size. It will lead to better momentum reconstruc-
1944 tion and finally more accurate neutrino energy estimations. The details about HATPC detector will
1945 be provided in [chapter 11](#).

1946 The Time of Flight (ToF) detectors will fully cover the upstream part of the ND280. It will be
1947 composed of scintillator bars and readout with the MPPC arrays. This detector will help with the
1948 reconstruction of the particle direction: to/from Super-FGD. Neutrino interacts quite often in the
1949 magnet coil and ECal and could produce a particle that will stop inside the SFGD. The relatively
1950 short track inside the scintillator target is not sufficient for the direction reconstruction, but the
1951 ToF detectors will give a clear answer. Also, this detector could help with particle identification.
1952 For example positrons and protons have very similar dE/dx around 1 GeV/c and could not be
1953 distinguished with the TPC but the time of flight is dramatically different.

1954 To sum up, the upgraded ND280 will have lost of benefits comparing to the present setup:

- 1955 ➤ full phase space coverage for the particles produced in neutrino interactions
- 1956 ➤ low threshold of the particle detection
- 1957 ➤ doubled fiducial mass
- 1958 ➤ better separation of the particles going "in" and "out" the target
- 1959 ➤ electron/gamma separation, resulting in better ν_e measurements
- 1960 ➤ neutron detection from $\bar{\nu}$ interactions

1961

C H A P T E R

10

1962

SIMULATIONS

1963

1964

1965

1 Concept

1966

1.1 Resistive MicroMegas technology

1969

2 Beamtest

1972

2.1 Cosmic test

1975

2.2 CERN beamtest

1978

2.3 DESY beamtest

1981

12

C H A P T E R

1983

1984

1985

1 Concept

1986

1987
1988**1.1 Assembly**

1989

1990
1991**2 Simulations**

1992

1993
1994**2.1 Expected light yield**

1995

1996
1997**2.2 Michell electron tagging**

1998

1999
2000**2.3 Pileups**

2001

2002
2003**3 Beamtest**

2004

2005
2006**3.1 First CERN beamtest**

2007

2008
2009**3.2 Second CERN beamtest**

2010

2011

SUPER FGD

2012

C H A P T E R

13

2013

NEUTRON TAGGING IN SUPERFGD

2014

1 Motivation

2015

2 Geant4 simulation

2016

2017

2018

3 Efficiency and energy resolution

2019

2020

2021

4 Background estimations

2022

2023

2024

5 Prospects for physics

2025

2026

2027

2028

2029

Part IV

2030

Conclusion

BIBLIOGRAPHY

- 2032 [1] J Chadwick. "Intensitätsverteilung im magnetischen Spectrum der β -Strahlen von radium
2033 B + C". In: *Verhandl. Dtsc. Phys. Ges.* 16 (1914), p. 383.
- 2034 [2] W. Pauli. *Letter to L. Meinter and other participants of the conference in Tübingen in 1930,*
2035 *a copy of the letter can be found in W. Pauli, Neutrino Physics ed. by K. Winter, Cambridge*
2036 *Univ. Press, Cambridge 1991, p.4, the first publication was given in W. Pauli. 1930.*
- 2037 [3] E. Fermi. "Versuch einer Theorie der β -Strahlen. I". In: *Zeitschrift für Physik* 88.3-4 (Mar.
2038 1934), pp. 161–177. DOI: [10.1007/BF01351864](https://doi.org/10.1007/BF01351864).
- 2039 [4] C. L. Cowan et al. "Detection of the free neutrino: A confirmation". In: *Science* 124.3212
2040 (1956), pp. 103–104. DOI: [10.1126/science.124.3212.103](https://doi.org/10.1126/science.124.3212.103).
- 2041 [5] G. Danby et al. "Observation of high-energy neutrino reactions and the existence of two
2042 kinds of neutrinos". In: *Physical Review Letters* 9.1 (1962), pp. 36–44. DOI: [10.1103/PhysRevLett.9.36](https://doi.org/10.1103/PhysRevLett.9.36).
- 2044 [6] C. N. Yang and R. L. Mills. "Conservation of isotopic spin and isotopic gauge invariance".
2045 In: *Physical Review* 96.1 (1954), pp. 191–195. DOI: [10.1103/PhysRev.96.191](https://doi.org/10.1103/PhysRev.96.191).
- 2046 [7] Sheldon L. Glashow. "Partial-symmetries of weak interactions". In: *Nuclear Physics* 22.4
2047 (Feb. 1961), pp. 579–588. DOI: [10.1016/0029-5582\(61\)90469-2](https://doi.org/10.1016/0029-5582(61)90469-2).
- 2048 [8] Steven Weinberg. "A model of leptons". In: *Physical Review Letters* 19.21 (1967), pp. 1264–
2049 1266. DOI: [10.1103/PhysRevLett.19.1264](https://doi.org/10.1103/PhysRevLett.19.1264).
- 2050 [9] Donald C Cundy. "Neutrino Physics - CERN". In: *17th International Conference on High-*
2051 *energy Physics*. London, 1974. URL: <http://cds.cern.ch/record/417920/>.
- 2052 [10] G. Arnison et al. "Experimental observation of isolated large transverse energy electrons
2053 with associated missing energy at $s=540 \text{ GeV}$ ". In: *Physics Letters B* 122.1 (Feb. 1983), pp. 103–
2054 116. DOI: [10.1016/0370-2693\(83\)91177-2](https://doi.org/10.1016/0370-2693(83)91177-2).
- 2055 [11] G. Aad et al. "Observation of a new particle in the search for the Standard Model Higgs bo-
2056 son with the ATLAS detector at the LHC". In: *Physics Letters, Section B: Nuclear, Elementary*
2057 *Particle and High-Energy Physics* 716.1 (Sept. 2012), pp. 1–29. DOI: [10.1016/j.physletb.2012.08.020](https://doi.org/10.1016/j.physletb.2012.08.020).
- 2059 [12] M. Goldhaber, L. Grodzins, and A. W. Sunyar. *Helicity of neutrinos*. 1958. DOI: [10.1103/PhysRev.109.1015](https://doi.org/10.1103/PhysRev.109.1015).
- 2061 [13] L. B. Auerbach et al. "Measurement of electron-neutrino electron elastic scattering". In:
2062 *Physical Review D* 63.11 (May 2001), p. 112001. DOI: [10.1103/PhysRevD.63.112001](https://doi.org/10.1103/PhysRevD.63.112001).
- 2063 [14] J. A. Formaggio and G. P. Zeller. "From eV to EeV: Neutrino cross sections across energy
2064 scales". In: *Reviews of Modern Physics* 84.3 (Sept. 2012), pp. 1307–1341. DOI: [10.1103/RevModPhys.84.1307](https://doi.org/10.1103/RevModPhys.84.1307).
- 2066 [15] B. Pontecorvo. "Inverse beta processes and nonconservation of lepton charge". In: *Zh.Eksp.Teor.Fiz.*
2067 7 (1957), p. 247.

- 2068 [16] Z Maki, M Nakagawa, and S Sakata. *REMARKS ON THE UNIFIED MODEL OF ELEMENTARY*
2069 *PARTICLES*. Tech. rep. 1962, p. 221.
- 2070 [17] Andrei D Sakharov. “Violation of CP invariance, C asymmetry, and baryon asymmetry of
2071 the universe”. In: *Journal of Experimental and Theoretical Physics Letters (JETP Letters)* 5
2072 (1967), pp. 24–27.
- 2073 [18] M. Tanabashi et al. *Review of Particle Physics*. Aug. 2018. DOI: [10.1103/PhysRevD.98.030001](https://doi.org/10.1103/PhysRevD.98.030001).
- 2075 [19] Sacha Davidson, Enrico Nardi, and Yosef Nir. *Leptogenesis*. Sept. 2008. DOI: [10.1016/j.physrep.2008.06.002](https://doi.org/10.1016/j.physrep.2008.06.002).
- 2077 [20] P. F. de Salas et al. “Status of neutrino oscillations 2018: 3σ hint for normal mass ordering
2078 and improved CP sensitivity”. In: *Physics Letters, Section B: Nuclear, Elementary Particle
2079 and High-Energy Physics* 782 (July 2018), pp. 633–640. DOI: [10.1016/j.physletb.2018.06.019](https://doi.org/10.1016/j.physletb.2018.06.019).
- 2081 [21] T. D. Lee and C. N. Yang. “Question of Parity Conservation in Weak Interactions”. In: *Physical
2082 Review* 104.1 (Oct. 1956), pp. 254–258. DOI: [10.1103/PhysRev.104.254](https://doi.org/10.1103/PhysRev.104.254).
- 2083 [22] C. S. Wu et al. “Experimental Test of Parity Conservation in Beta Decay”. In: *Physical Review*
2084 105.4 (Feb. 1957), pp. 1413–1415. DOI: [10.1103/PhysRev.105.1413](https://doi.org/10.1103/PhysRev.105.1413).
- 2085 [23] M. Gormley et al. “Experimental test of C Invariance in $\eta \rightarrow \pi^+ \pi^- \pi^0$ ”. In: *Physical Review
2086 Letters* 21.6 (1968), pp. 402–406. DOI: [10.1103/PhysRevLett.21.402](https://doi.org/10.1103/PhysRevLett.21.402).
- 2087 [24] J. H. Christenson et al. “Evidence for the 2π decay of the K20 meson”. In: *Physical Review
2088 Letters* 13.4 (July 1964), pp. 138–140. DOI: [10.1103/PhysRevLett.13.138](https://doi.org/10.1103/PhysRevLett.13.138).
- 2089 [25] A. Alavi-Harati et al. “Observation of Direct CP Violation in K S , L $\rightarrow \pi \pi$ Decays”. In:
2090 *Physical Review Letters* 83.1 (July 1999), pp. 22–27. DOI: [10.1103/PhysRevLett.83.22](https://doi.org/10.1103/PhysRevLett.83.22).
- 2091 [26] V. Fanti et al. “A new measurement of direct CP violation in two pion decays of the neu-
2092 tral kaon”. In: *Physics Letters B* 465.1-4 (Oct. 1999), pp. 335–348. DOI: [10.1016/S0370-2693\(99\)01030-8](https://doi.org/10.1016/S0370-2693(99)01030-8).
- 2094 [27] B. Aubert et al. “Measurement of CP -Violating Asymmetries in B 0 Decays to CP Eigen-
2095 states”. In: *Physical Review Letters* 86.12 (Mar. 2001), pp. 2515–2522. DOI: [10.1103/PhysRevLett.86.2515](https://doi.org/10.1103/PhysRevLett.86.2515).
- 2097 [28] K. Abe et al. “Observation of Large CP Violation in the Neutral B Meson System”. In: *Physical
2098 Review Letters* 87.9 (Aug. 2001), p. 091802. DOI: [10.1103/PhysRevLett.87.091802](https://doi.org/10.1103/PhysRevLett.87.091802).
- 2099 [29] R. Aaij et al. “Observation of CP Violation in Charm Decays”. In: *Physical Review Letters*
2100 122.21 (May 2019). DOI: [10.1103/PhysRevLett.122.211803](https://doi.org/10.1103/PhysRevLett.122.211803).
- 2101 [30] L. Wolfenstein. “Neutrino oscillations in matter”. In: *Physical Review D* 17.9 (May 1978),
2102 pp. 2369–2374. DOI: [10.1103/PhysRevD.17.2369](https://doi.org/10.1103/PhysRevD.17.2369).
- 2103 [31] S. P. Mikheyev and A. Yu. Smirnov. “Resonance enhancement of oscillations in matter and
2104 solar neutrino spectroscopy”. In: *Yadernaya Fizika* 42 (1985), p. 1441.
- 2105 [32] A. Yu. Smirnov. “Solar neutrinos: Oscillations or No-oscillations?” In: (Sept. 2016). arXiv:
2106 [1609.02386](https://arxiv.org/abs/1609.02386).
- 2107 [33] Evgeny Kh. Akhmedov and Joachim Kopp. “Neutrino oscillations: Quantum mechanics vs.
2108 quantum field theory”. In: (Jan. 2010). DOI: [10.1007/JHEP04\(2010\)008](https://doi.org/10.1007/JHEP04(2010)008).
- 2109 [34] Evgeny Akhmedov. “Do charged leptons oscillate?” In: (June 2007). DOI: [10.1088/1126-6708/2007/09/116](https://doi.org/10.1088/1126-6708/2007/09/116).

- 2111 [35] Raymond Davis, Don S. Harmer, and Kenneth C. Hoffman. "Search for neutrinos from
2112 the sun". In: *Physical Review Letters* 20.21 (May 1968), pp. 1205–1209. DOI: [10.1103/PhysRevLett.20.1205](https://doi.org/10.1103/PhysRevLett.20.1205).
- 2114 [36] T. A. Kirsten et al. "GALLEX solar neutrino results and status of GNO". In: *Nuclear Physics B - Proceedings Supplements* 77.1-3 (May 1999), pp. 26–34. DOI: [10.1016/S0920-5632\(99\)00389-8](https://doi.org/10.1016/S0920-5632(99)00389-8).
- 2117 [37] J. N. Abdurashitov et al. "Measurement of the solar neutrino capture rate with gallium metal". In: *Physical Review C - Nuclear Physics* 60.5 (Oct. 1999), p. 32. DOI: [10.1103/PhysRevC.60.055801](https://doi.org/10.1103/PhysRevC.60.055801).
- 2120 [38] Y. Oyama et al. "Experimental study of upward-going muons in Kamiokande". In: *Physical Review D* 39.6 (Mar. 1989), pp. 1481–1491. DOI: [10.1103/PhysRevD.39.1481](https://doi.org/10.1103/PhysRevD.39.1481).
- 2122 [39] Q. R. Ahmad et al. "Direct Evidence for Neutrino Flavor Transformation from Neutral-
2123 Current Interactions in the Sudbury Neutrino Observatory". In: *Physical Review Letters* 89.1
2124 (June 2002), p. 011301. DOI: [10.1103/PhysRevLett.89.011301](https://doi.org/10.1103/PhysRevLett.89.011301).
- 2125 [40] Y. Fukuda et al. "Measurement of the flux and zenith-angle distribution of upward through-
2126 going muons by super-kamiokande". In: *Physical Review Letters* 82.13 (Mar. 1999), pp. 2644–
2127 2648. DOI: [10.1103/PhysRevLett.82.2644](https://doi.org/10.1103/PhysRevLett.82.2644).
- 2128 [41] K. Eguchi et al. "First Results from KamLAND: Evidence for Reactor Antineutrino Disap-
2129 pearance". In: *Physical Review Letters* 90.2 (Jan. 2003), p. 6. DOI: [10.1103/PhysRevLett.90.021802](https://doi.org/10.1103/PhysRevLett.90.021802).
- 2131 [42] J. K. Ahn et al. "Observation of reactor electron antineutrinos disappearance in the RENO
2132 experiment". In: *Physical Review Letters* 108.19 (May 2012), p. 191802. DOI: [10.1103/PhysRevLett.108.191802](https://doi.org/10.1103/PhysRevLett.108.191802).
- 2134 [43] Y. Abe et al. "Improved measurements of the neutrino mixing angle θ_{13} with the double
2135 chooz detector". In: *Journal of High Energy Physics* 2014.10 (Oct. 2014), pp. 1–44. DOI: [10.1007/JHEP10\(2014\)086](https://doi.org/10.1007/JHEP10(2014)086).
- 2137 [44] F. P. An et al. "Independent measurement of the neutrino mixing angle θ_{13} via neutron
2138 capture on hydrogen at Daya Bay". In: *Physical Review D - Particles, Fields, Gravitation and
2139 Cosmology* 90.7 (Oct. 2014), p. 071101. DOI: [10.1103/PhysRevD.90.071101](https://doi.org/10.1103/PhysRevD.90.071101).
- 2140 [45] M. H. Ahn et al. "Measurement of neutrino oscillation by the K2K experiment". In: *Physical
2141 Review D - Particles, Fields, Gravitation and Cosmology* 74.7 (Oct. 2006), p. 072003. DOI:
2142 [10.1103/PhysRevD.74.072003](https://doi.org/10.1103/PhysRevD.74.072003).
- 2143 [46] P. Adamson et al. "Combined analysis of ν_μ disappearance and $\nu_\mu \rightarrow \nu_e$ appearance in MI-
2144 NOS using accelerator and atmospheric neutrinos". In: *Physical Review Letters* 112.19 (May
2145 2014), p. 191801. DOI: [10.1103/PhysRevLett.112.191801](https://doi.org/10.1103/PhysRevLett.112.191801).
- 2146 [47] K. Abe et al. "First combined measurement of the muon neutrino and antineutrino charged-
2147 current cross section without pions in the final state at T2K". In: (Feb. 2020). arXiv: [2002.09323](https://arxiv.org/abs/2002.09323).
- 2149 [48] M. A. Acero et al. "First measurement of neutrino oscillation parameters using neutrinos
2150 and antineutrinos by NOvA". In: *Physical Review Letters* 123.15 (Oct. 2019), p. 151803. DOI:
2151 [10.1103/PhysRevLett.123.151803](https://doi.org/10.1103/PhysRevLett.123.151803).
- 2152 [49] M Jiang et al. "Atmospheric neutrino oscillation analysis with improved event reconstruc-
2153 tion in Super-Kamiokande IV". In: *Progress of Theoretical and Experimental Physics* 2019.5
2154 (May 2019). DOI: [10.1093/PTEP/PTZ015](https://doi.org/10.1093/PTEP/PTZ015).

- 2155 [50] Ivan Esteban et al. “Global analysis of three-flavour neutrino oscillations: synergies and
2156 tensions in the determination of θ_{23} , δ_{CP} , and the mass ordering”. In: *Journal of High*
2157 *Energy Physics* 2019.1 (Jan. 2019). DOI: [10.1007/JHEP01\(2019\)106](https://doi.org/10.1007/JHEP01(2019)106).
- 2158 [51] Peter W. Higgs. “Broken Symmetries and the Masses of Gauge Bosons”. In: *Physical Review*
2159 *Letters* 13.16 (Oct. 1964), pp. 508–509. DOI: [10.1103/PhysRevLett.13.508](https://doi.org/10.1103/PhysRevLett.13.508).
- 2160 [52] M. Aker et al. “An improved upper limit on the neutrino mass from a direct kinematic
2161 method by KATRIN”. In: (Sept. 2019). arXiv: [1909.06048](https://arxiv.org/abs/1909.06048).
- 2162 [53] C. Athanassopoulos et al. “The liquid scintillator neutrino detector and LAMPF neutrino
2163 source”. In: *Nuclear Instruments and Methods in Physics Research, Section A: Accelerators,*
2164 *Spectrometers, Detectors and Associated Equipment* 388.1-2 (Mar. 1997), pp. 149–172. DOI:
2165 [10.1016/S0168-9002\(96\)01155-2](https://doi.org/10.1016/S0168-9002(96)01155-2).
- 2166 [54] Y. J. Ko et al. “Sterile Neutrino Search at the NEOS Experiment”. In: *Physical Review Letters*
2167 118.12 (Mar. 2017), p. 121802. DOI: [10.1103/PhysRevLett.118.121802](https://doi.org/10.1103/PhysRevLett.118.121802).
- 2168 [55] I. Alekseev et al. “Search for sterile neutrinos at the DANSS experiment”. In: *Physics Letters,*
2169 *Section B: Nuclear, Elementary Particle and High-Energy Physics* 787 (Dec. 2018), pp. 56–63.
2170 DOI: [10.1016/j.physletb.2018.10.038](https://doi.org/10.1016/j.physletb.2018.10.038).
- 2171 [56] H. Almazán et al. “Sterile Neutrino Constraints from the STEREO Experiment with 66 Days
2172 of Reactor-On Data”. In: *Physical Review Letters* 121.16 (Oct. 2018), p. 161801. DOI: [10.1103/PhysRevLett.121.161801](https://doi.org/10.1103/PhysRevLett.121.161801).
- 2174 [57] J. Ashenfelter et al. “First Search for Short-Baseline Neutrino Oscillations at HFIR with
2175 PROSPECT”. In: *Physical Review Letters* 121.25 (Dec. 2018), p. 251802. DOI: [10.1103/PhysRevLett.121.251802](https://doi.org/10.1103/PhysRevLett.121.251802).
- 2177 [58] A. P. Serebrov et al. “Neutrino-4 experiment on the search for a sterile neutrino at the SM-3
2178 reactor”. In: *Journal of Experimental and Theoretical Physics* 121.4 (Oct. 2015), pp. 578–586.
2179 DOI: [10.1134/S1063776115100209](https://doi.org/10.1134/S1063776115100209).
- 2180 [59] K. N. Abazajian et al. “Light Sterile Neutrinos: A White Paper”. In: (Apr. 2012). arXiv: [1204.5379](https://arxiv.org/abs/1204.5379).
- 2182 [60] Takehiko Asaka, Steve Blanchet, and Mikhail Shaposhnikov. “The ν MSM, Dark Matter and
2183 Neutrino Masses”. In: *Physics Letters B* 631.4 (Mar. 2005), pp. 151–156. DOI: [10.1016/j.physletb.2005.09.070](https://doi.org/10.1016/j.physletb.2005.09.070).
- 2185 [61] Takehiko Asaka and Mikhail Shaposhnikov. “The ν MSM, Dark Matter and Baryon Asym-
2186 metry of the Universe”. In: *Journal of Physics: Conference Series* 39.1 (May 2005), pp. 9–11.
2187 DOI: [10.1016/j.physletb.2005.06.020](https://doi.org/10.1016/j.physletb.2005.06.020).
- 2188 [62] Ch Kraus et al. “Final results from phase II of the Mainz neutrino mass searchin tritium β
2189 decay”. In: *European Physical Journal C* 40.4 (Apr. 2005), pp. 447–468. DOI: [10.1140/epjc/s2005-02139-7](https://doi.org/10.1140/epjc/s2005-02139-7).
- 2191 [63] V. N. Aseev et al. “Upper limit on the electron antineutrino mass from the Troitsk exper-
2192 iment”. In: *Physical Review D - Particles, Fields, Gravitation and Cosmology* 84.11 (Dec.
2193 2011). DOI: [10.1103/PhysRevD.84.112003](https://doi.org/10.1103/PhysRevD.84.112003).
- 2194 [64] A. Gando et al. “Search for Majorana Neutrinos Near the Inverted Mass Hierarchy Region
2195 with KamLAND-Zen”. In: *Physical Review Letters* 117.8 (Aug. 2016). DOI: [10.1103/PhysRevLett.117.082503](https://doi.org/10.1103/PhysRevLett.117.082503).
- 2197 [65] Nathalie Palanque-Delabrouille et al. “Neutrino masses and cosmology with Lyman-alpha
2198 forest power spectrum”. In: *Journal of Cosmology and Astroparticle Physics* 2015.11 (Nov.
2199 2015). DOI: [10.1088/1475-7516/2015/11/011](https://doi.org/10.1088/1475-7516/2015/11/011).

- 2200 [66] Kenny C.Y. Ng et al. "New constraints on sterile neutrino dark matter from NuSTAR M31
2201 observations". In: *Physical Review D* 99.8 (Apr. 2019), p. 083005. DOI: [10.1103/PhysRevD.99.083005](https://doi.org/10.1103/PhysRevD.99.083005).
- 2203 [67] Kerstin Perez et al. "Almost closing the ν mSM sterile neutrino dark matter window with
2204 NuSTAR". In: *Physical Review D* 95.12 (June 2017), p. 123002. DOI: [10.1103/PhysRevD.95.123002](https://doi.org/10.1103/PhysRevD.95.123002).
- 2206 [68] Andrea Caputo, Marco Regis, and Marco Taoso. *Searching for Sterile Neutrino with X-ray
2207 Intensity Mapping*. Tech. rep. 2020. arXiv: [1911.09120v2](https://arxiv.org/abs/1911.09120v2).
- 2208 [69] Dmitry Gorbunov and Mikhail Shaposhnikov. "How to find neutral leptons of the ν MSM?"
2209 In: *Journal of High Energy Physics* 2007.10 (Oct. 2007), pp. 015–015. DOI: [10.1088/1126-6708/2007/10/015](https://doi.org/10.1088/1126-6708/2007/10/015).
- 2211 [70] CMS Collaboration. "Search for heavy Majorana neutrinos in $\mu\pm\mu\pm$ in proton–proton col-
2212 lisions at $\sqrt{s}=7$ TeV". In: *Physics Letters B* 748 (2015), pp. 144–166.
- 2213 [71] P Abreu. "DELPHI Collaboration: Search for neutral heavy leptons produced in Z decays".
2214 In: *Zeitschrift fur Physik C-Particles and Fields* 74.1 (1997), pp. 57–72.
- 2215 [72] O Adriani et al. "Search for isosinglet neutral heavy leptons in Z 0 decays". In: *Physics Letters
2216 B* 295.3 (1992), pp. 371–382.
- 2217 [73] Roel Aaij et al. "Search for Majorana neutrinos in $B \rightarrow \pi^+ \mu^- \mu^-$ decays". In: *Physical review
2218 letters* 112.13 (2014), p. 131802.
- 2219 [74] D Liventsev et al. "Search for heavy neutrinos at Belle". In: *Physical Review D* 87.7 (2013),
2220 p. 071102.
- 2221 [75] Amanda M Cooper-Sarkar et al. "Search for heavy neutrino decays in the BEBC beam dump
2222 experiment". In: *Physics Letters B* 160.1 (1985), pp. 207–211.
- 2223 [76] E Gallas et al. "Search for neutral weakly interacting massive particles in the Fermilab Teva-
2224 tron wideband neutrino beam". In: *Physical Review D* 52.1 (1995), p. 6.
- 2225 [77] AV Artamonov et al. "Search for heavy neutrinos in $K^+ \rightarrow \mu^+ \nu H$ decays". In: *Physical Review
2226 D* 91.5 (2015), p. 052001.
- 2227 [78] M Aoki et al. "Search for massive neutrinos in the decay $\pi \rightarrow e \nu$ ". In: *Physical Review D*
2228 84.5 (2011), p. 052002.
- 2229 [79] DI Britton et al. "Improved search for massive neutrinos in $\pi^+ \rightarrow e^+ \nu$ decay". In: *Physical
2230 Review D* 46.3 (1992), R885.
- 2231 [80] G. Bernardi et al. "Further limits on heavy neutrino couplings". In: *Physics Letters B* 203.3
2232 (Mar. 1988), pp. 332–334. DOI: [10.1016/0370-2693\(88\)90563-1](https://doi.org/10.1016/0370-2693(88)90563-1).
- 2233 [81] Pierre Vilain et al. "Search for heavy isosinglet neutrinos". In: *Physics Letters B* 351.1 (1995),
2234 pp. 387–392.
- 2235 [82] Arturas Vaitaitis et al. "Search for neutral heavy leptons in a high-energy neutrino beam".
2236 In: *Physical Review Letters* 83.24 (1999), p. 4943.
- 2237 [83] J Badier et al. "Direct photon production from pions and protons at 200 GeV/c". In: *Zeitschrift
2238 für Physik C Particles and Fields* 31.3 (1986), pp. 341–347.
- 2239 [84] T. Yamazaki T. Ishikawa Y. Akiba M. Iwasaki K. H. Tanaka S. Ohtake H. Tamura and M. Naka-
2240 jima. *et al.* 1984.
- 2241 [85] RS Hayano et al. "Heavy-Neutrino Search Using $K \mu 2$ Decay". In: *Physical Review Letters*
2242 49.18 (1982), p. 1305.

- 2243 [86] Marco Drewes and Björn Garbrecht. “Experimental and cosmological constraints on heavy
2244 neutrinos”. In: *arXiv preprint arXiv:1502.00477* (2015).
- 2245 [87] JV Allaby et al. “A search for decays of heavy neutrinos in the mass range 0.5–2.8 GeV”. In:
2246 *Physics Letters B* 166.4 (1986), pp. 473–478.
- 2247 [88] S Baranov et al. “Search for heavy neutrinos at the IHEP-JINR neutrino detector”. In: *Physics*
2248 *Letters B* 302.2 (1993), pp. 336–340.
- 2249 [89] Jean Orloff, A Rozanov, and C Santoni. “Limits on the mixing of tau neutrino to heavy neu-
2250 trinos”. In: *Physics Letters B* 550.1 (2002), pp. 8–15.
- 2251 [90] P Astier D Autieroh A Baldissari et al. “Search for heavy neutrinos mixing with tau neu-
2252 trinos”. In: *arXiv preprint hep-ex/0101041* (2001).
- 2253 [91] K. Abe et al. “Proposal for an Extended Run of T2K to 20×10^{21} POT”. In: (Sept. 2016). arXiv:
2254 [1609.04111](https://arxiv.org/abs/1609.04111).
- 2255 [92] Hyper-Kamiokande Proto-Collaboration et al. “Hyper-Kamiokande Design Report”. In: (May
2256 2018). arXiv: [1805.04163](https://arxiv.org/abs/1805.04163).
- 2257 [93] R. Acciarri et al. “Long-Baseline Neutrino Facility (LBNF) and Deep Underground Neutrino
2258 Experiment (DUNE) Conceptual Design Report Volume 1: The LBNF and DUNE Projects”.
2259 In: (Jan. 2016). arXiv: [1601.05471](https://arxiv.org/abs/1601.05471).
- 2260 [94] Cedric Cerna. “The Jiangmen Underground Neutrino Observatory (JUNO)”. In: *Nuclear In-
2261 struments and Methods in Physics Research, Section A: Accelerators, Spectrometers, Detectors
2262 and Associated Equipment* 958 (Apr. 2020), p. 162183. DOI: [10.1016/j.nima.2019.05.024](https://doi.org/10.1016/j.nima.2019.05.024).
- 2263 [95] N. Di Marco. “Searching for neutrinoless double-beta decay with GERDA”. In: *Nuclear In-
2264 struments and Methods in Physics Research, Section A: Accelerators, Spectrometers, Detectors
2265 and Associated Equipment* 958 (Apr. 2020), p. 162112. DOI: [10.1016/j.nima.2019.04.066](https://doi.org/10.1016/j.nima.2019.04.066).
- 2266 [96] L. Cardani. “Final Results of the CUPID-0 Phase I Experiment”. In: *Journal of Low Temper-
2267 erature Physics* (Feb. 2020), pp. 1–8. DOI: [10.1007/s10909-020-02382-w](https://doi.org/10.1007/s10909-020-02382-w).
- 2268 [97] M.G. Aartsen et al. “The IceCube Neutrino Observatory: instrumentation and online sys-
2269 tems”. In: *Journal of Instrumentation* 12.03 (Mar. 2017), P03012–P03012. DOI: [10.1088/1748-0221/12/03/P03012](https://doi.org/10.1088/1748-0221/12/03/P03012).
- 2270 [98] Rémy Le Breton. *KM3NeT: Next-generation neutrino telescope in the Mediterranean Sea*.
2271 Aug. 2019. DOI: [10.1016/j.nima.2018.10.103](https://doi.org/10.1016/j.nima.2018.10.103).
- 2272 [99] the FCC Collaboration. “FCC-ee: The Lepton Collider: Future Circular Collider Conceptual
2273 Design Report Volume 2”. In: *European Physical Journal: Special Topics* 228.2 (June 2019),
2274 pp. 261–623. DOI: [10.1140/EPJST/E2019-900045-4](https://doi.org/10.1140/EPJST/E2019-900045-4).
- 2275 [100] SHiP SHiP Collaboration. “The experimental facility for the Search for Hidden Particles at
2276 the CERN SPS”. In: (Oct. 2018). DOI: [10.1088/1748-0221/14/03/P03025](https://doi.org/10.1088/1748-0221/14/03/P03025).
- 2277 [101] K Abe et al. *The T2K Neutrino Flux Prediction*. Tech. rep. 2013, p. 37. arXiv: [1211.0469v3](https://arxiv.org/abs/1211.0469v3).
- 2278 [102] P. A. Amaudruz et al. “The T2K fine-grained detectors”. In: *Nuclear Instruments and Meth-
2279 ods in Physics Research, Section A: Accelerators, Spectrometers, Detectors and Associated
2280 Equipment* 696 (2012), pp. 1–31. DOI: [10.1016/j.nima.2012.08.020](https://doi.org/10.1016/j.nima.2012.08.020).
- 2281 [103] N Abgrall et al. “Time projection chambers for the T2K near detectors”. In: *Nuclear Instru-
2282 ments and Methods in Physics Research, Section A: Accelerators, Spectrometers, Detectors
2283 and Associated Equipment* 637.1 (2011), pp. 25–46. DOI: [10.1016/j.nima.2011.02.036](https://doi.org/10.1016/j.nima.2011.02.036).
- 2284 [104] J. A. Aguayo et al. “Performance of the T2K near detector time projection chamber”. In:
2285 *Nuclear Instruments and Methods in Physics Research, Section A: Accelerators, Spectrometers,
2286 Detectors and Associated Equipment* 637.1 (2011), pp. 47–60. DOI: [10.1016/j.nima.2011.02.037](https://doi.org/10.1016/j.nima.2011.02.037).

- 2287 [104] S. Fukuda et al. "The Super-Kamiokande detector". In: *Nuclear Instruments and Methods in Physics Research, Section A: Accelerators, Spectrometers, Detectors and Associated Equipment* 501.2-3 (Apr. 2003), pp. 418–462. DOI: [10.1016/S0168-9002\(03\)00425-X](https://doi.org/10.1016/S0168-9002(03)00425-X).
- 2288
- 2289
- 2290 [105] K. Abe et al. "Measurement of neutrino and antineutrino oscillations by the T2K experiment including a new additional sample of ve interactions at the far detector". In: *Physical Review D* 96.9 (Nov. 2017), p. 092006. DOI: [10.1103/PhysRevD.96.092006](https://doi.org/10.1103/PhysRevD.96.092006).
- 2291
- 2292
- 2293 [106] K. Abe et al. "Measurement of the charged-current electron (anti-)neutrino inclusive cross-sections at the T2K off-axis near detector ND280". In: (Feb. 2020). arXiv: [2002.11986](https://arxiv.org/abs/2002.11986).
- 2294
- 2295 [107] Takehiko Asaka, Shintaro Eijima, and Atsushi Watanabe. "Heavy neutrino search in accelerator-based experiments". In: *Journal of High Energy Physics* 2013.3 (Dec. 2012), p. 125. DOI: [10.1007/JHEP03\(2013\)125](https://doi.org/10.1007/JHEP03(2013)125).
- 2296
- 2297
- 2298 [108] Loretta M. Johnson, Douglas W. McKay, and Tim Bolton. "Extending Sensitivity for Low-Mass Neutral Heavy Lepton Searches". In: *Physical Review D* 56.5 (Mar. 1997), pp. 2970–2981. DOI: [10.1103/PhysRevD.56.2970](https://doi.org/10.1103/PhysRevD.56.2970).
- 2299
- 2300
- 2301 [109] R. Acciarri et al. "Measurements of Inclusive Muon Neutrino and Antineutrino Charged Current Differential Cross Sections on Argon in the NuMI Antineutrino Beam". In: *Physical Review D* 89.11 (Apr. 2014), p. 112003. DOI: [10.1103/PhysRevD.89.112003](https://doi.org/10.1103/PhysRevD.89.112003).
- 2302
- 2303
- 2304 [110] The NA61/SHINE Collaboration et al. "Measurements of π^\pm , K^\pm and proton yields from the surface of the T2K replica target for incoming 31 GeV/c protons with the NA61/SHINE spectrometer at the CERN SPS". In: *The European Physical Journal C* 79.2 (Aug. 2018), p. 100. DOI: [10.1140/epjc/s10052-019-6583-0](https://doi.org/10.1140/epjc/s10052-019-6583-0).
- 2305
- 2306
- 2307
- 2308 [111] N Abgrall et al. "NA61/SHINE facility at the CERN SPS: beams and detector system". In: *Journal of Instrumentation* 9.06 (June 2014), P06005–P06005. DOI: [10.1088/1748-0221/9/06/P06005](https://doi.org/10.1088/1748-0221/9/06/P06005).
- 2309
- 2310
- 2311 [112] Robert D. Cousins and Virgil L. Highland. "Incorporating systematic uncertainties into an upper limit". In: *Nuclear Inst. and Methods in Physics Research, A* 320.1-2 (Aug. 1992), pp. 331–335. DOI: [10.1016/0168-9002\(92\)90794-5](https://doi.org/10.1016/0168-9002(92)90794-5).
- 2312
- 2313
- 2314 [113] Lev Davidovich Landau. *The classical theory of fields*. Vol. 2. Elsevier, 2013. ISBN: 0-08-025072-6. DOI: [10.1063/1.3067575](https://doi.org/10.1063/1.3067575).
- 2315
- 2316 [114] S Agostinelli et al. "Geant4 – a simulation toolkit". In: *Nuclear Instruments and Methods in Physics Research Section A: Accelerators, Spectrometers, Detectors and Associated Equipment* 506.3 (2003), pp. 250–303. DOI: [10.1016/S0168-9002\(03\)01368-8](https://doi.org/10.1016/S0168-9002(03)01368-8).
- 2317
- 2318
- 2319 [115] Y. Hayato. "Neut". In: *Nuclear Physics B - Proceedings Supplements* 112.1-3 (Nov. 2002), pp. 171–176. DOI: [10.1016/S0920-5632\(02\)01759-0](https://doi.org/10.1016/S0920-5632(02)01759-0).
- 2320
- 2321 [116] C. Andreopoulos et al. "The GENIE neutrino Monte Carlo generator". In: *Nuclear Instruments and Methods in Physics Research Section A: Accelerators, Spectrometers, Detectors and Associated Equipment* 614.1 (Feb. 2010), pp. 87–104. DOI: [10.1016/j.nima.2009.12.009](https://doi.org/10.1016/j.nima.2009.12.009).
- 2322
- 2323
- 2324 [117] Jakub Zmuda et al. "NuWro monte carlo generator of neutrino interactions-first electron scattering results". In: *Acta Physica Polonica B*. Vol. 46. 11. Jagellonian University, Nov. 2015, pp. 2329–2334. DOI: [10.5506/APhysPolB.46.2329](https://doi.org/10.5506/APhysPolB.46.2329).
- 2325
- 2326
- 2327 [118] K. Abe et al. "Constraint on the Matter-Antimatter Symmetry-Violating Phase in NeutrinoOscillations". In: (Oct. 2019). arXiv: [1910.03887](https://arxiv.org/abs/1910.03887).
- 2328
- 2329 [119] K. Abe et al. "T2K ND280 Upgrade - Technical Design Report". In: (Jan. 2019). arXiv: [1901.03750](https://arxiv.org/abs/1901.03750).
- 2330

- 2331 [120] K. Abe et al. "Constraint on the matterantimatter symmetry-violating phase in neutrino
2332 oscillations". In: *Nature* 580.7803 (Apr. 2020), pp. 339–344. DOI: [10.1038/s41586-020-2177-0](https://doi.org/10.1038/s41586-020-2177-0).
- 2334 [121] K. Abe et al. "J-PARC Neutrino Beamline Upgrade Technical Design Report". In: (Aug. 2019).
2335 arXiv: [1908.05141](https://arxiv.org/abs/1908.05141).